國立交通大學

機械工程學系

碩士論文

空氣吹離法與時間因子對 PEMFC CO 容忍度之改善研究

Investigations of air-bleeding technique and specific poisoned duration for CO tolerance improvement of PEM fuel cell

研 究 生：翁德正

指導教授：陳俊勳　教授

中華民國九十三年六月

空氣吹離法與時間因子對 PEMFC CO 容忍度之改善研究

學生：翁德正　　指導教授：陳俊勳

國立交通大學機械工程學系

摘要

本論文可分為三大部分。第一部分為運用不同的操作條件去做暫態 CO 毒化實驗。暫態實驗中操作條件分別為固定電池電位(0.5、0.6、0.7)與固定電池電流(600、1000、1200 mA/cm^2)，CO 濃度為 52.7ppm。由實驗結果可知，不論定何種電位執行暫態實驗所得到的穩態毒化性能都是一樣的。但發現如果固定越高的電流去做毒化實驗，電池的 CO 容忍度能夠被提升，相對地有較佳的電池性能。第二部分為討論空氣吹離法與其注入時機對燃料電池 CO 容忍度的影響。在暫態毒化實驗中空氣注入時間分別為三分鐘與三十分鐘。結果可知不論空氣何時注入都能有效提升電池的 CO 容忍度，使性能回復。但空氣越早注入越能更有效降低 CO 毒化效應，而所需的空氣量也會因此減少。第三部分為比較不同陽極觸媒(Pt alloy and Pt)對 CO 容忍度之差異。當沒有配合使用空氣吹離法時，使用 Pt alloy 陽極觸媒可以較有效地降低毒化效應，可得到較高的電池性能。但運用空氣吹離法後，發現陽極觸媒成分對 CO 容忍度的影響變的不明顯。那是因為不論何種觸媒(Pt alloy and Pt)空氣吹離法都能大幅提升電池對抗 CO 毒化的能力。

Investigations of air-bleeding technique and specific poisoned duration for CO tolerance improvement of PEM fuel cell

Student: De-Zheng Weng Advisor: Prof. Chiun-Hsun Chen

Institute of Mechanical Engineering

National Chiao Tung University

ABSTRACT

This thesis consists of three parts. The first one carries out the transient CO (52.7ppm) poisoning test with fixed cell voltage (0.5, 0.6 and 0.7V) and current density conditions (600, 1000 and 1200 mA/cm^2), respectively. For the fixed cell voltage case, the results of transient CO poisoning test indicate that varying cell voltage does not change the stable poisoned polarization behaviors. For the fixed current density one, the higher current density can improve CO tolerance. The second one investigates the effects of air-bleeding with different introduced timing (3 and 30min) in the transient poisoning CO tests (10.1, 25 and 52.7ppm). With air-bleeding, it is able to improve the fuel cell CO tolerance and recover the poisoned performance no matter what the air introducing timing. With an earlier introducing timing, 3min, it can obtain a better recovery performance and the optimum ratio of air-bleeding is lower. The third one studies the effect of using different anode catalyst component (Pt alloy and Pt) on the cell performance in CO poisoning tests. Without air-bleeding, Pt alloy anode catalyst has a better CO tolerance comparing to pure Pt anode catalyst. With air-bleeding, it can increase CO tolerance effectively no matter what kind anode catalyst (Pt or Pt alloy) is used.

致謝

兩年的時間過的真快，轉眼間已經要畢業了。想當初剛進實驗室時對燃料電池還一無所知，可是現在已完成了相關的研究論文。當然如果不是許多人的指導與協助論文是不可能順利完成的。所以要感謝的人真的非常多。首先要感謝指導教授陳俊勳老師，兩年來的教導使我成長許多。還有如果不是老師給我機會，我也無法去工研院做研究與到加拿大增廣見聞。還想跟老師說聲不好意思，因為我的英文文法使的給老師增加不少困擾。

家人默默的陪伴一直我往前走的原動力，雖然我的父親、母親還有姐姐不善於言語表達，但只要一個眼神我全都能了解了。更要感謝父母的栽培養育之恩，如不是父母全心的投入與付出也不會有現在健全的我。

實驗的同學們好像就快要各奔東西了，兩年的相處時間似乎不太夠。皓然、平吉、慧真很高興在研究生活中，可以一起歡笑、一起被罵、一起克服許多難題，大家以後都要朝著自己的方向前進喔。還有老師的助理雅雪，雅雪不只是個稱職的助理，還會像朋友一樣的關心我們，真的很感謝。當然怎麼能忘記學弟跟博班學長呢，尤其是耀慶。

朋友可說是我心靈上的支柱，研究生的生活常常有許多不順心與困境。小龜、學長、滷蛋、宜祥、裕博、智超...謝謝你們一路上的陪伴。還有今年的國際書展我遇到了我等待已久的那個她，宜惠，真的很慶幸能遇到妳。

當然怎麼能漏掉工研院的同事們，比較怕生的我因為有你們的熱情還不厭其煩的教導，讓我很快就能融入這個環境中，實驗上也是你們給我許多的方便，不然我可能還在作實驗呢。要感謝的人真的很多，何姐、賜岱、吳伯、淑卿、銘晃、張大哥、許大哥、宋大哥、阿燦哥、顏博、林博...你們不但是工作上的好夥伴更是生活上的好朋友，再會了阿。

CONTENTS

LIST OF TABLES

LIST OF FIGURES

NOMENCLATURE

I	Current (A) produced from fuel cell
i	Current density (mA/cm^2)
OCV	Open circuit voltage (V)
V	Cell voltage (V)
V_A	Anode potential (V)
T	Temperature (℃)
t	Time (sec)
C	CO concentration (ppm)

CHAPTER 1

INTRODUCTION

1.1 Background

Today, people's lives are more and more convenient, but we have no sense of propriety to waste natural resources and bring more serious pollution on the earth. So we face many difficult problems, such as greenhouse effect, natural resources insufficiency and so on. The search for renewable and clear energy has grown tremendously in recent years. Fuel cell is one of the most promising sources for achieving our goals. There are three major reasons to explain why we need fuel cell.

The first reason is the resource problem. After 2004, we will begin to face the decline in oil production about 3% per year. In accordance with BP Statistical Review of World Energy's statistics, the oil will be exhaust after about 40 to 50 years. If we do not have sense to hold down the waste rate, then, the time will be shorter. We know that the supply of fossil fuels has a limit eventually, but the resource of hydrogen is unlimited. The fuel cell uses hydrogen, a clean and new energy resource, as its fuel.

The second is environmental problem. Traditional technologies, such as internal combustion engines, will produce greenhouse gases and other pollution into the air, whereas fuel cells only produce water and heat. Comparing with to the damage effects of oil spill, the hydrogen spill would quickly disperse into the air without harmful effects, provided that

no explosion occurs. So it is an environmental protection method to generate energy.

The third is efficiency problem. Because fuel cell converts fuel directly into energy through an electrochemical reaction, so it can get more energy in the same amount of fuel relatively by comparing to traditional combustion. This direct process can reduce energy waste and in the fuel cell system we can further utilize the surplus heat, increasing the efficiency up to 80~90%. On the other hand, combustion-based energy generation first converts the fuel into heat, subjected to a maximum efficiency limited by Carnot cycle in thermodynamics, and then it converts into mechanical energy to provide motion or drive a turbine to produce work. The additional steps involved in combustion generation allow energy to escape as heat, friction and conversion losses, resulting in the lower overall efficiencies. So fuel cell can provide higher efficiency than tradition generation energy method.

There are many types of fuel cells such as PEMFC, AFC, SOFC, PAFC, MCFC, DMFC and so on, however, their operation theories are almost the same. Usually, a fuel cell is made up of three major compositions. They are anode side, cathode side, and in between an electrolytic component, which it may be a solid polymer or electrolyte solution such that proton can pass through to the cathode side.

The research target in the present study is PEMFC. In next section we will introduce the PEMFC basic theory and its advantages.

PEM fuel cell uses solid electrolyte to replace traditional liquid electrolyte. The electrolyte used is a solid organic polymer poly-perflourosulfonic acid. It is a very thin membrane so that it can

reduce the space and also can reduce corrosion and management problems. So Proton Exchange Membrane has many advantages than the other types of electrolytes. The membrane is coated on both sides with highly dispersed metal alloy particles (mostly platinum), which are active catalysts. Hydrogen and oxygen are fed into anode- and cathode-catalyst on each side. In the anode, hydrogen is oxidized into hydrogen ions and electrons. The protons diffuse through the membrane (electrolyte) to reach the cathode, in the meantime, the electrons travel in the form of electric current to the cathode. Finally, in the cathode hydrogen ions, electrons and oxygen will proceed the reduction reaction to form water. The reactions are given as follows.

Reaction in the anode:

$$H_{2(g)} \rightarrow 2H^{+}_{(aq)} + 2e^{-} \qquad (1\text{-}1)$$

Reaction in the cathode:

$$\tfrac{1}{2}O_{2(g)} + 2H^{+}_{(aq)} + 2e^{-} \rightarrow H_2O_{(l)} \qquad (1\text{-}2)$$

Overall reaction:

$$H_{2(g)} + \tfrac{1}{2}O_{2(g)} \rightarrow H_2O_{(l)} \qquad (1\text{-}3)$$

This cell is a type of low temperature fuel cell, usually it operates at a temperature about 80℃. It has high power density and can change power output, generally ranged from 50W to 250kW, very quickly. As expected, it is the primary candidate of power supply for light-duty vehicles and buildings, and potentially for much smaller applications, such as replacements for rechargeable batteries.

The mechanism for hydrogen oxidation reaction is [1], [2]:

$$H_2 + 2S \rightarrow 2S - H \qquad \text{(Tafel)} \quad (1\text{-}4)$$

$$S - H \rightarrow S + H^+ + e^- \qquad \text{(Volmer)} \quad (1\text{-}5)$$

where “S” means the active site in the catalyst surface and the Tafel and Volmer reactions are always very fast.

Proton Exchange Membrane Fuel Cell (PEMFC) needs hydrogen and oxygen to operate. However, the direct storage of hydrogen is difficult, so it is usually to use hydrocarbon fuels, such as methanol (CH_3OH), methane (CH_4), gasoline, to pass through a fuel reformer to generate hydrogen. When hydrocarbon fuel passes through fuel reformer, it produces not only hydrogen but also carbon monoxide (CO). The latter one will be adsorbed by catalyst, leading to a less number of available catalytic sites. It is so-called poisoning. The CO poisoning reaction on catalyst surface is:

$$S + CO \rightarrow S - CO \qquad (1\text{-}6)$$

The active adsorption of CO by catalyst will cause the Tafel reaction to become the rate determining step, so it is a critical effect to PEMFC performance. Dhar et al. [3] experimentally studied the CO poisoning effect with cell performance. They found that when PEMFC electrode is Pt, as little as 10ppm CO in the anode fuel stream can lower the power output by 50%. So it is a very crucial problem that needs to solve. This work is motivated to experimentally study the CO poisoning effect in PEMFC.

1.2 Literature Review

There are many theoretical and experimental literatures concerning with the improvement of PEMFC CO tolerance. In order to reduce CO poisoning effect, there are some techniques suggested by many investigators. These include to increase catalytic ability to oxidize CO, to weaken CO adsorption of these catalysts; to add an oxidant into anode fuel stream to oxidize CO; to increase anode potential to let CO be oxidized, and to change the thermodynamic operation conditions.

Up to now, Pt is one of best catalysts for PEMFC. However, PEMFC operation temperature is between 60 to 100℃, under this operation temperature CO will be actively adsorbed by Pt catalyst. Then, it will reduce catalyst activity and lower the power output. One solution is to use alloyed catalysts. This method is to add second or third metal to Pt catalyst to become a new alloy to improve CO tolerance. Pt-Ru alloy is the most general one used as PEMFC catalyst in commercial fuel cells. It is because that Pt-Ru catalyst has a good effect to increase CO tolerance. There are some literatures to investigate CO reaction mechanism on Pt-Ru catalyst.

Watanabe and Motoo [4] used Ru surface to form RuOH to oxidize with CO, adsorbed on the catalyst. It will become CO_2 as CO proceeds oxidation reaction. Since CO is removed from catalyst surface, the catalyst now has more reaction area, improving cell performance. Ru can increase the ability of CO oxidation reaction, consequently, Pt-Ru catalyst can improve CO tolerance. The reactions are as follows:

$$S + H_2O \rightarrow OH_{ads} + H^+ + e^- \qquad (1\text{-}7)$$

$$CO_{ads} + OH_{ads} \rightarrow CO_2 + H^+ + 2S + e^- \qquad (1\text{-}8)$$

where “ads” represents the adsorption on the catalyst surface and S the extra available reaction area of catalyst after CO oxidization.

There has another explanation to depict why Pt-Ru can increase CO tolerance in other literatures.

Christoffersen et al. [5] used “density functional theory” to calculate every kind of dual metal catalyst surface characteristics and the corresponding CO adsorptive power. They considered that CO is adsorbed by Ru of Pt-Ru to the catalyst surface, then, the adsorbability of Pt with CO decreases. Therefore, Ru can reduce CO poison effect. Watanabe et al. [6] applied theoretical calculation for Pt-Ru catalyst adsorptive power with CO. Their results can support Chirstoffersen’s conclusion [5]. So there are two ways that Pt-Ru can increase CO tolerance. One is that RuOH can oxidatize CO, the other is that Ru can reduce the CO adsorption by Pt. These two effects exist simultaneously.

Gastiger et al. [7] considered that the optimum ratio between Pt and Ru is 1:1. Hongmei Yu et al. [8] experimentally studied the structural composition of Pt-Ru catalyst. They used inner and outer catalysts to make up a complete catalyst to test. As long as anode is fed with pure hydrogen, Pt still is the best catalyst for PEMFC. However, Pt-Ru alloy catalyst can effectively improve CO tolerance. Therefore, they used Pt-Ru as outer catalyst, and used pure Pt as inner catalyst. They found that such catalyst has higher CO tolerance and better performance than those of the traditional Pt-Ru alloy catalyst. Also, it is unnecessary to add catalyst

loading that can effectively improve CO poison effect. However, the inner to outer catalyst ratio is very important, too.

Hung et al. [9] conducted an experimental investigation for a carbon-supported Ru embedded between the Pt catalyst and GDL to form a filter. They used Pt+Ru filter catalyst to do CO poison experiment and compare the results with those of Pt-Ru alloy. When 100ppm CO and 2% oxygen are in the anode fuel stream, Pt+Ru filter catalyst has a better CO tolerance and performance than those of Pt-Ru alloy electrode. It is likely that CO oxidation within the Ru filter is primarily due to oxygen reaction to form OH, which then electrochemically reacts with CO to form CO_2 and protons. But when CO concentration is higher than 100ppm and oxygen injection less than 2%, Ru cannot complete oxidize CO and poisons Pt catalyst. They suggested that a Ru filter be placed in font of and adjacent to Pt:Ru alloy incorporating with proper oxygen injection to achieve an optimal CO tolerance.

Lee et al. [10] experimentally studied the CO tolerance of Pt/C, PtSn/C and PtRu/C electrocatalysts in PEMFCs. In order to investigate CO and hydrogen reaction mechanism on three types of catalyst, they changed operation temperature and CO concentration to do the tests. They proposed that CO adsorption step would change for different catalyst component. For PtRu/C and Pt/C catalysts, CO adsorption step would through a free site attack path and for PtSn/C catalyst, it would through a displacement path. There are two types of bonded adsorbed CO on catalyst. PtSn/C and PtRu/C $(T \le 55°C)$ are linear bonded adsorbed. Pt/C and PtRu/C $(T \ge 70°C)$ are bridged bonded adsorbed. Lee used

cyclic voltammograms method (CV) to define CO onset oxidation potential on the catalyst. They found that this reaction occurs first for PtSn/C, followed by PtRu/C and finally for Pt/C. Increasing the operation temperature would lower onset oxidation potential. The onset reaction potential is very important to CO tolerance, but the kinetics of the CO adsorption process and thermodynamics conditions also affect CO tolerance.

Lee et al. [11] further analyzed these catalyst kinetic mechanisms by kinetic model analysis. They compared model predictions with experiment results and found that both bridge- and linear-bonded adsorbed CO appear on catalyst. For all catalysts, the CO oxidation initiates at bridge-bonded sites, and oxidation at linear-bonded sites only at high anode potential. Lee considered that the hydrogen oxidation reaction and the CO poisoning mechanisms were all the same in all catalysts. But the reaction kinetics of the CO oxidation/adsorption steps were changed by the following different catalyst alloys.

The use of alloyed catalysts is the most convenient method to improve CO tolerance because it does not introduce any additional procedures or hardware's. But it only can control poisoning effect under 10ppm CO concentrations. If CO concentration is higher, then it cannot improve cell performance. Therefore, the higher CO concentration requires additional procedure to bleed an oxidant into the anode fuel stream to oxidize CO. The bleeding oxidant can be air, oxygen and hydrogen peroxide. There are some literatures that study about bleeding oxidant.

Gottesfeld and Pafford [12] made a new approach to the poisoning problem in PEMFCS. They attempted to generate an oxidative surface environment at the anode Pt catalyst, so that CO_{ads} would be removed by oxidation to form CO_2. It was known that CO oxidation by oxygen at Pt catalyst the temperature needed was higher than 100℃ and PEMFC operation temperature was about 80℃. But when they injected oxygen into impure anode fuel stream, it could increase cell performance. So this new approach is useful to improve CO tolerance. When CO concentration was 100ppm, injection 2~5% oxygen could complete restored cell performance. The reaction is shown as follows:

$$O_2 + 2Pt \rightarrow 2O_{ads} \qquad (1\text{-}9)$$

$$CO_{ads} + O_{ads} \rightarrow CO_2 + 2Pt \qquad (1\text{-}10)$$

Gottesfeld [13] experimentally studied about injection oxygen technique further. This patent studied CO concentration ranged from 100 to 1000ppm. He found when CO concentration is 100-500ppm injection 2~6% oxygen can substantially restore cell performance. If injection oxygen levels are too high, it may cause decrease in cell efficiency. Because the remaining oxygen chemically combusts with hydrogen to consume hydrogen from the fuel stream. It is very important to find proper oxygen ratio for different CO concentration.

Knights et al. [14] built an air-bleed system to investigate CO poisoning test. This system included a CO sensor, a sensor cell and one air-bleed meter. The sensor cell was more sensitive than that of test fuel cell, so it could find CO in the fuel stream earlier. If sensor cell voltage

lost than 100mV, then, air-bleed would introduce air to the fuel stream. The method could prevent from poisoning without wasting air. In the lower CO concentration (40ppm), this system might form a periodic or pulsed air-bleed. In this situation pulsed air-bleed would have better CO tolerance than average.

Murthy et al. [15] used commercial MEA to do CO test. They compared different GDL to find which one had better CO tolerance. They had different baseline data so they needed to define which one was better. In the steady-state test, it showed that injection of 5% air would almost completely recover the performance of the PEMFC at 500ppm CO. With 3000ppm CO, complete recovery is not achievable even with 15% air bleed. In the transient measurement, CO concentration would change with time. They considered that air bleeding technique will lower the CO poison rate and recover the cell performance substantially.

Murthy et al. [16] studied thermodynamic effect on CO tolerance. They still used the same commercial MEA to test, and changed cell operation temperature and backpressure. Raising the cell temperature from 70 to 90°C at 202kPa backpressure would increase performance with 500ppm CO. It might be due to a temperature dependence of the adsorption and the fact that this MEA has a large number of available catalytic sites. Increasing backpressure from 101kPa to 202kPa might have an increase in the permeability for both hydrogen and oxygen. When oxygen arriving to the anode side would oxidize CO and improve cell performance. In the transient measurements, they found that poisoning rates were substantially four times lower with an increase in pressure and fourteen times with an increase in temperature.

Zhang et al [17] studied the influence of anode flow rate and cathode oxygen pressure on CO poisoning. They used H_2/CO(100ppm) as the PEMFC anode fuel. The cell voltage decreases dramatically by increasing anode flow rate at a constant current density due to an increase of CO content in the anode chamber. And increasing flow rate would accelerate poisoning rate. They considered that increasing cathode oxygen pressure would cause diffusion through the membrane and improve CO tolerance. Increasing oxygen pressure with a thinner membrane would have a better effect to improve CO tolerance.

Bellows et al. [18] studied the diluted H_2O_2 in the anode humidifier technique to increase CO tolerance. H_2O_2 would decompose into oxygen and water as it meets metallic walls in the humidifier. At 100ppm CO, the cell performance would almost restore with 0.75% H_2O_2 in the stainless steel.

Divisek et al. [19] considered that the addition of H_2O_2 to the humidification has advantages regarding the safety problem as comparing to mixtures of hydrogen and oxygen.

Carrette et al. [20] studied CO tolerance effect by a pulsing technique. The fuel cell was operated with hydrogen or hydrogen containing CO as fuel gas at the anode and hydrogen gas at the cathode. The cathode in this case acts as a reference for characterization of the anode process only. This technique made use of electrical pulses to increase the anode potential to which the CO was oxidized to CO_2. Using this technique, the catalyst surface was continuously cleaned and the loss of cell voltage was

lowest. The pulse height must adjust for each catalyst component with the specified CO oxidization potential. For each CO concentration, it has own optimum operation frequency.

Table 1.1 summarizes the literatures of CO tolerance on PEM fuel cells with different investigative schemes.

1.3 Scope of Present Study

The research mainly concerns on the improvement of PEMFC CO tolerance by using oxygen-bleeding technique. In the experiment, it will inject oxidant (air) into the fuel stream at anode and investigate if it has influence on CO tolerance of PEMFC. The reason for using air instead of pure oxygen in the oxygen-bleed test is the safety concern, of course, the former can be obtained directly from the atmosphere without extra cost for supply.

The present work is divided into three parts, as shown in Fig. 1.1. The first one is to define suitable CO poisoning test condition for PEMFC that include cell voltage and current density. In such test, it will fix different cell voltages or current density, respectively, to perform poisoning experiment. Then, it will determine which one (cell voltage or current density) has a better performance in CO poisoning test and find out the difference between these two methods.

The second part is to bleed air into anode fuel stream (H_2/CO), which contains CO at different concentrations (10.1, 25, 52.7ppm). At the beginning, it should first identify the cell baseline before poisoned, and then the steady state poisoned polarization curve before the application of

air bleed. The two sets of data will compare with the recovered performance obtained by air bleed. In this test, the experiments, either fixing the cell voltage or current density, are transient, and the cell performance will decay with the time. In the transient test, it can be further divided into two parts that are long- (30min.) and short-duration (3min.) poisoning, respectively. As the duration is reached, the air is injected into anode fuel stream. Then, it will determine the air injection rate for a given CO-concentration fuel stream that can effectively improve the CO tolerance and recover cell performance. Finally, the results from theses two specific times (30min. and 3min.) are compared with each other and a corresponding discussion will be given.

The third part is to use pure Pt catalyst to perform the CO poisoning tests with and without air-bleeding. The results will compare with the ones of Pt alloy catalyst.

CHAPTER2

EXPERIMENTAL APPARATUS

The experimental apparatus are set up in the Energy & Resources Laboratories of the ITRI (Industrial Technology Research Institute). It is the sole fuel cell test/research center in Taiwan. The present study uses their apparatus to carry out this research and the corresponding experiments. The apparatus consists of two major elements, which are the fuel cell test station and the test sample of PEMFC. The above-mentioned elements are described in detail as follows.

2.1 Fuel Cell Test Station

This fuel cell test station consists of four components, which are the electronic load, MFC readout power supply, power supply, gas pipelines controller. Utilizing this system can change operation conditions, like temperature, humidification, flow rate, pressure, cell potential, etc, required by PEMFC performance evaluation. The schematic configuration is shown in Fig. 2.1. The elements of test station are described as follows.

2.1.1 Electronic Load

The electronic load uses the style of HP6060b. This DC electronic load is ideal for the test and evaluation of dc power sources and components, and is well suited for applications in areas, such as research and development, production, and incoming inspection. This load box

operation mode has constant current and voltage. It measures current range between 0 and 60 A. The maximum power output that load box can support is 300 watts. Electronic load can measure cell voltage and be used to control cell voltage and current. Eventually, it will consume cell power production in the test. The load box will display the cell performance on its monitor. The HP6060b load box is shown in Fig. 2.2.

2.1.2 MFC Readout Power Supply

The PC-540 MFC Readout Power Supply (Fig. 2.3) can display and control units for precision gas control in conjunction with MFCs. This apparatus has multiple channel instrumentation that it can completely control up to four MFCs at the same time.

In the present experiment, the flow rate controller will control three flow meters, which include anode gas, cathode gas and additional gas meter. These gas meters are anode (H_2), cathode (O_2 or air) and bleeding (O_2 or air), respectively.

2.1.3 Power Supply

This apparatus (Fig. 2.4) is a power source switch that provides power to each component in this test station. It includes mass flow controller, solenoid valve, heater (anode, cathode and cell), and three thermocouples plugs. In the power supply, it has three temperature controllers and monitors that the controlled temperature range is between 25 and 95℃. These temperature controllers will control anode, cathode humidity bottle and cell temperature that can change temperature by direct input buttons. When press power button, it will start all instruments of test station. On

the other hand, pressing power off will shut down all power.

2.1.4 Gas Pipelines Controller

The gas pipelines controller (Fig. 2.5) can manage what kind gas can feed into anode and cathode fuel stream. It also can control gas humidity, temperature, back pressure and flow rate. There are five gas inlets behind this apparatus that both anode and cathode have two gas channels respectively, the last one is nitrogen channel. The anode channels always feed with H_2 and reformation gas (H_2/CO). The cathode channels always feed with O_2 and air. On the operation board, it has anode and cathode globe valve, which can change the gas that test cell needs and can shut the valve that the gas cannot pass through it into the test sample. In addition to globe valve, there have three solenoid valves in the instrumentation. They are the safe valves. When this test station is in danger or overload condition, the solenoid valves will shut off anode and cathode gas channel and the other valve will open to purge nitrogen into test cell. Before fuel gas enters anode and cathode sides, it must go through humidity bottle first. This bottle will fill up water and has a heater and thermocouple inside that can heat the water when gas pass through it to increase the humidity of fuel gas before it enters the fuel cell. Finally, the board also has two adjust pressure valves that can change outlet backpressures for both anode and cathode fuel streams.

2.1.5 Liquid-Gas Separator

After fuel gas passes through test cell, there will have some remnant gas and water discharged from the cell fuel outlet. If there is too much water in the waste gas channel, then it will prevent remnant gas from

entering into the atmosphere. Therefore, it must enter a liquid-gas separator first so that the water can be kept in a bottle and only let the gas go out. Then the waste gas will discharge to the atmosphere by an exhaust fan.

Finally, the photo of complete test station is shown in Fig. 2.6. In this photo, each apparatus from top to bottom is MFC readout power supply, electronic load, power output, gas pipelines controller and liquid-gas separator, respectively.

2.2 Test Sample of PEMFC

The PEMFC has six major components, which include MEA (membrane electrode assembly), GDL (gas diffusion layer), gasket, gas flow channel and current collector. The MEA (Fig. 2.7) is Gore's commercial product, PRIMEA series 5561 MEA. The membrane in the middle has a thickness of 35 μm and catalyst loads are of 0.45 mg/cm^2 Pt alloy on the anode and 0.6 mg/cm^2 Pt on cathode. The active area of the membrane is 25 cm^2 and the border area is 100 cm^2. The GDL (Fig. 2.7) used in the experiment is CARBEL CL GDL and its thickness is of 0.4 mm. The Ucar carbon is used as the material of flow field channels. It will be processed serpentine flow channels (Fig. 2.8) on the carbon board. These flow fields consist of 26 equally spaced channels of 1 mm width, 1 mm height and 1mm width. The current collector (Fig. 2.9) composes of copper plating gold. This current collector board can conduct electric current from test cell. The end plank (Fig. 2.10) is made by nickel-plating steel, used as fixing and protecting this fuel cell structure. The

dimensions of carbon board, current collector and end plank all are 100 mm $\times$ 100 mm.

Fig. 2.11 shows each constituting component of PEMFC. There is a sequence to compose a cell. The MEA is always in middle of the cell and both anode and cathode electrode have a GDL. In the outer circle of GDL, it places a gasket (Fig. 2.7) to prevent the gas leakage to environment. This composing sequence is shown in Fig. 2.12. Finally, this PEMFC test sample is shown in Fig.2.13.

2.3 Test conditions

The experimental conditions for these tests are fixed. The fuel flow rates of anode and cathode are calculated from the theoretic volume, which can produce one ampere of current. They are 7.6 and 3.8cc/min/Amps for hydrogen and oxygen, respectively. Then, for the anode, it is multiplied by the stoichiometry of 1.37 to obtain a value of 10.4 cc/min/Amps), whereas for the cathode, it is 1.84 to get 7 cc/min/Amps. This can guarantee the fuel flow rate being sufficient to initiate the electrochemistry reaction. The reason for the cathode stoichiometry higher than the anode one is the lower oxygen activity to reaction. The fuel cell temperature always fixes at $65^{o}C$. The pressures at the outlet of fuel stream for both anode and cathode are 101kPa. The humidification temperatures are $80^{o}C$ and $70^{o}C$ for anode and cathode fuel streams, respectively. These temperatures can let fuel possess enough humidity to crossover membrane and obtain the optimum cell performance with a cell temperature of $65^{o}C$.

2.4 Procedure of the Experimental Operation

1. Connect all lines of test station with fuel cell before the experiment. For instance, connect potential sensors to the anode and cathode current collectors; connect positive pole loading line to the cathode current collector. On the other hand, connect anode with negative pole, insert the heater into the end plank hole, insert the thermocouple into the carbon board hole, and connect pipelines to the fuel cell.
2. Add the water to the humidification bottle by the atmosphere style water bottle.
3. Open the valves of H_2, O_2, N_2 and H_2/CO fuel cylinders and retain the inlet pressure up to 80 psi.
4. Turn on the globe valves of the gas pipelines on the controller operation board; anode side turns to H_2 or H_2/CO pipeline, cathode side turns to O_2 pipeline.
5. Turn on the power source of the exhaust fan. Because this laboratory is in the airtight space and the experimental gases contain CO and H_2, so it is a necessary procedure.
6. Check if any fuel gases leakage from pipeline's connection by applying suds on them. It is a very important procedure, especially for the uses of CO and, H_2.
7. Push down the power button of the test station to star this system.

8. Activate the software of the test system.
9. Set the minimum fuel flow rate and the flow rate per ampere current of anode and cathode. The minimum flow rates of anode and cathode are 104cc/min and 70cc/min, respectively, and the flow rates per ampere current are 10.4cc/min/Amp and 7cc/min/Amp, respectively.
10. Set anode and cathode humidification temperature.
11. Push down the gas reset button on the power supply board. At the same time, solenoid valve will shut off N_2, which stops to purge the fuel cell.
12. Push down the applying fuel icon of software window. Now, anode and cathode fuel pipeline solenoid valve will open and the fuel gas is fed into fuel cell.
13. Set the cell temperature to star the cell heater as the humidification temperature is up. It is to protect MEA from drying to damage the MEA.
14. Push down the “apply load” icon of the window that the electronic load will start loading from the test sample as the OCV (open-circuit voltage) reaches the steady value.
15. Set the same cell overpotential to activate the test fuel cell. In general, a new cell needs to activate several hours until it achieves optimum or steady performance.
16. Define proper CO poisoning test condition for PEMFC that include cell voltage and current density for the first part of the present study.

17. For the second and third parts, hold the same cell potential to record current-time curve. At first, feed pure H_2 as the anode fuel, then observe the current change by transferring the fuel to H_2/CO mixed gas.
18. Then inject air into anode fuel stream by the equivalent or periodic method; or change fuel gas back to the pure H_2 to observe current recovery rate.
19. In present study, replace CO concentration of the anode fuel and try different air bleeding ratio or frequency. Repeat the procedure from (17)-(18) steps.

CHAPTER 3

UNCERTAINTY ANALYSIS

All of the data from experimental results may not be equally good to adopt. Their accuracy should be confirmed before the analyses of experimental results are carried out. Uncertainty analysis (or error analysis) is a procedure used to quantify data validity and accuracy [21]. Errors always are presented in experimental measuring. Experimental errors can be categorized into the fixed (systematic) error and random (non-repeatability) error, respectively [21]. Fixed error is the same for each reading and can be removed by proper calibration and correction. Random error is different for every reading and hence cannot be removed. The objective of uncertainty analysis is to estimate the probable random error in experimental results.

From the viewpoint of reliable estimation, it can be categorized into single-sample and multi-sample experiments. If experiments could be repeated enough times by enough observers and diverse instruments, then the reliability of the results could be assured by the use of statistics [22]. Like such, repetitive experiments would be called multi-sample ones. Experiments of the type, in which uncertainties are not found by repetition because of time and costs, would be called single-sample experiments.

3.1 Analyses of the Propagation of Uncertainty in Calculations

Uncertainty analysis is carried out here to estimate the uncertainty levels in the experiment. Formulas for evaluating the uncertainty levels in the experiment can be found in many papers [22, 23] and textbooks [21, 24 and 25]. They are presented as follows:

Suppose that there are n independent variables, $x_1, x_2, \ldots, x_n$, of experimental measurements, and the relative uncertainty of each independently measured quantity is estimated as u_i. The measurements are used to calculate some experimental result, R, which is a function of independent variables, $x_1, x_2, \ldots, x_n$; $R = R(x_1, x_2, ..., x_n)$.

An individual x_i, which affects error of R, can be estimated by the deviation of a function. A variation, δx_i, in x_i would cause R to vary according to

$$\delta R_i = \frac{\partial R}{\partial x_i}\delta x_i . \tag{3-1}$$

Normalize above equation by dividing R to obtain

$$\frac{\delta R_i}{R} = \frac{1}{R}\frac{\partial R}{\partial x_i}\delta x_i = \frac{x_i}{R}\frac{\partial R}{\partial x_i}\frac{\delta x_i}{x_i} \tag{3-2}$$

Eq. (3-2) can be used to estimate the uncertainty interval in the result due to the variation in x_i. Substitute the uncertainty interval for x_i,

$$u_{R_i} = \frac{x_i}{R}\frac{\partial R}{\partial x_i}u_{x_i} \tag{3-3}$$

To estimate the uncertainty in R due to the combined effects of uncertainty intervals in all the x_i's, it can be shown that the best representation for the uncertainty interval of the result is [23]

$$u_R = \pm\left[\left(\frac{x_1}{R}\frac{\partial R}{\partial x_1}u_1\right)^2 + \left(\frac{x_2}{R}\frac{\partial R}{\partial x_2}u_2\right)^2 + ... + \left(\frac{x_n}{R}\frac{\partial R}{\partial x_n}u_n\right)^2\right]^{1/2} \tag{3-4}$$

3.2 The Analysis of CO Concentration

In the present experiment, it will discuss the poisoning influence with the lower CO concentrations, which are 50, 25 and 10ppm, respectively. The SAN FU GAS company provides the specific H_2/CO mixing gases according to the experimental requirements. It analyzes these gases by using the GC-DID method so that the accurate value of CO concentration contained in the H_2 gas can be ensured. These concentrations are 52.7, 25 and 10.1ppm, respectively. Finally, these mixing gases are stuffed into the steel cylinders by the high pressure of 120 Kg/cm^2.

3.3 The uncertainty of test station apparatus

The apparatus must correct with other standard instruments to make sure that it can normally operate and let the inaccuracy of the experimental result reduce to the minimum. However, the test apparatus used in present experiment are in the Energy & Resource Laboratories of ITRI and they have been corrected by their own researchers periodically.

(1) The uncertainty of HP 6060B electronic load: u_V, u_A

The HP 6060B electronic load in the test station had corrected its potential and current meter before experiment. The research uses FLUKE 8060A Digital Multimeter and Chroma Smart N300-040 Electronic Load to correct HP load box. These correction instruments had corrected by the Center for Measurement Standards of ITRI. At the beginning, set the

potential of the load box and the readout value will show on its monitor. Then, use FLUKE digital meter to measure the actual potential. If the inaccuracy of potential is lower than $\pm 2\%$, it can consider the load box being normal. In Table 3.1, it shows the error for different potentials. The standard value is the load box readout, whereas the digital value is the actual measured value.

Next, the researchers correct the DC current meter of HP load box. They use Chroma Smart electronic load and FLUKE digital meter to find the impedance of the shunt. After that, they connect the shunt between HP load box and DC power source. And adjust different potentials of power source so it can change the measurement current of load box meter. At the same time, the shunt will measure a signal of current. After converting this signal, it can define the actual current of this circuit. In Table 3.2, it shows the error for different current. The conversion value is the actual current, the other is load box measurement value.

(1) The uncertainty of mass flow controller

In this study, there have three MFCs in this test station that includes anode, cathode and oxygen bleeding flow meter. The researchers correct these MFC according to MFG handbook. The specified error is shown as follows:

$$ERROR(\%) = CALAUATED - TARGET \Big/ FULLSCALE \times 100\%$$

The ranges of MFC specified accuracy are $1000 \pm 5\%$ with anode MFC, $2000 \pm 5\%$ with cathode MFC and $500 \pm 1\%$ with bleeding MFC. They use the same company instrument, series 5850 MFC, as the standard correction apparatus to correct these MFCs. The results are listed in next

three tables (Table 3.3, 3.4, 3.5). They are anode, cathode and air-bleeding flow meter respectively. In these tables, the standard value means the setting flow rate, the Brooks MFC read value means the test station MFC readout value, the measurement value is the actual measured value. Then, these data can define the errors in different flow rates.

(2) The uncertainty of temperature controller

The correction standard is base on MFG handbook. They use the standard temperature controller, corrected by the Center for Measurement Standards, as the correction apparatus. The error of this must be lower than 5%. There are three temperature controllers in the test station. They include anode, cathode humidifier and fuel cell, respectively. The results of analyses are listed in Table 3.6, 3.7, 3.8. In these tables, standard value means the setting temperature and the measure value means actual value, measured by the correction apparatus.

3.4 The Experimental Repeatability

In general, the life of the commercial MEA is about 300hr, so the fuel cell performance will decline with an increase of test time. Because CO makes anode catalyst decaying and ageing in the poisoning test, the life of fuel cell is expected to be shorter. In order to improve the cell CO tolerance, it uses air-bleeding technique as the CO oxidant to remove the adsorbed CO from catalyst surface. However, the major amount of O_2 will react with H_2 to form water and resultant reaction heat is quite high. This is the other factor that may cause anode catalyst decay. Therefore, it must complete experiment as quick as possible to reduce the time effect,

which influences the experiment results. Due to these factors, it is difficult to the perform repeatability test. In order to confirm the accuracy and confidence of the experiment, the cell performance must recover to the base performance before it carries out the next poisoning experiment. The present experimental works can be divided into three parts, therefore, there are three test samples available to perform tests. The repeatability of baseline performances is shown in Table 3.9, 3.10 and 3.11, which correspond to each part's sample. However, these data are too many to list, so it only shows the three average performances to determine the error.

CHAPTER 4

RESULT AND DISSCUSSION

The test results of air-bleeding experiments are given and discussed in this chapter. They include two scenarios, which one is to fix cell voltage and the other is to fix current density, to carry out CO poisoning tests, respectively, to identify which one has a better CO tolerance. After that, it will discuss the timing effects of air bleeding into the CO poisoning tests under the case of fixed current density. They consist of the long- (30min) and short-duration (3min) poisonings, separately, and the results from theses two specific durations are compared with each other. Finally, the effects of using two different catalysts, Pt and Pt alloy, on CO poisoning tests with and without air-bleeding are discussed.

4.1 Poisoning Effects of Fixed Cell Voltage and Current Density

First, the test samples of fuel cell are fixed at two specific conditions to perform the transient CO poisoning experiments. One is to fix the voltage, the other is to fix the current density. In the former condition, the voltages are fixed at 0.5, 0.6, 0.7V, respectively, whereas the current densities are fixed at 600, 1000, 1200 mA/cm^2, respectively, in the latter one. In these tests, the anode is fed by pure hydrogen in the first 5min., then, it is changed to H_2/CO, where the CO concentration is specified as 52.7ppm. The cell performance will be varied with time. The

poisoned polarization curves are determined as soon as the performance subjected to CO poisoning reaches a steady state.

The results of transient experiments, whose cell potentials are fixed at 0.5, 0.6, and 0.7V are shown in the Fig. 4.1. In general, it can be found when fuel is changed to H_2/CO, the cell performance of resultant current density decays very quickly. It is because that fuel cell operation temperature is always maintained between 65^oC and 85^oC, in this range, CO has a stronger adsorbability with Pt catalyst than that of H_2. In other words, it will take over the active site of catalyst when CO presents in reaction chamber. Therefore, the less active site of catalyst is available for the hydrogen reaction that reduces the cell performance.

In Fig. 4.1, the current density declines from $735\,mA/cm^2$ (pure H_2) to a stable poisoned current $370\,mA/cm^2$ after 65min in the case of 0.7V. As the cell voltage fixes at 0.6V, the current density decreases from $1460\,mA/cm^2$ (pure H_2) to $530\,mA/cm^2$ after 40min. For 0.5V case, it declines from $2200\,mA/cm^2$ to $700\,mA/cm^2$ after 35min. From these observations, it is found that the performance decline rate becomes faster at the lower fixed cell voltage. The reason is that the lower cell voltage produces a higher current density, which requires higher fuel flow rate. Consequently, it results in a higher supply amount of CO, consequently, the accumulation and adsorbed rate of CO becomes higher in the reaction chamber. Finally, the competition of adsorbed reaction with Pt alloy catalyst between hydrogen and CO reaches to a balance state, defined as the steady state. The corresponding times for each fixed voltage to reach

steady state are mentioned above.

When the steady state is reached, the anode fuel is turned back to pure hydrogen and no CO exists in the fuel stream at all. Under this circumstance, the CO must be desorbed from catalyst surface by pure hydrogen or oxidized by the anode catalyst alloy. The recovery of cell performance almost simultaneously takes place as the fuel is turned back to pure hydrogen as shown in Fig 4.1. However, it can only recover to about 80 percentage of the original performance after 30min of purging pure hydrogen, indicating that there is a lot of CO still adsorbed on the catalyst and cannot be removed completely.

Figure 4.2 shows the baseline polarization curve, the poisoned and recovered polarization curves with different poisoning conditions (0.5, 0.6 and 0.7V). In this figure, it is significant to find that for a given concentration of CO (52.7ppm) the resultant steady state poisoning polarization curves are almost coincident no matter the applications of different fixed cell voltage in these transient tests, which the cell operations and fuel humid temperatures are the same. It implies that under a given CO concentration, the hydrogen and CO adsorption reactions to the Pt alloy catalyst have a fixed balance state, or a constant polarization behavior. The only difference is the duration to reach the steady state.

In Fig. 4.2, it also shows that the recovery rate after purging the pure hydrogen is faster for the case of lower cell voltage (V) in the transient tests. The similar reason for poisoning effect has been given in the discussion of Fig. 4.1. The cell at the lower voltage gains a higher current density, which requires the higher fuel flow rate. The higher rate

may accelerate CO desorption from catalyst. The other reason is that the fuel cell at low voltage can force CO to proceed oxidation reaction to remove itself from catalyst. Therefore, the transient experiment at a lower fixed voltage, such as 0.5V, can get a better recovered rate (more than 85%) in the Fig. 4.1. This explains why the different polarization behaviors show up in recovered performance with different transient poisoned conditions (0.5, 0.6 and 0.7V).

Next, the transient poisoning tests are performed at different fixed current densities. In Fig. 4.3, it shows three cell voltages transient curves, which the corresponding fixed current density are 600, 1000 and 1200 mA/cm^2, respectively. In this case, the cell performance, expressed as cell voltage, decays very fast when H_2/CO (52.7ppm) fuel stream is introduced into anode. It can cause a rise of anode potential, relatively, a decrease in cell potential because CO adsorption reduces the catalyst active site. Finally, the performance subjected to CO poisoning reaches to a steady state as shown in Fig.4.3. The cell voltage for a fixed cell current density of 600 mA/cm^2 decays from 0.725V to a stable voltage 0.55V when anode fuel contains 52.7ppm CO after 50min. The one fixes at 1000 mA/cm^2, the voltage decays from 0.662 to 0.410V after 45min and the one at 1200 mA/cm^2 decays from 0.632 to 0.355V after 30min. It can find that the higher fixed current density can result in a faster poisoned rate. The reason is same as that in Fig. 4.1.

There exists a different phenomenon between the fixed cell voltage case and current density one in the transient tests. In the fixed current density transient test, the cell voltage shows the oscillation sometimes

when the poisoning performance reaches a balance condition as shown in Fig.4.3, whereas no such phenomenon happens in Fig. 4.1. The CO adsorption can raise anode potential and the higher current density causes a higher anode potential. These effects quickly reach to CO onset oxidation potential and lead CO to be removed from catalyst locally, which results in a bit of cell voltage recovery. The CO adsorption and oxidation reaction form a repeated influence to each other and this interaction causes the voltage oscillation.

In Fig. 4.4, it shows the baseline polarization curve, the poisoned and recovered polarization curves with different poisoning conditions (600, 1000 and 1200 mA/cm^2). It can observe that a better CO poisoned tolerance performance can be obtained when cell is fixed at higher current density (1200 mA/cm^2) to perform the transient test. In this situation, the CO poisoned phenomenon is indicated by the decrease of cell voltage. The CO poisoning effect always makes anode potential rising and causes overall cell performance to decline. However, CO on the catalyst surface can perform oxidative reaction if the anode potential rises to the CO onset potential of oxidation. In the literature [10], it indicated that the onset of CO oxidation with Pt alloy catalyst occurs when anode potential is about 0.2V. The higher anode potential, greater than 0.2V, can raise CO oxidation rate in a specific range. In Fig. 4.3, it can calculate the rise of stable anode potential under 52.7ppm of CO in different current density conditions, such as 600, 1000 and 1200 mA/cm^2. They are 0.175, 0.252 and 0.277V, respectively. The higher anode potential cause more CO removed from catalyst surface and obtain a better CO tolerance. Therefore, the transient condition with 1200 mA/cm^2

has the best steady poisoned polarization performance as shown in Fig. 4.4. On the contrary, the transient poisoned condition of fixed cell voltage may limit the change of anode potential. Therefore, it cannot oxidize CO from catalyst surface in the stable poisoned state. The stable values of CO adsorption are the same for any transient conditions (0.5, 0.6 and 0.7V), and the steady poisoned polarization behaviors are almost coincident to each other.

In Fig. 4.5, it shows the anode polarization curves obtained from the poisoned polarization curves in Figs. 4.2 and 4.4. At first, it should describe the polarization behaviors with pure hydrogen fuel; no CO poisoning. The typical polarization behavior, fed with pure hydrogen, for fuel cell is shown in the baseline curve of Fig. 4.2 and 4.4. There are three main effects that cause cell potential to drop. They are the kinetic losses, ohmic losses and mass transport limitations [26]. The initial fall is associated with the poor electrode kinetics at a voltage close to the rest voltage. This sharply sudden drop is due to the sluggish kinetics of the oxygen reduction reaction. As the current density rises, the cell potential varies nearly linearly with current density. It is mainly due to ohmic and mass transport losses in solution between electrodes. The anode overpotential can be neglected when anode is fed with pure hydrogen. So, the cell potential drop in the typical polarization curve can be treated as the drop of cathode potential. The anode potential is calculated from the difference between the cell potential with pure hydrogen and the one with H_2/CO at the same current density. Then, the polarization curve is obtained from the collection of anode potentials

for all of current densities. In Fig. 4.5, it can observe that the rising rate is smaller with a higher current density in the transient poisoning test. The higher fixed current density can force anode potential to rise to the value above onset one of CO oxidation and, then, to remove CO from catalyst surface. Therefore, it causes a better CO tolerance, which has a lower anode potential slope. On the other hand, in the transient condition of $600\,mA/cm^2$, its anode potential slope is higher than the others (1000, $1200\,mA/cm^2$). It is because that the anode potential only rises to 0.175V in the stable poisoned state when the current density is fixed at $600\,mA/cm^2$. This resultant potential is lower than the onset potential of CO oxidation, so it cannot improve CO tolerance.

In the transient test of fixed cell voltage, the discrepancy among the stable poisoned polarization curves with different poisoning conditions is insignificant. The anode polarization curves are more or less the same in this case. Its potential slope is higher than the one in fixed current density case (1000, $1200\,mA/cm^2$). It can conclude that changing cell current density to a higher value can improve CO tolerance, whereas it cannot change the stable poisoned polarization behaviors in the transient experiment of fixed cell voltage.

4.2 Effect of Air-Bleeding Timing

In this case, it will investigate the effect of air-bleeding on CO tolerance improvement. The parameters are the specific air-bleeding timings, after which the air is injected into anode poisoned fuel stream, and the CO concentration. Two timings (3min. and 30min.) and 3 CO

concentrations (10.1, 25 and 52.7ppm) are selected. The current density is fixed at 800 mA/cm^2.

4.2.1 Long Duration Poisoning (30min)

In the present experimental work, it discusses the effect of CO concentrations on the performance of PEMFC. In order to determine the influence on CO tolerance by using air-bleeding technique, it should obtain the stable poisoned cell performance as the base line first without air-bleeding. In Fig. 4.6, three transient curves under fixed current density at 800 mA/cm^2 are obtained by performing the poisoning tests with three CO concentrations (52.7, 25 and 10.1ppm). Remind that the fuel streams are pure hydrogen at the first 5min. in all transient tests, after that, the streams are changed to H_2/CO ones with specified CO concentration.

In this figure, the initial cell voltages for all tests are the same (0.701V) at the first 5min due to no CO poisoning. In the transient experiments, the cell voltage decays with the time when CO is contained in the anode fuel stream. The transient curve declines to the steady potential of 0.417V with 52.7ppm CO that spends only 40min. With 25ppm of CO, it takes 85min to achieve the steady poisoned potential of 0.476V. It needs over 3.5hr to get the steady state potential of 0.588V when the anode fuel stream contains 10.1ppm of CO. It can be seen that the higher CO concentration, the faster poisoning and cell voltage decay rates. The higher CO concentration has a greater probability to attack the active site on the catalyst surface and cause more serious CO poisoning effect. In the curve of 52.7ppm CO, it shows a potential

oscillation after reaching the steady poisoned potential. The anode potential may be up to the onset potential of CO oxidation in this situation. Therefore, it can cause some CO desorption from catalyst surface and let cell voltage have a sudden recovery. The interaction between adsorption and desorption makes the cell to form an oscillation. In the 25 and 10.1ppm CO curves, the anode potential can not reach up to the CO onset oxidation potential. Therefore, no cell voltage oscillation in the steady poisoned state is found. The anode poisoned fuel turns back to pure hydrogen when the transient curves decay to the steady state as shown in Fig. 4.6. After that, the cell voltage is recovered very quickly since CO is removed from catalyst surface by pure hydrogen. These cell performances recover to the value of about 0.675V after purging pure hydrogen for 30min.

In Fig. 4.7, it shows the steady polarization curves with different CO concentrations and the baseline performance curve, fed with pure hydrogen. It can be found that the higher CO poisoning concentration results in a lower cell power output. The cell power output declines to $0.22285 W/cm^2$ at 0.51V with 52.7ppm of CO. It is only 20% of the performance of baseline value ($1.1628 W/cm^2$). In the 10ppm of CO condition, the power output ($0.64111 W/cm^2$) decays to the half of baseline value at 0.51V cell potential. Even the anode catalyst uses the Pt alloy catalyst, it still cannot reduce CO poisoning effect significantly in many cases of only very little CO concentration. The polarization curves, after purging pure hydrogen for 30min, recover to 80% of the baseline performance at 0.51V.

The results by air-bleeding in the long duration poisoning (30min) with 52.7ppm of CO are shown in Figs. 4.8a and 4.8b. The long duration transient poisoning test introduces air into anode fuel stream after 30min. of CO poisoning application. The initial cell potential is 0.701V with a current density 800 mA/cm^2.

Fig. 4.8a is the cell voltage versus time. It shows the different cell voltage recovery curves with different air-bleeding ratio in anode fuel stream. It indicates that the cell potential is recovered very quickly when the air is introduced into fuel stream at 30min. The oxygen is absorbed by the catalyst (O_{ads}), then it can proceed the oxidation reaction with CO_{ads} to form CO_2. Therefore, CO is depleted from catalyst surface and the hydrogen can obtain more active sites to carry out the oxidation reaction. This makes anode potential to drop and recovers the cell potential. Apparently, air-bleeding technique can improve the CO tolerance for PEM fuel cell. In this case, air-bleeding ratios change from 2% to 8% in the transient tests. It is found that the recovery rate of cell performance increases with an increase of air ratio. The cell potentials recover to 0.681, 0.684 and 0.687V as the air-bleeding ratios are 2, 3 and 4%, respectively. Moreover, it takes about 15min after the injection of air into anode fuel stream to recover the cell potential to a steady-state value. There is an interesting phenomenon occurred in the transient curves. It can no long achieve a better performance of CO tolerance as the air ratio is over 4%. Apparently, the optimum air-bleeding ratio is 4% with 52.7ppm of CO poisoning. It is because CO adsorption and desorption by oxygen reach a steady state as air-bleeding ratio above

4%, and no more contribution can be made by adding more air.

In Fig. 4.8b, it continues changing air ratio until the air-bleeding condition gets to a steady state. The transient curve shows that the cell potential recovers to a constant value (0.687V) even the air ratio is raised to 8%. The major consumption of O_2 is used for H_2 oxidation reaction and just a little fraction is for CO oxidation reaction. Therefore, the excess of O_2 reacts with H_2 in the anode to produce H_2O or H_2O_2. On the contrary, the air-bleeding ratio above 8% may cause a decline in cell performance. The excess of O_2 lessens the amount of H_2, which can proceed oxidation with catalyst surface. On the other hand, the oxidation of H_2 with O_2 generates heat in the catalyst surface. The heat may destroy anode catalyst and cell membrane to cause a loss of cell performance. The air-bleeding technique is useful to improve the CO tolerance, however, a suitable air ratio is a more important factor.

In Fig. 4.9, it shows the steady polarization behaviors as a function of air-bleeding ratio after long duration CO (52.7ppm) poisoning condition. From these polarization curves, it can be seen that an increase of air ratio from 2% to 4% increases the cell performance. Comparing the recovered polarization curves using air-bleeding with the one without air-bleeding, it can be seen that a remarkable improvement of cell performance is achieved with this technique. The cell performance can recover to over 94% of baseline data at the same current density by using 4% of air-bleeding. Fig. 4.9 also shows the different performance recovery rates with various cell current densities. For example, the

recovery rate is 98% with 4% air-bleeding at 800 mA/cm^2 in the recovery polarization curve. However, the recovery rate declines to 94.3% at 2000 mA/cm^2 with respect to the baseline datum. At this current density (2000 mA/cm^2), the cell voltages of the baseline and recovery are 0.544V and 0.513V, respectively. This is because that the anode potential linearly increases with the cell current density and it causes the different recovery rate with various current densities. It also can be seen that the air-bleeding technique constrains the anode potential under 0.04V and prevents cell performance from decay under the 52.7ppm of CO poisoning.

Two more CO poisoning concentrations are considered in this long duration poisoning experiments. The experiment procedures are the same as the previous one. The resultant transient air-bleeding curves with 25 and 10.1ppm of CO poisoning are shown in Figs. 4.10 and 4.12, respectively. The corresponding steady-state recovery polarization curves with different air ratios are shown in Fig. 4.11 and 4.13.

In Fig. 4.10.a, it can observe a large discrepancy of cell poisoning rates before and after air is introduced into anode fuel stream. The cell operation conditions are the same at the first 35min. It should make sure that the cell performance is completely recovered, then, it can perform the next transient poisoning test. So, the initial cell potentials are the same in all of transient experiments. The cell performance seems completely recovered on the surface. However, these transient tests are repeatedly performed and it may cause some irreversible and harmful reactions on the catalyst surface by CO poisoning that may lead to the different cell poisoning rate in different transient test. The results of transient

air-bleeding test are not changed by this drawback. It may reduce this drawback by increasing the duration between two consecutive transient experiments.

Figure 4.14 summarizes the recovered steady-state polarization curves by air-bleeding technique with different CO poisoning concentrations (52.7, 25 and 10.1ppm). It is found when the anode fuel stream, containing 10.1ppm of CO, is injected by 1.5% of air, it can obtain the optimum CO tolerance for fuel cell. Comparing with baseline polarization curve, it has over 97% recovery rate under the same current density. For the fuel stream with 25ppm of CO poisoning, injecting 3% of air to the fuel stream has the optimum CO tolerance, which has over 96% recovery rate from the baseline curve.

4.2.2 Short Duration Poisoning (3min)

In this section, it will study in the influence of air-bleeding in a short duration (3min) of CO poisoning. The experimental procedures are similar to the previous one. The only difference between these two cases is the poisoning duration. In the short duration transient test, the air is introduced into the anode fuel steam after 3min of CO poisoning. The air-bleeding ratio is tried from the higher value to low one in this case because the optimum air-bleeding ratio has been found for each CO poisoning concentration in the previous case.

The transient polarization curves are shown in Figs. 4.15a, 4.15b and 4.15c. Because the differences for various air-bleeding ratio conditions are quite insignificant, therefore, it only shows the optimum air ratio for each CO poisoning concentration in these figures. In Fig. 4.15, the initial cell potential of transient curves is fixed at 0.701V with current

density 800 mA/cm^2. It can be observed that the drop of cell voltage is quite small which is about 0.698 to 0.701V for each CO concentration after the short duration (3min) of poisoning in the transient experiment. After that the air is injected into the anode fuel stream. These reactants can reach the newly chemical reaction balance about 20min later. With 3% air-bleeding, it can obtain optimum CO tolerance when anode fuel contains 52.7ppm of CO. In this situation, the balance of cell potential is 0.693V with a current density 800 mA/cm^2 which can reach 98.9% of baseline performance as shown in Fig. 4.15.a. It only needs 1.5% of air-bleeding to have the best CO tolerance (0.696V) with 25ppm of CO poisoning and the balance potential can recover to 99.3% of baseline datum as illustrated in Fig. 4.15.b. Due to the limitation of air-bleeding flow meter, the flow rate cannot be less than 1% of full capacity (500cc/min). For 10.1ppm of CO poisoning condition, it may need to try the air-bleeding technique by using periodic mode in order to find the optimum air-bleeding ratio. In the periodic mode of air-bleeding test, the cycle is 15s (sec) and the air-bleeding duration is 10s in a cycle. However, it only needs 1.5% periodic air-bleeding to get the best CO tolerance (0.6965V) in the short duration transient poisoned test as shown in Fig. 4.15.c.

Fig. 4.16 shows the resultant polarization curves with air-bleeding technique after short duration CO transient test to reach the steady state. In this figure, it can be observed that the CO tolerance can be improved effectively if the air can be introduced into anode fuel stream in the initial poisoning stage (3min). The cell performances can be recovered over 97% of baseline curve at the same current density. In the lower CO

poisoning concentrations (10.1, 25ppm), the effect of CO poisoning can almost be cleared by using the air-bleeding technique.

4.2.3 Effect of specific poisoning duration

In last two cases, it performs the transient CO poisoning experiments with different air-bleeding introducing timings (30 and 3min). With air-bleeding, the fuel cell has a larger CO tolerance and reduces effectively the performance dropping due to CO poisoning. It now discusses whether the introducing timing of air into anode fuel stream can cause the different CO tolerance of fuel cell. Tables 4.1, 4.2 and 4.3 show the summary data from the transient CO poisoning experiments with two different specific times. The current density is fixed at 800 mA/cm^2 in the transient test. The specific time means the air-bleeding timing, the reference potential (V_{ref}) the initial potential of every transient test, V_{spe} the cell potential after specific poisoning duration and recovery potential (V_{re}) the steady recovery value of cell voltage by air-bleeding technique. In these tables, it can be seen that the shorter duration time (3min) only needs a lower air-bleeding ratio to get optimum CO tolerance. With 52.7ppm of CO, the optimum air ratio is reduced from 4% to 3%. With 25ppm of CO, the optimum air ratio is reduced from 3% to 1.5%. It only needs 1.5% of periodic air-bleeding when anode fuel contains 10.1ppm CO. In addition, it has the better cell performance for the recover rates in short duration poisoning transient test. For the longer poisoning duration (30min), it causes more CO accumulating in the anode reaction chamber. Therefore, the less active sites of catalyst are available because it is attacked by CO with long

duration CO poisoning. So, it has a lower probability for adsorption reaction of O_2 the with catalyst surface when air is introduced into the anode fuel stream, consequently, the oxidation reaction rate of CO and O_2 becomes very slow. It must introduce the higher air-bleeding ratio to achieve the optimum CO tolerance after the long poisoning duration. On the other hands, the catalyst surface has more active sites after short duration poisoned (3min). In this situation, O_2 has a higher probability to be adsorbed on the catalyst surface to react with CO to form CO_2. The faster reaction rate between O_2 and CO causes the higher utility rate of air-bleeding. So, it only needs a lower air-bleeding ratio to get optimum CO tolerance when air is injected to anode fuel at initial stage of CO poisoning test. The CO adsorption and desoprtion, which is removed by oxidation reaction with O_2, can reach a balance state eventually and the air introducing timing will cause the difference of this balance. O_2 has a faster reaction rate with CO in the short poisoning duration and it can reduce the adsorption rate of CO on the catalyst surface. H_2 can get more active sites to perform oxidation reaction. Therefore, the cell has a higher CO tolerance by using air-bleeding with earlier introducing timing in the CO poisoning tests. These are indicated in Tables 4.1, 4.2 and 4.3. It can conclude that air-bleeding timing is the important factor to CO tolerance and performance recovery rate in CO poisoning experiment. The comparisons of steady polarization curves with different specific poisoning durations in transient experiments are

shown in Figs. 4.17, 4.18 and 4.19. The concentrations of CO poisoning in Fig. 4.17, 4.18 and 4.19 are 52.7, 25 and 10.1ppm, respectively. In these figures, it can be seen that the better recovery performance is with an earlier introducing timing (3min) of air-bleeding. However, the difference of recovery polarization behaviors between two specific poisoning durations is insignificant in the 10.1ppm of CO poisoning as shown in Fig. 4.19. Because the anode catalyst is made of Pt alloy, it can decrease CO poisoning effectively even with the long poisoning duration (30min). The poisoned potentials (V_{spe}) with different poisoning durations (3 and 30min) are shown in Table 4.3. It indicates that the difference of CO poisoning effect between two poisoning durations is very small (0.693, 0.701V). Therefore, the air-bleeding introducing timing does not change the balance of recovery rate very much in the lower CO concentration (10.1ppm). However, it becomes very important for the introducing timing of air-bleeding into anode fuel stream with the higher CO poisoning concentration (over 25ppm). The fuel cell can obtain a better CO tolerance with the earlier timing of air-bleeding in the CO poisoning experiment as shown in Fig. 4.17 and 4.18.

4.3 Effect of Different Catalyst Components

In this case, the effects of using different anode catalysts, which are pure Pt and Pt alloy, respectively, on CO tolerance are investigated. In the literature [4], it indicates that Pt alloy anode catalyst has a better CO tolerance for fuel cell. In generally, the anode catalyst for the

commercial MEA usually is Pt alloy and the cathode one is always the pure Pt. Because the activity of oxygen is lower than that of hydrogen, so, it needs a higher loading of Pt to perform reaction with catalyst. The Gore's commercial MEA is used as fuel cell sample in present CO poisoning study. The loadings of Pt alloy and pure Pt are 0.45 and $0.6\,mg/cm^2$, respectively, in this MEA. In present study, it uses pure Pt in anode catalyst to perform poisoning test. However, there is no such design in the existent commercial MEA. Therefore, the present work switches the cathode to anode and vice versa. Now, the cathode catalyst is Pt alloy and the anode one is pure Pt. Under this circumstance, the original baseline performance is expected to be different from the present one due to the different loadings. Therefore, it definitely causes the difficult to compare the CO tolerances directly for these two samples. However, we still try to find the relation and trend between these two cases from the results of CO poisoning tests with and without air-bleeding.

The procedure of CO poisoning tests are complete the same as the previous two sections. In the transient tests, the cell current density fixes at $800\,mA/cm^2$ and the anode is fed by pure hydrogen in the first 5min. then, it is changed to H_2/CO, where the CO concentration is specified as 52.7ppm. In the transient air-bleeding tests, the introducing timing of air is 35min.

Fig. 4.20 shows the transient curves with different anode catalysts, such as Pt alloy and pure Pt. In Fig. 20, the cell voltage declines very quickly when the CO contains in the anode fuel. The initial cell voltage

with anode catalyst of Pt alloy is 0.701V and the one with pure Pt anode catalyst is 0.657V. After switch, the cathode catalyst loading becomes 0.45 mA/cm^2, less than the original one, 0.6 mA/cm^2. The reduced loading causes the lower baseline performance and initial potential (0.657V) in transient test. In the original case with Pt alloy anode catalyst, it will reach a steady state after 45min in the CO poisoning test and the cell voltage is decayed to 0.417V (59.5%). In the switched case with pure Pt anode catalyst, it declines to a stable poisoned value of 0.303V (46%) after 47min. It can observe that the Pt alloy anode catalyst has a better CO tolerance and can reduce the decay rate of cell voltage as shown in Fig. 4.20. Also, it can reduce the CO adsorbability to Pt surface and causes an oxidation reaction of CO to remove it from Pt catalyst. Although the Pt alloy catalyst can improve CO tolerance in fuel cell, the reduction of CO poisoning effect is not so significant. Even using Pt alloy as anode catalyst, the cell performance has a substantial drop by 52.7ppm of CO poisoning, especially after a long duration poisoning. The anode fuel will be turned back to pure H_2 when the CO poisoning effect reaches to a steady state in transient experiment. From these transient curves in Fig. 4.20, it can observe that the cell voltage is recovered rapidly for both pure Pt and Pt alloy anode catalyst because purging pure H_2 can change the balanced poisoning state. The Pt alloy catalyst has faster cell voltage recovery rate after purging pure H_2 into anode fuel stream. In other words, Pt alloy catalyst can remove CO more effectively.

Fig. 4.21 shows the steady polarization curves includes the baseline,

poisoned and recovery performances with different anode catalysts. In this figure, the performance of baseline polarization curve with pure Pt anode catalyst is only 70% of that with Pt alloy one. The reason has been given previously. In Fig. 4.21, it also can find that the power output of poisoned polarization curve is very small with pure Pt anode catalyst. The cell current density is only 137 mA/cm^2 less than 10% of base performance (1744 mA/cm^2) when the cell voltage is 0.496V. The pure Pt catalyst cannot avoid the poisoning of CO because CO almost occupies the whole active sites on catalyst surface when CO poisoning effect reaches the steady state. The Pt alloy catalyst has a better CO tolerance comparing with pure Pt catalyst. However, it only can increase cell performance from 10% to 20% (437 mA/cm^2) with respect to the baseline datum (2280.8 mA/cm^2) at the cell voltage of 0.51V. There is an obvious recovery of cell performance after purging pure H_2 for 30min.

After that, it will discuss the CO tolerance by using air-bleeding technique with pure Pt anode catalyst. It has been verified that the air-bleeding technique can effectively improve fuel cell CO (52.7ppm) tolerance previously when the anode catalyst uses Pt alloy as shown in Fig. 4.8, 4.9.

Fig. 4.22 shows the transient curves with 52.7ppm of CO poisoning by using air-bleeding technique with pure Pt as anode catalyst. The procedure of this transient test is the same as that in the previous case. In this test, the CO of 52.7ppm is introduced into anode fuel stream at the time of 5min and the air is injected into anode at the instant of 35min.

From these curves, it can observe that the cell voltage is recovered quickly as air is injected into anode fuel stream. With 7% of air-bleeding, the cell has the optimum CO tolerance and the cell voltage can be recovered to 0.649V (98.8%) with current density $800\,mA/cm^2$ in the transient curve. In Table 4.4, it makes a summary of the transient test results, which can serve as a comparison between the Pt alloy and pure Pt anode catalysts. It shows that the air-bleeding can increase CO tolerance and improve cell performance no matter what kind anode catalyst is (pure Pt or Pt alloy). With Pt alloy anode catalyst, the cell voltage has optimum recovery rate of 98% when 4% air-bleeding is introduced into anode. However, the recovery rate can be further increased to 98.8% with 7% air-bleeding when the anode catalyst is pure Pt. It is because the loading becomes higher ($0.6\,mA/cm^2$) as pure Pt is used as anode catalyst, comparing with the original one ($0.45\,mA/cm^2$), it causes more adsorption of O_2 with Pt and more desorption of CO from Pt surface. Note that in this table, the resultant poisoning rates are different for these transient tests after the specific poisoning duration (30min). It was explained in the last section. However, the discrepancies among the poisoning rates are larger by using pure Pt as anode catalyst. It can be found a trend that the poisoning rate becomes greater as the number of continuous transient poisoned tests increases. The reason may be that the interval between two consecutive transient tests is too short and the catalyst features may have some changes after the repeat transient poisoning experiments. It is believed that the results of transient air-bleeding tests are not affected by this drawback.

Fig. 4.23 shows the steady polarization curves with different anode catalysts and the percentage of air-bleeding. Without air-bleeding, it is observed that the Pt alloy anode catalyst has a better CO tolerance than that of pure Pt catalyst. With air-bleeding, it can remarkably improve the CO tolerance for both Pt alloy and pure Pt anode catalysts.

CHAPTER5
CONCLUSIONS

This thesis consists of three parts. The first one is to experimentally investigate the transient CO (52.7ppm) poisoning test with fixed cell voltage and current density conditions, respectively. With fixed cell voltage to perform transient CO poisoning test, the anode potential is restricted to change. Therefore, the CO adsorption rates at anode catalyst with any voltage conditions reaches to the same steady-state values. So, the poisoned polarization curves under different cell voltages to do CO poisoning tests are alike. For the CO poisoning tests with fixed current density, using higher current density can increase cell CO tolerance. The higher current density can promote the anode potential to achieve the onset potential of CO oxidation that causes CO removed from Pt surface. The steady adsorption rate of catalyst is decreased following the rise of current density condition in the transient tests. Apparently, it can improve the cell performance, CO tolerance, by using this method.

The second one is to investigate the effects of air-bleeding with different introduced timing (3 and 30min) in the transient poisoning CO tests. The CO concentrations are 52.7, 25 and 10.1ppm, respectively. With the air-bleeding ratios of 4, 3 and 1.5% applied to each CO concentration, the fuel cell can obtain the optimum CO tolerance when the air-bleeding introducing timing is 30min. The steady recovery polarization behaviors can reach to 94, 96 and 97% of baseline performance, respectively, under the same current density. With the

air-bleeding ratios of 3, 1.5 and periodic 1.5% applied to each CO concentration, the cell can obtain the optimum CO tolerance while the air-bleeding timing is 3min in the transient experiments. With 3min air-bleeding timing, the steady recovery polarization curves can achieve over 97% of baseline performance for each CO concentration under the same current density. In this situation, the effect of CO poisoning is almost disappeared with lower CO concentration condition (25 and 10.1ppm). The air-bleeding is able to improve the fuel cell CO tolerance and recovery poisoned performance no matter what the air introducing timing. CO absorbed on catalyst surface reacts with injected O_2 to carry out the oxidation reaction, and it is removed from Pt surface to recover cell performance. The air-bleeding timing is very important factor for the cell CO tolerance performance. The optimum ratio of air-bleeding is decreased and the cell performance recovery rate is increased when the air-bleeding timing is short (3min). The adsorption ratio of Pt surface is lowered as the CO poisoning duration is shorter. In this situation, the injected O_2 has more chance to be adsorbed on the catalyst surface and then increase the reaction rate of O_2 and CO. Therefore, it costs a lower air-bleeding ratio to get better CO tolerance performance by a shorter air injecting timing.

The third one is to investigate the effect on the cell performance by using different anode catalyst component (Pt alloy and pure Pt) to perform the CO poisoning tests with and without air-bleeding. Without air-bleeding, the Pt alloy anode catalyst has a better CO tolerance comparing to the pure Pt anode catalyst. With the pure Pt catalyst, it

cannot reduce the CO (52.7ppm) poisoning effect and the power output is less than 10% of baseline datum at the cell potential of 0.5V. However, it is insignificant to increase cell CO tolerance by using Pt alloy anode catalyst. With air-bleeding, it can increase CO tolerance effectively no matter what kind anode catalyst (pure Pt or Pt alloy) is used to perform CO poisoning tests.

Finally, there are some suggestions for the future extensions of the present experiment. It could determine the life of a commercial MEA when CO is contained in the anode fuel stream. Also, the effect of air bleeding on the MEA life would be interesting since oxygen could cause the damage of MEA due to the heat generated from its reaction with hydrogen and the change of catalyst properties. Eventually, it might determine the fuel cell life that anode fuel is from reformer gas, which contains CO, and then it is subjected to air-bleeding.

REFERENCE

1. W. Nogel, J. Lundquist, P. Ross, P. Stonehart, Electrochim. Acta 20, pp.79 (1975).
2. R.M.Q Mello, E.A. Ticianelli, Electrochim. Acta 42, pp.1031 (1997).
3. H. P. Dhar, L. G. Christner, A. K. Kush, and H. C. Maru, Nature of CO adsorption during H_2 oxidation in relation to modeling for CO poisoning of a fuel cell anode, Journal of The Electrochemical Society, 134, pp.3021 (1987).
4. Watanabe M. and S. Motoo, Journal of Electroanalytical Chemistry, 63, pp.97 (1975).
5. Christoffersen E., P. Liu, A. Ruban, H. L. Skriver and J. K. Noskov, Anode materials for low-temperature fuel cells: A density functional theory study, Journal of Catalysis, 199, pp.123 (2001).
6. Watanabe M., H. Igarashi and T. Fujino, Design of CO tolerance anode catalysts for polymer electrolyte fuel cell, Electrochemistry, 67, pp.1194-1196 (1999).
7. H. A. Gastiger, N. Markovic, P. N. Ross Jr., E.J. Cairns, **CO** Electroxidation on Well-Characterized Pt-Ru Alloys, Journal of Physical Chemistry, 98, pp.617 (1994).
8. Hongmei Yu, Zhongjun Hou, Baolian Yi, Zhiyin Lin, Composite anode for CO tolerance PEMFC, Journal of power sources, 105 pp.52-57 (2002).
9. Andrew T. Haug, Ralph E. White, John W. Weidner Wayne Huang, Steven Shi, Narender Rana, Stephan Grunow, Timothy C. Stoner and Alain E. Kaloyeros, Using Sputter Deposition to Increase CO Tolerance in a Proton-Exchange Membrane Fuel Cell, Journal of The Electrochemical Society, 149 (7) A868-A872 (2002).
10. S. J. Lee, S. Mukerjee, E. A. Ticianelli, J. McBreen, Electrocatalysis of CO tolerance in hydrogen oxidation reaction in PEM fuel cells, Electrochimica Acta, 44, 3283-3293 (1999).
11. G. A. Camara, E. A. Ticianelli,S. J. Lee and J. McBreen, The CO poisoning Mechanism of the Hydrogen Oxidation Reacting in Proton Exchange Membrane Fuel Cells, Journal of The Electrochemical Society, 149 (6), A748-A753 (2002).
12. Shimshon Gottesfeld and Judith Pafford, A new approach to the

problem of Carbon Monoxide Poisoning in fuel cells Operating at Low Temperatures, Journal of The Electrochemical Society, 135, 2651-2652 (1988).
13. Shimshon Gottesfeld, Preventing CO poisoning in fuel cells, United States Patent, NO. 4,910,099 Date: Mar. 20,1990.
14. Knights et al., Method for operating fuel cells on impure fuels, United States Patent, NO: US6,500,572 B2 Date: Dec. 31, 2002.
15. Mahesh Murthy, Manual Esayian, Alex Hobson, Steve MacKensie, Performance of a Polymer Electrolyte Membrane Fuel Cell Exposed to Transient CO Concentrations, Journal of The Electrochemical Society, 148 (10), A1141-1147 (2001).
16. Mahesh Murthy, Manual Esayian, Woo-kum Lee and J. W. Van Zee, The Effect of Temperature and Pressure on the Performance of a PEMFC exposed to Transient CO Concentrations, Journal of The Electrochemical Society, 150 (1), A29-A34 (2003).
17. Jingxin Zhang, Tony Thampan and Ravindra Datta, Influence of Anode Flow Rate and Cathode Oxygen Pressure on CO Poisoning of Proton Exchange Membrane Fuel Cells, Journal of The Electrochemical Society, 149 (6), A765-A772 (2002).
18. R. J. Bellows, E. Marucchi-Soos and R. P. Reynolds, The Mechanism of CO Mitigation in PEMFC using Dilute H_2O_2 in the Anode Humidifier, Electrochemical and State Letters, 1 (2), 69-70 (1998).
19. J. Divisek, H. F. Oetjen, V. Peinecke, V. M. Schmidt and U. Stimming, Components for PEM fuel cell systems using hydrogen and CO containing fuels, Electrochimica Acta, Vol 43, NO.24, pp.3811-3815 (1998).
20. L. P. Carrette, K. A. Friedrich, M. Huber and U. Stimming, Improvement of CO tolerance of proton exchange membrane fuel cells by a Pulsing technique, Physical Chemistry Chemical Physics, 3, 320-324 (2001).
21. R. W. Fox and A. T. McDonald, Introduction to Fluid Mechanics, John Wiley and Sons, Canada, 1994
22. S. J. Kline and F. Mcclintock, Describing Uncertainties in Single-Sample Experiments, Mechanical Engineering, vol. 75, pp.3-8, 1953.
23. R. J. Moffat, Contributions to the Theory of Single-Sample Uncertainty Analysis, Journal of Fluid Engineering, vol. 104,

pp.250-260, 1982.
24. R. S. Figliola and D. E. Beasley, Theory and Design for Mechanical Measurements, 2nd Ed., John Wiley and Sons, Canada, 1995.
25. J. P. Holman, Experimental Methods for Engineers, 5th Ed., McGraw-Hill, New York, 1989.
26. A. Weber, R. Darling, J. Meyers and J. Newman, Handbook of Fuel Cells, Volume2 Fundamentals and survey of systems, pp.49, John Wiley & Sons (2003).

Table 1.1 Summary of investigation of CO tolerance on PEM fuel cells:

Catalyst:

Author	Investigation method	Parameter	Results	Remarks
Watanabe M. et al. **(4)**	Pt-Ru alloy catalyst	CO	Ru form RuOH, CO oxidized by RuOH to remove from catalyst	
Christoffersen E. et al. **(5)**	Used density functional theory to calculate dual metal catalyst surface characteristics and the corresponding CO adsorptive power	Pt-Ru dual metal catalyst	CO adsorbs on Ru of Pt-Ru alloy catalyst Decrease CO adsorbability with Pt surface	
Hougmei Yu et al. **(8)**	Composite anode: inner and outer catalyst	Inner: Pt, outer: Pt-Ru alloy	Outer catalyst improves CO tolerance Inner + outer catalyst has better performance to traditional Pt-Ru alloy catalyst	The ratio of inner and outer catalyst
Ralph E. White et al. **(9)**	Sputter deposition Ru on Pt surface Ru to form CO filter, Pt + Ru filter catalyst	100ppm CO, O_2 : 2%	With suitable O_2 -bleeding ratio, this has better CO tolerance	Pt-Ru alloy replaced Ru may better
J. Mcbreen et al. **(10)**	investigate CO and hydrogen reaction mechanism on three types of catalyst	Pt, PtSn and PtRu catalyst	CO adsorption step, form of CO bonded and onset potential of CO oxidation change with different catalyst	
J. Mcbreen et al. **(11)**	further analyzed these catalyst kinetic mechanisms by kinetic model analysis	Pt, PtSn and PtRu catalyst	both bridge- and linear-bonded adsorbed CO appear on catalyst, CO oxidation initiates at bridge-bonded, CO oxidation/adsorption steps change by different catalyst	

Table 1.1 Summary of investigation of CO tolerance on PEM fuel cells: (continuity)

Air-bleeding:

Author	Investigation method	Parameter	Results	Remarks
Shimshon G. et al. **(12)**	Inject oxidant of CO, oxygen-bleeding	CO: 100ppm O_2 : 2~5%	Injection 2~5% oxygen could complete restored cell performance (100ppm CO)	First literature of air-bleeding
Shimshon G. et al. **(13)**	oxygen-bleeding	CO: 100~1000ppm O_2 : 2~6%	2~6% oxygen substantially restore cell performance (100~500ppm), exceed O_2 cause performance decreasing	
Knights et al. **(14)**	Air-bleeding system by using a sensor cell Periodic air-bleeding	Air-bleeding timing: sensor cell voltage lost than 100 mV	prevent from poisoning without wasting air, pulsed air-bleed would have better CO tolerance than constant	
J. W. Van Zee et al. **(15)**	Compare with different GDL, transient poisoning test, air-bleeding	GDL: SSE, CARBEL CO: 500, 3000ppm Air-bleeding	With bleed: decay rate lower, recovery rate higher, 5% air improve CO tolerance effectively (500ppm)	GDL: cannot define which one is better
J. W. Van Zee et al. **(16)**	Discuss cell temperature and cathode backpressure, transient test	T: 70^oC,90^oC P: 101, 202KPa Air-bleeding	Increase T: decrease CO adsorbability and poisoning rate of forteen times Increase cathode backpressure: O_2 may crossover to anode and decrease poisoning rate of four times	

Table 1.1 Summary of investigation of CO tolerance on PEM fuel cells: (continuity)

Others:

Author	Investigation method	Parameter	Results	Remarks
Ravindra Datta et al. **(17)**	The effect of anode flow rate and cathode oxygen pressure	CO: 100ppm, fixed current density	flow rate ↑ :poisoning rate↑ , increasing cathode oxygen pressure would cause diffusion through the membrane and improve CO tolerance	The thick of MEA
R. J. Bellows et al. **(18)**	diluted H_2O_2 in the anode humidifier, decompose into oxygen and water	CO: 100ppm, 0.75% H_2O_2 in the stainless steel	At 100 ppm CO, the cell performance would almost restore with 0.75% H_2O_2 in the stainless steel	More safe then oxygen-bleeding
L. P. Carrette et al. **(20)**	pulsing technique to change anode potential	Cathode: reference electrode	the catalyst surface was continuously cleaned and the loss of cell voltage was lowest	pulse height: adjust for different catalyst

Table 2.1 Fuel cell operation conditions.	
Cell temperature	65℃
Humidification temperature	Anode: 80℃, Cathode: 70℃
Backpressure	Anode, Cathode: 1atm
Fuel flow rates	H_2: 10.4 cc/min/Amps O_2: 7 cc/min/Amps
Min. fuel flow rates	H_2: 104 cc/min/Amps O_2: 70 cc/min/Amps
Stoichiometry	H_2: 1.37, O_2:1.84
Case 1	
Feed stream	Anode: H_2, H_2 + CO Cathode: O_2
Transient conditions:	Fix cell voltage: 0.5, 0.6 and 0.7V Fix current density: 600, 1000 and 1200 mA/cm^2
CO concentration	52.7ppm
Case 2	
Feed stream	Anode: H_2, H_2 + CO, H_2 + CO + air-bleeding Cathode: O_2
Transient condition	Fix current density: 800 mA/cm^2
CO concentration	10.1, 25 and 52.7ppm
Air-bleeding timing	30 and 3min
Case 3	
Feed stream	Anode: H_2, H_2 + CO, H_2 + CO + air-bleeding Cathode: O_2
Transient condition	Fix current density: 800 mA/cm^2
CO concentration	52.7ppm
Anode catalyst	Pt alloy and Pt
Air-bleeding timing	30min

Table 3.1 Uncertainty of electronic load potential meter

Standard value (V)	Digital meter (V)	Uncertainty (%)
20.00	19.81	-0.95
9.95	9.85	-1.00
8.02	7.95	-0.87
6.04	5.95	-0.99
5.00	4.97	-0.60
3.03	3.00	-0.99
1.00	0.998	-0.50
0.00	0.00	0.00

Table 3.2 Uncertainty of electronic load current meter

Fluke digital meter (mV)	Electronic load (A)	Conversion value ($\overline{A}$)	Uncertainty (%)
0.00	0.00	0.00	0.00
1.69	1.00	1.02	1.96
5.05	3.00	3.04	1.32
8.37	5.00	5.03	0.60
16.71	10.00	10.05	0.50
25.04	15.00	15.06	0.40
33.41	20.00	20.09	0.45
50.21	30.00	30.19	0.63

Table 3.3 Uncertainty of anode MFC

Standard value (sccm)	Brooks MFC read value (sccm)	Measure value (sccm)	Uncertainty (%)
1000	1002	1001	-0.10
500	501	499.8	-0.23
250	250.2	249.7	-0.23
0	0	0	0

Table 3.4 Uncertainty of cathode MFC

Standard value (sccm)	Brooks MFC read value (sccm)	Measure value (sccm)	Uncertainty (%)
2000	1999.8	1999.4	-0.02
1250	1255	1253	-0.15
1000	1000.3	1000.2	-0.01
500	500.2	500	-0.03
0	0	0	0

Table 3.5 Uncertainty of air-bleeding MFC

Output Voltage	Brooks MFC read value (sccm)	Measure value (sccm)	Uncertainty (%)
5	500	500.34	0.07
3.75	375	374.54	-0.09
2.5	250	250.32	0.06
1.25	125	124.54	-0.09
-0.001	0.0	0	0

Table 3.6 Uncertainty of anode temperature controller

Standard value (℃)	Measure value (℃)	Uncertainty (%)
25	25	0
35	35	0
50	50	0
70	70	0
85	84	-1.17
95	94	-1.05
100	99	-1

Table 3.7 Uncertainty of cathode temperature controller

Standard value (℃)	Measure value (℃)	Uncertainty (%)
25	25	0
35	35	0
50	50	0
70	70	0
85	85	0
95	94	-1.05
100	99	-1

Table 3.8 Uncertainty of cell temperature controller

Standard value (℃)	Measure value (℃)	Uncertainty (%)
25	25	0
35	35	0
50	50	0
70	70	0
85	85	0
95	95	0
100	100	0

Table 3.9 The table of experimental repeatability for baseline performance (case 1)

Cell voltage (V)	Current Density (mA/cm^2) (1^{st} averaged)	Current Density (mA/cm^2) (2^{nd} averaged)	Current Density (mA/cm^2) (3^{rd} averaged)	Averaged value of three times (mA/cm^2)	Error (%)
0.948	0	0	0	0	0
0.889	18.8	18.8	19.3	18.96667	1.25
0.874	30.4	31.2	31.1	30.9	1.15
0.842	72.4	72.8	72.9	72.7	0.30
0.823	108.8	107.2	109.6	108.5333	0.92
0.796	202	191.2	202.9	198.7	2.68
0.779	271.2	264.4	271.2	268.9333	1.20
0.747	421.2	409.6	422.3	417.7	1.38
0.713	609.2	582.4	609.2	600.2667	2.10
0.698	724.4	700.8	724.8	716.6667	1.57
0.667	927.2	917.6	930.5	925.1	0.60
0.649	1046	1041.6	1055.2	1047.6	0.54
0.618	1243.2	1268	1273.3	1261.5	1.04
0.598	1378	1404.8	1394	1392.267	0.79
0.569	1626.8	1642.8	1609.1	1626.233	0.85
0.554	1748.4	1768.4	1737.3	1751.367	0.73
0.525	1990	1986.4	1986.4	1987.6	0.09
0.488	2215.6	2234.8	2231.2	2227.2	0.37

Table 3.10 The table of experimental repeatability for baseline performance (case 2)

Cell voltage (V)	Current Density (mA/cm^2) (1^{st} averaged)	Current Density (mA/cm^2) (2^{nd} averaged)	Current Density (mA/cm^2) (3^{rd} averaged)	Averaged value of three times (mA/cm^2)	Error (%)
0.948	0	0	0	-0.8	0
0.913	10.4	8.4	8.8	9.2	9.39
0.896	19.6	16.4	17.6	17.86667	7.39
0.864	48.8	42.8	46.4	46	5.36
0.833	112	101.6	109.2	107.6	4.08
0.815	160	147.6	157.6	155.0667	3.46
0.786	276.8	262.4	275.2	271.4667	2.37
0.769	361.6	344.8	360.4	355.6	2.15
0.737	530.4	513.6	532	525.3333	1.58
0.72	645.6	626.4	646.4	639.4667	1.45
0.686	851.6	833.6	855.6	846.9333	1.13
0.669	988.4	966	991.2	981.8667	1.15
0.64	1223.2	1204	1231.2	1219.467	0.96
0.61	1486.8	1464	1495.2	1482	0.89
0.591	1637.6	1606.8	1646.4	1630.267	1.04
0.559	1868	1852.4	1893.6	1871.333	0.91
0.544	2022	2000	2040	2020.667	0.81
0.51	2280.8	2242.8	2294.4	2272.667	0.96

Table 3.11 The table of experimental repeatability for baseline performance (case 3, Pt anode catalyst)

Cell voltage (V)	Current Density (mA/cm^2) (1^{st} averaged)	Current Density (mA/cm^2) (2^{nd} averaged)	Current Density (mA/cm^2) (3^{rd} averaged)	Averaged value of three times (mA/cm^2)	Error (%)
0.96	-0.8	-0.8	-0.8	-0.8	0
0.896	12	11.6	12.8	12.13333	4.11
0.864	31.6	31.6	35.2	32.8	5.17
0.85	49.6	49.6	55.2	51.46667	5.13
0.818	101.2	101.2	111.6	104.6667	4.68
0.798	142.8	140.8	156	146.5333	4.60
0.767	240.4	238	258.8	245.7333	3.78
0.752	306.4	303.6	328.4	312.8	3.55
0.72	439.6	438	466	447.8667	2.87
0.688	596	595.6	627.2	606.2667	2.44
0.671	689.6	688.8	722.8	700.4	2.26
0.64	860	861.6	896.4	872.6667	1.92
0.625	963.6	964	998.8	975.4667	1.69
0.591	1143.6	1145.6	1180	1156.4	1.44
0.574	1250.8	1251.2	1286.8	1262.933	1.34
0.544	1428	1434.8	1466.4	1443.067	1.16
0.527	1544	1535.6	1572.4	1550.667	1.02
0.496	1744.4	1721.2	1750.4	1738.667	0.72

Table 4.1 Summary data from the transient CO poisoning experiments with two different specific times for 52.7ppmCO

52.7ppm CO, Specific time: 30min					
V_{ref} (V)	V_{spe} (V)	Air (%)	V_{re} (V)	$\nu = V_{re}/V_{ref}$	Rate (%)
0.701	0.427	2	0.681	0.971	97.1
0.701	0.41	3	0.684	0.976	97.6
0.701	0.417	4	0.687	0.98	98
52.7ppm CO, Specific time 3min					
V_{ref} (V)	V_{spe} (V)	Air (%)	V_{re} (V)	$\nu = V_{re}/V_{ref}$	Rate (%)
0.701	0.696	2	0.687	0.98	98
0.701	0.698	3	0.693	0.989	98.9
0.701	0.698	4	0.693	0.989	98.9

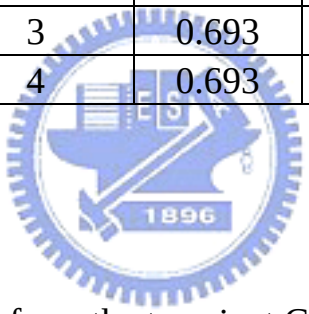

Table 4.2 Summary data from the transient CO poisoning experiments with two different specific times for 25ppmCO

25ppm CO, Specific time: 30min					
V_{ref} (V)	V_{spe} (V)	Air (%)	V_{re} (V)	$\nu = V_{re}/V_{ref}$	Rate (%)
0.701	0.659	2	0.688	0.981	98.1
0.701	0.625	3	0.691	0.986	98.6
25ppm CO, Specific time: 3min					
V_{ref} (V)	V_{spe} (V)	Air (%)	V_{re} (V)	$\nu = V_{re}/V_{ref}$	Rate (%)
0.701	0.698	1.5	0.696	0.993	99.3
0.701	0.701	2	0.696	0.993	99.3
0.701	0.701	3	0.695	0.991	99.1

Table 4.3 summary data from the transient CO poisoning experiments with two different specific times for 10.1ppmCO

10.1ppm CO, Specific time: 30min					
V_{ref} (V)	V_{spe} (V)	Air (%)	V_{re} (V)	$\nu = V_{re}/V_{ref}$	Rate (%)
0.701	0.693	1.5	0.695	0.991	99.1
0.701	0.693	2	0.695	0.991	99.1
10.1ppm CO, Specific time: 3min					
V_{ref} (V)	V_{spe} (V)	Air (%)	V_{re} (V)	$\nu = V_{re}/V_{ref}$	Rate (%)
0.701	0.701	1.5(P)	0.6965	0.994	99.4
0.701	0.701	2(P)	0.6965	0.994	99.4
0.701	0.701	1.5	0.697	0.994	99.4

Table 4.4 summary data from the transient CO poisoning experiments with two different anode catalysts for 52.7ppmCO

52.7ppm CO, Pt alloy					
V_{ref} (V)	V_{spe} (V)	Air (%)	V_{re} (V)	$\nu = V_{re}/V_{ref}$	Rate (%)
0.701	0.427	2	0.681	0.971	97.1
0.701	0.41	3	0.684	0.976	97.6
0.701	0.417	4	0.687	0.98	98
52.7ppm CO, pure Pt					
V_{ref} (V)	V_{spe} (V)	Air (%)	V_{re} (V)	$\nu = V_{re}/V_{ref}$	Rate (%)
0.657	0.518	3	0.605	0.921	92.1
0.657	0.488	4	0.620	0.944	94.4
0.657	0.410	5	0.637	0.97	97
0.657	0.444	6	0.642	0.977	97.7
0.657	0.366	7	0.649	0.988	98.8

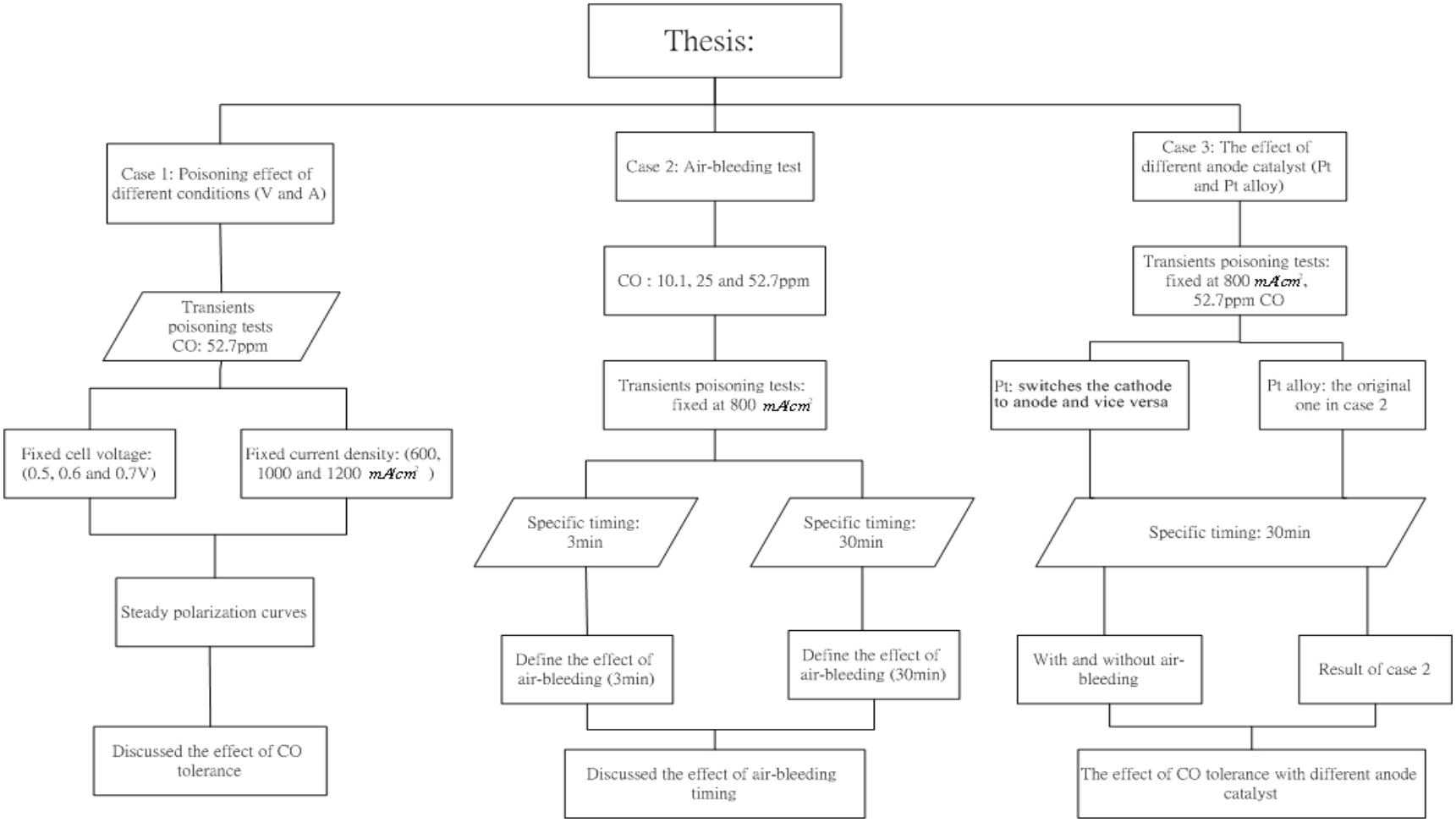

Fig. 1.1 Scheme diagram of the thesis

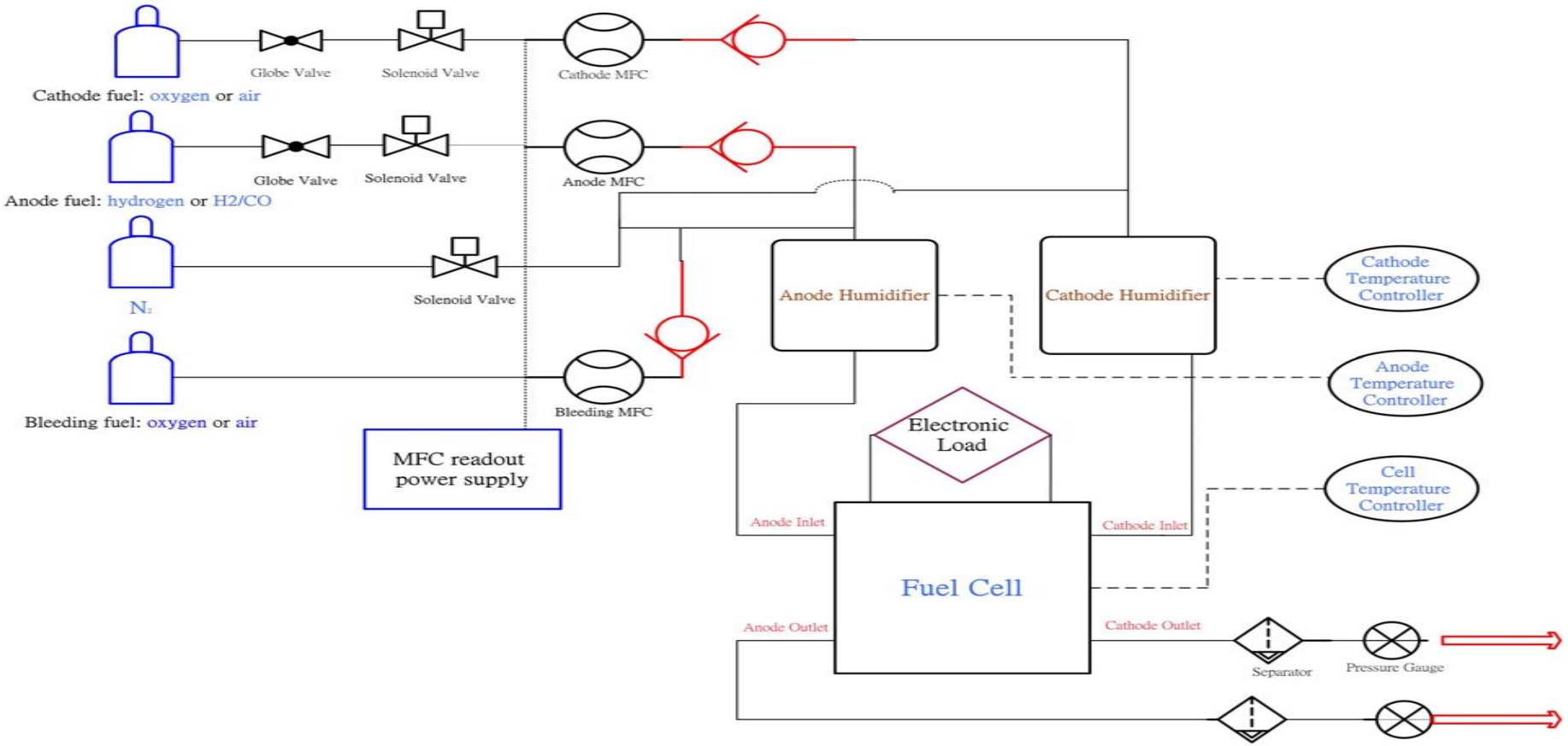

Fig 2.1 Schematic drawing of overall experimental system

Fig. 2.2 The HP 6060B electronic load

Fig. 2.3 The MFC readout power supply

Fig. 2.4 The power supply of the test station

Fig. 2.5 The gas pipelines controller

Fig. 2.6 The fuel cell test station

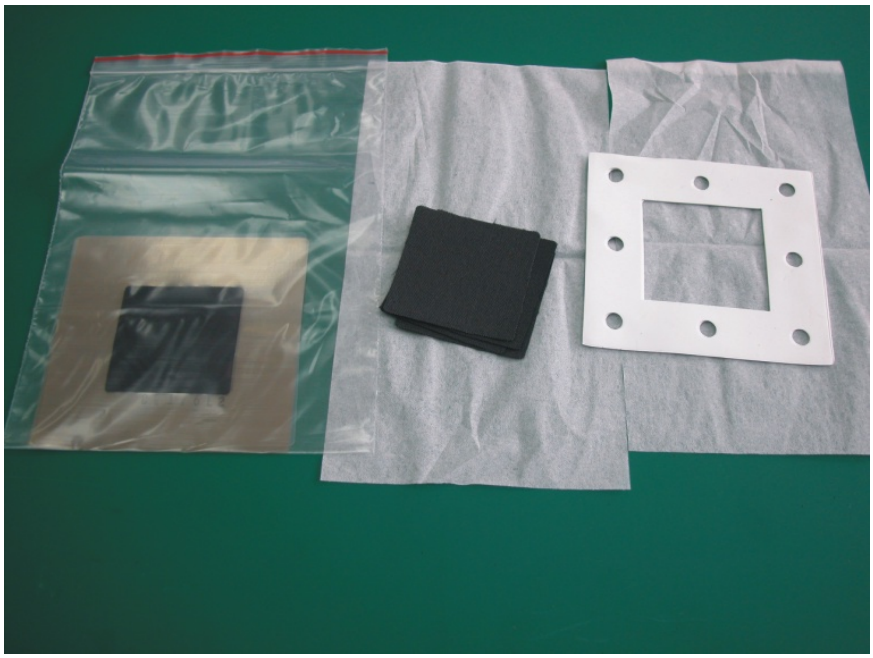

Fig. 2.7 The MEA, GDL, gasket

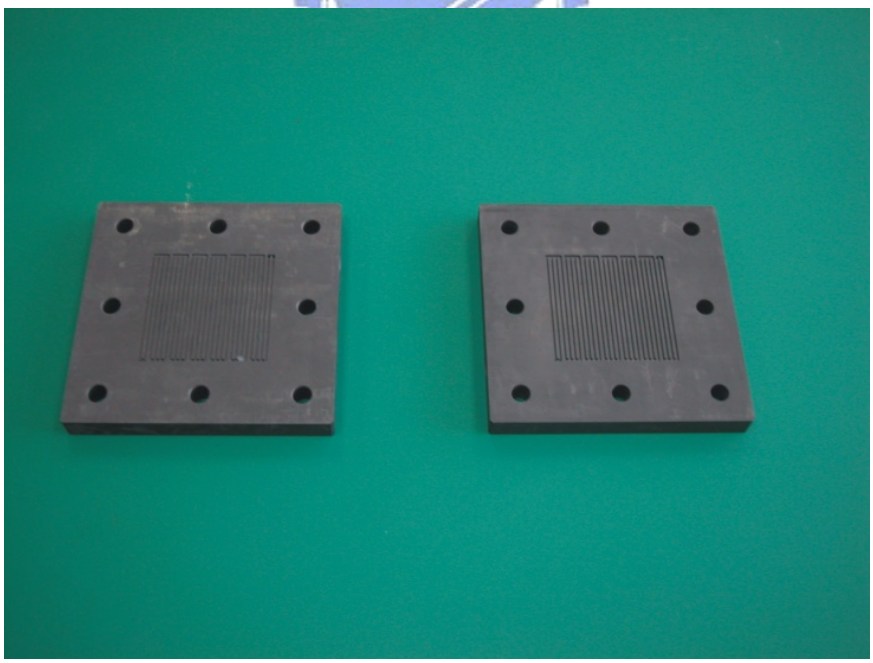

Fig. 2.8 The flow channels

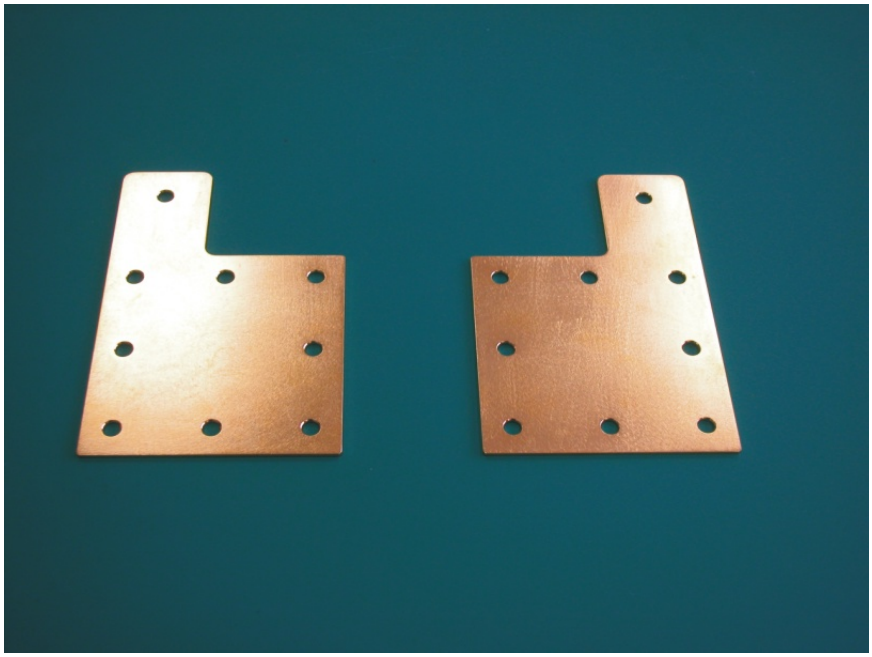

Fig. 2.9 The current collector

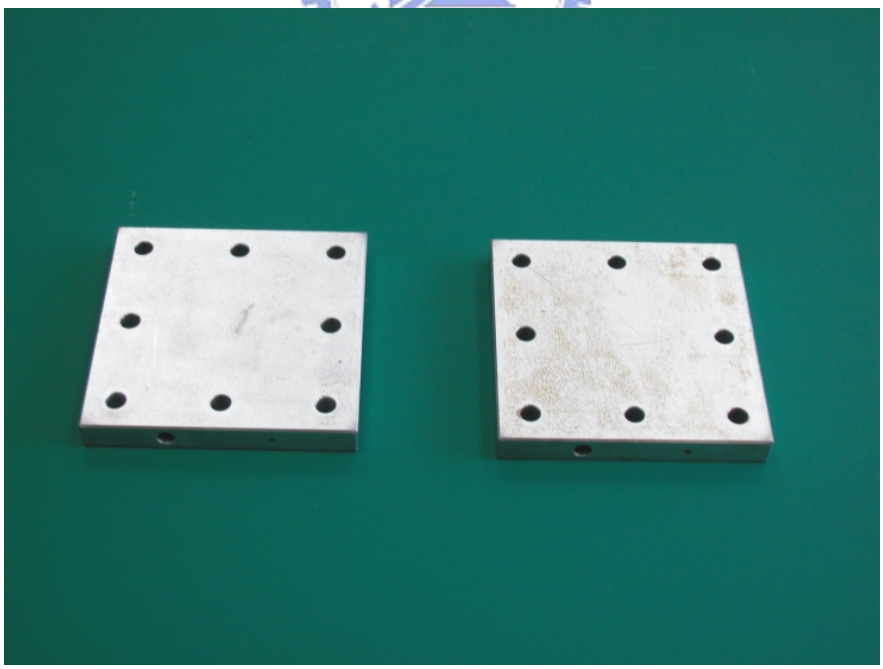

Fig. 2.10 The end plank

Fig. 2.11 All components of PEMFC

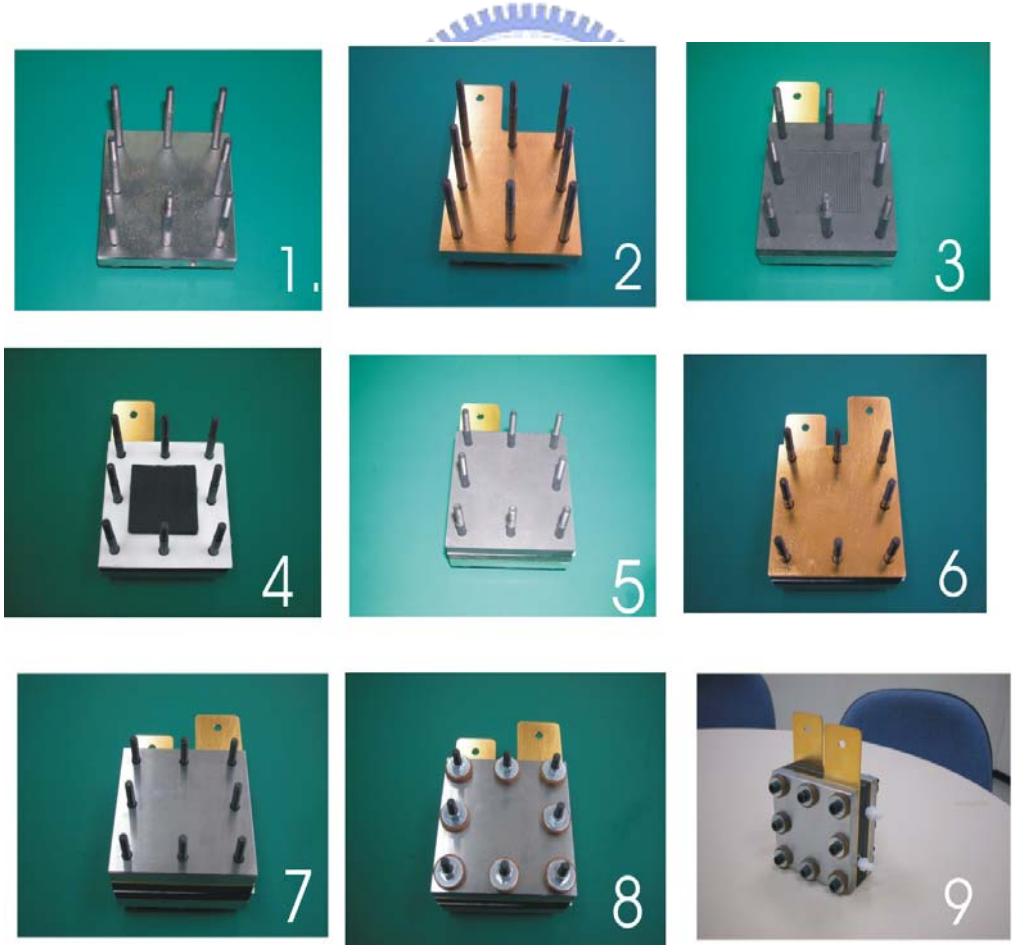

Fig. 2.12The sequence of fabricated fuel cell

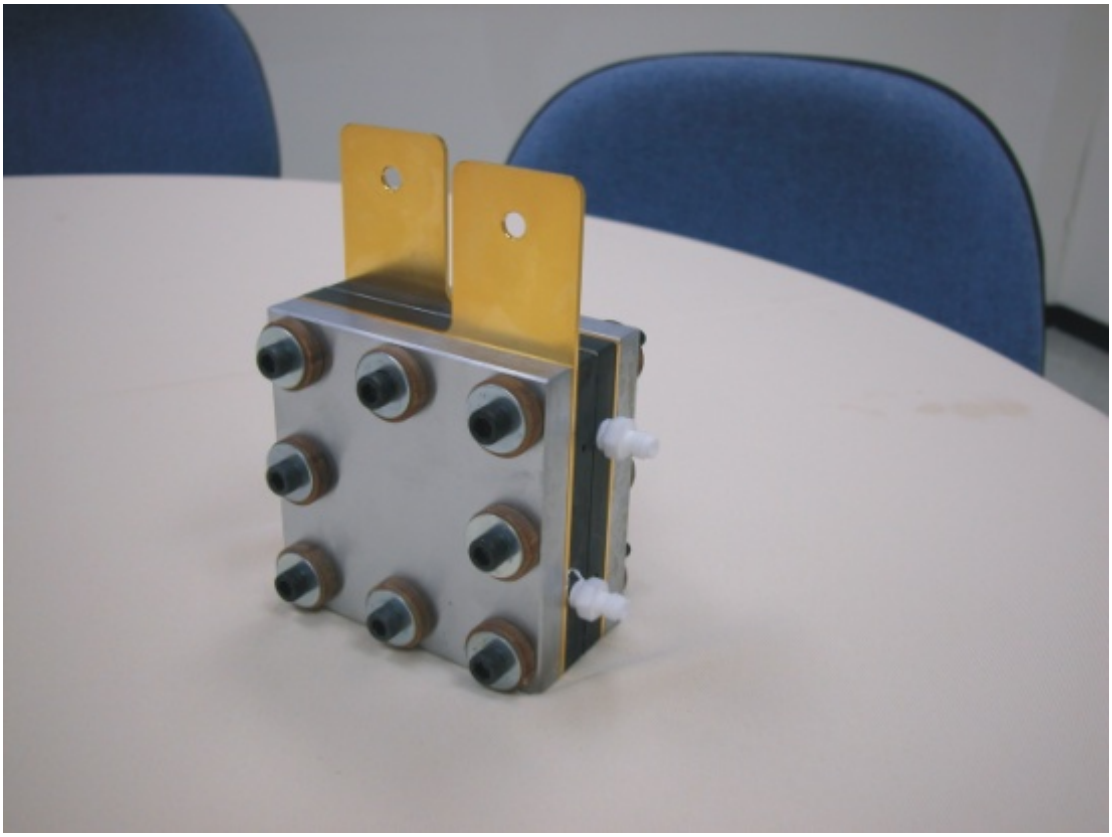

Fig. 2.13 The test fuel cell

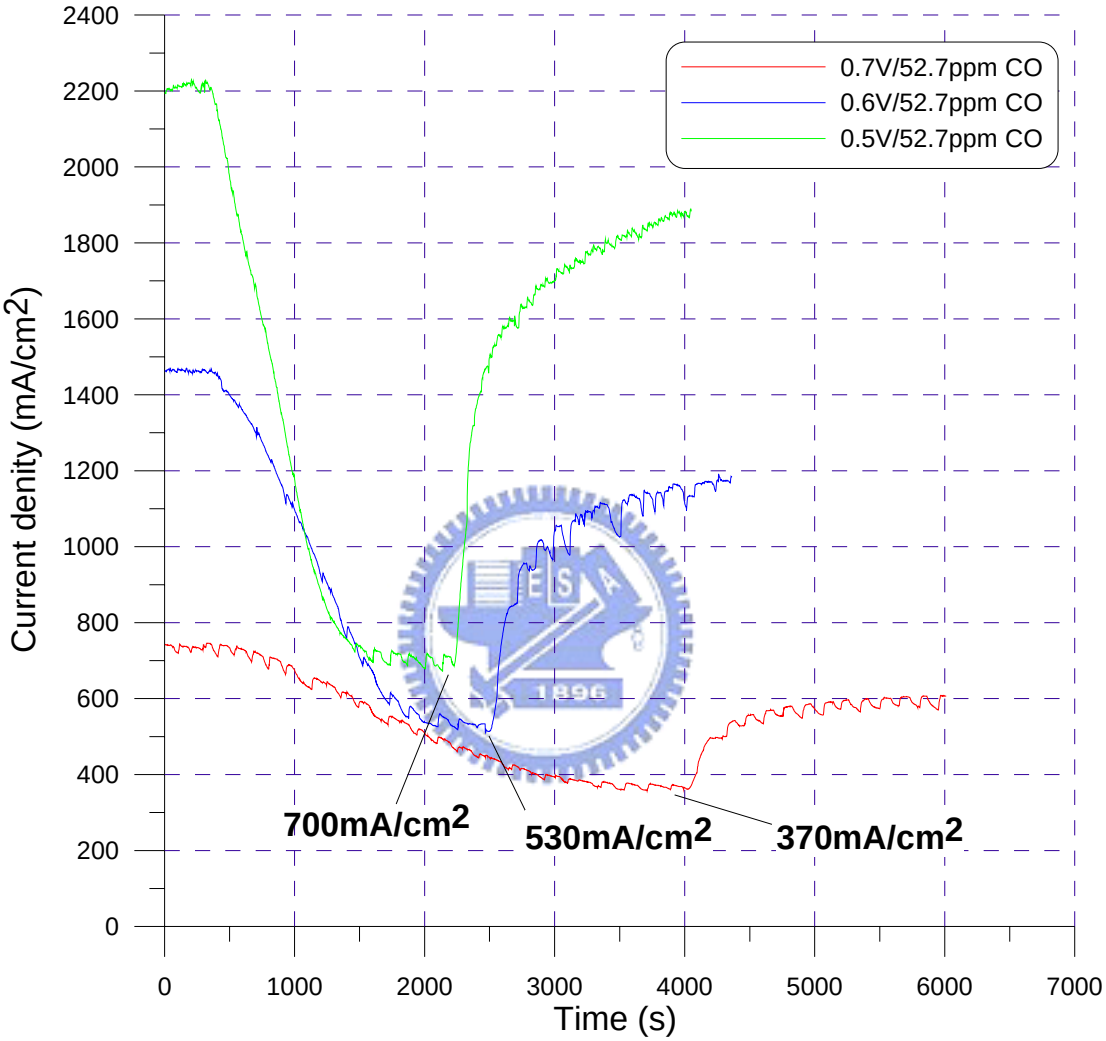

Fig. 4.1 Transients poisoning and recovery performances with different poisoning conditions (0.5, 0.6 and 0.7V)

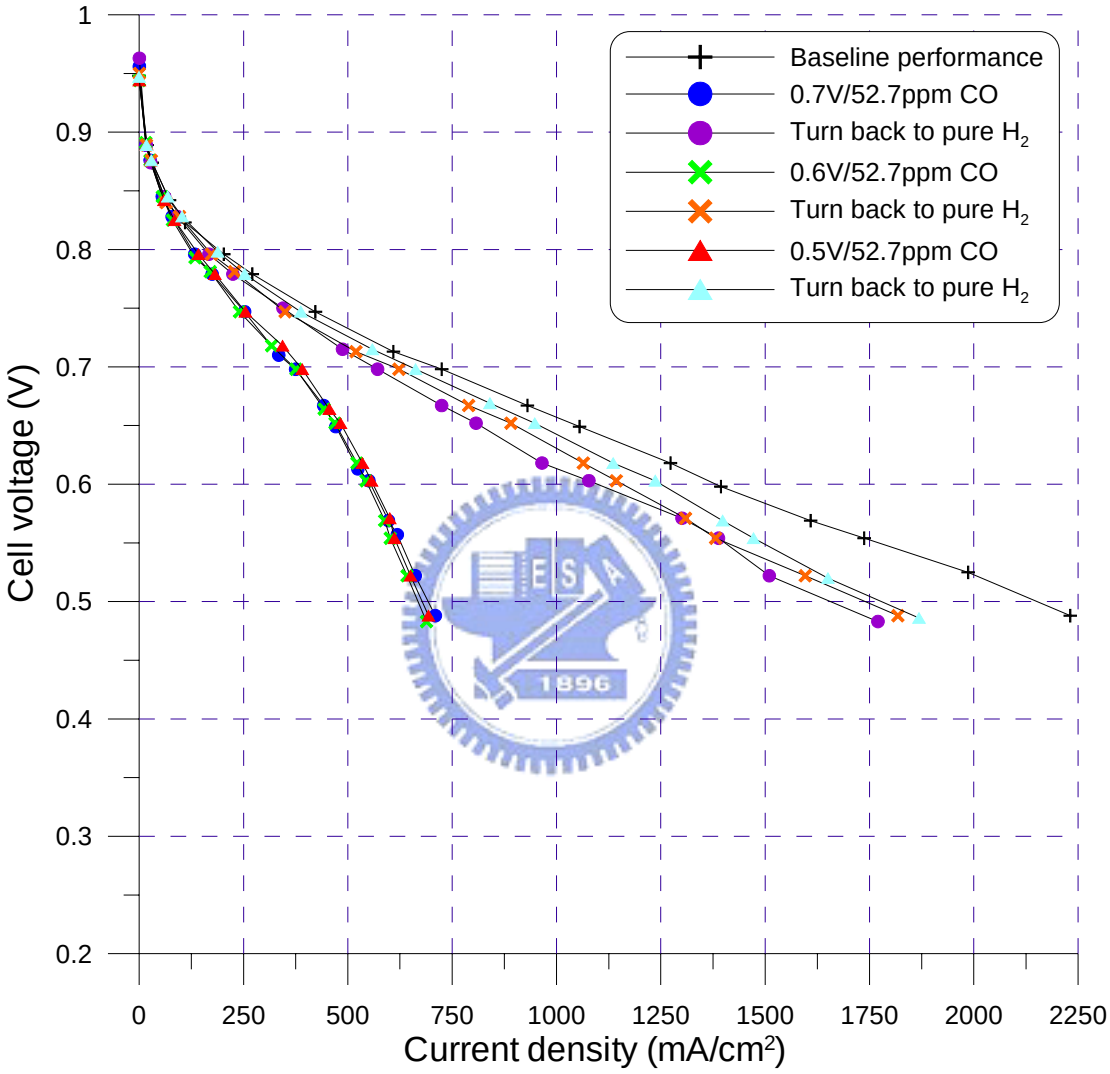

Fig. 4.2 The baseline polarization curve, the poisoned and recovered polarization curves with different poisoning conditions (0.5, 0.6 and 0.7V)

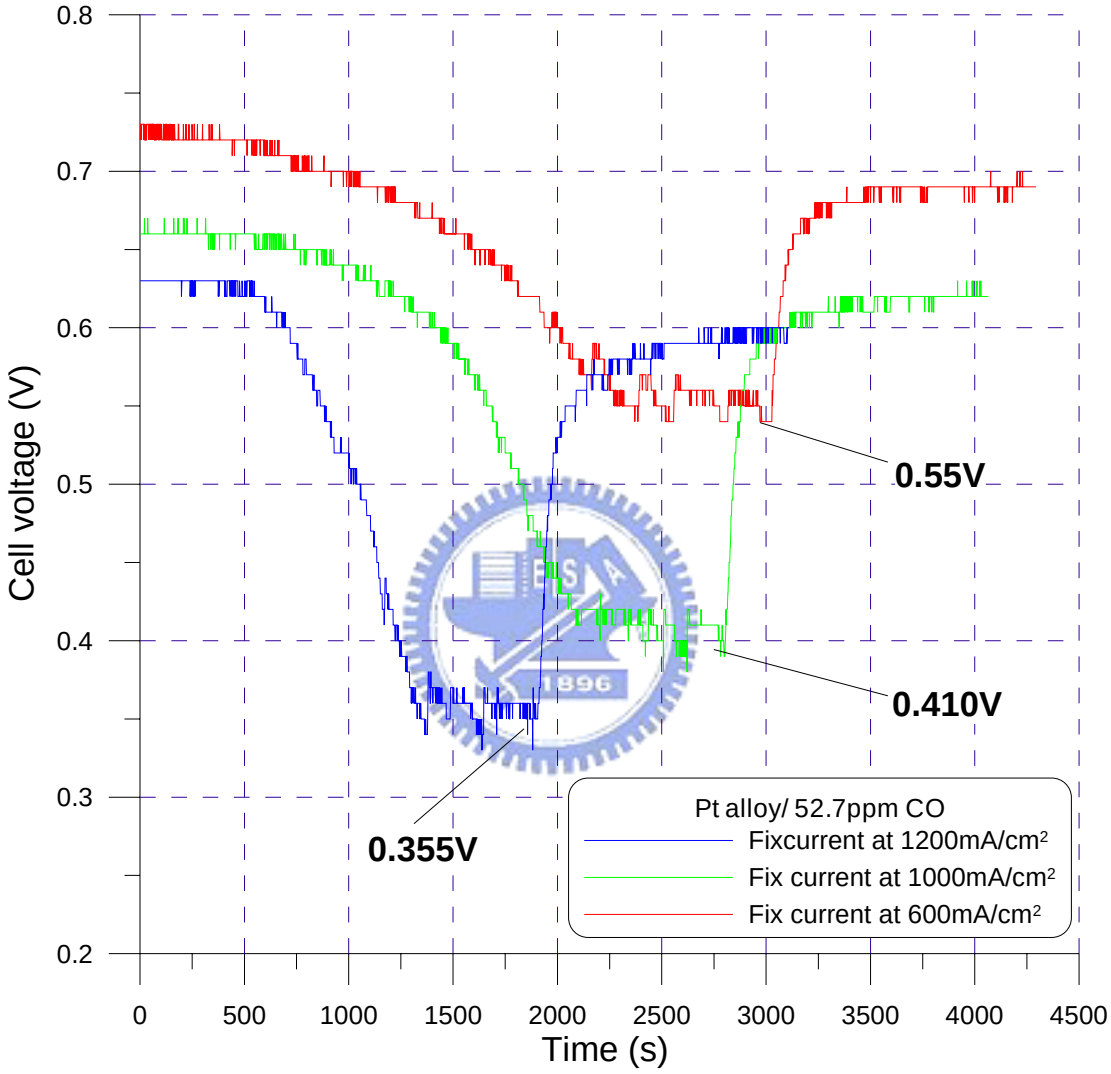

Fig. 4.3 Transients poisoning and recovery performances with different poisoning conditions (600, 1000 and 1200 mA/cm^2)

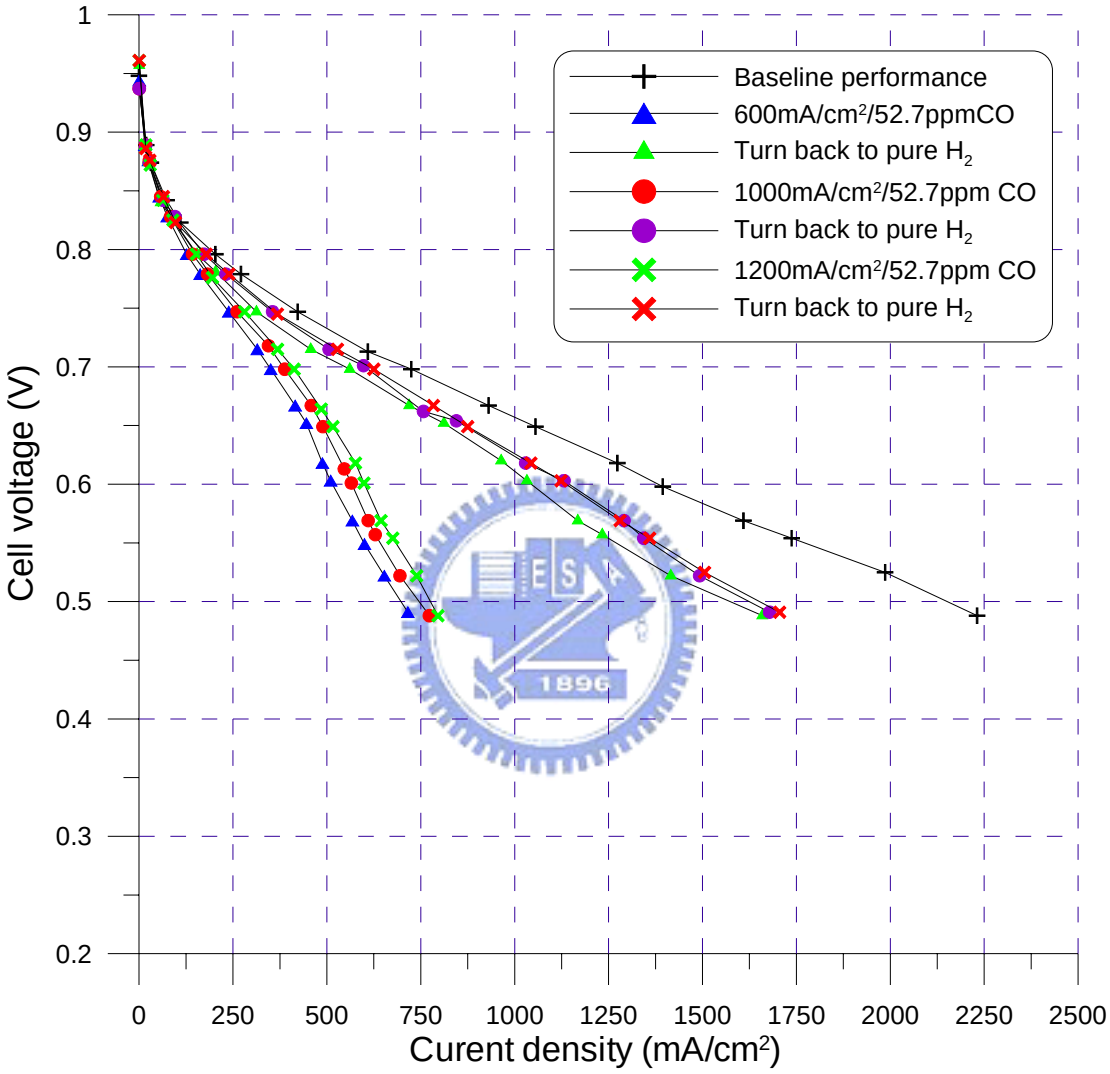

Fig. 4.4 The baseline polarization curve, the poisoned and recovered polarization curves with different poisoning conditions (600, 1000 and 1200 mA/cm^2)

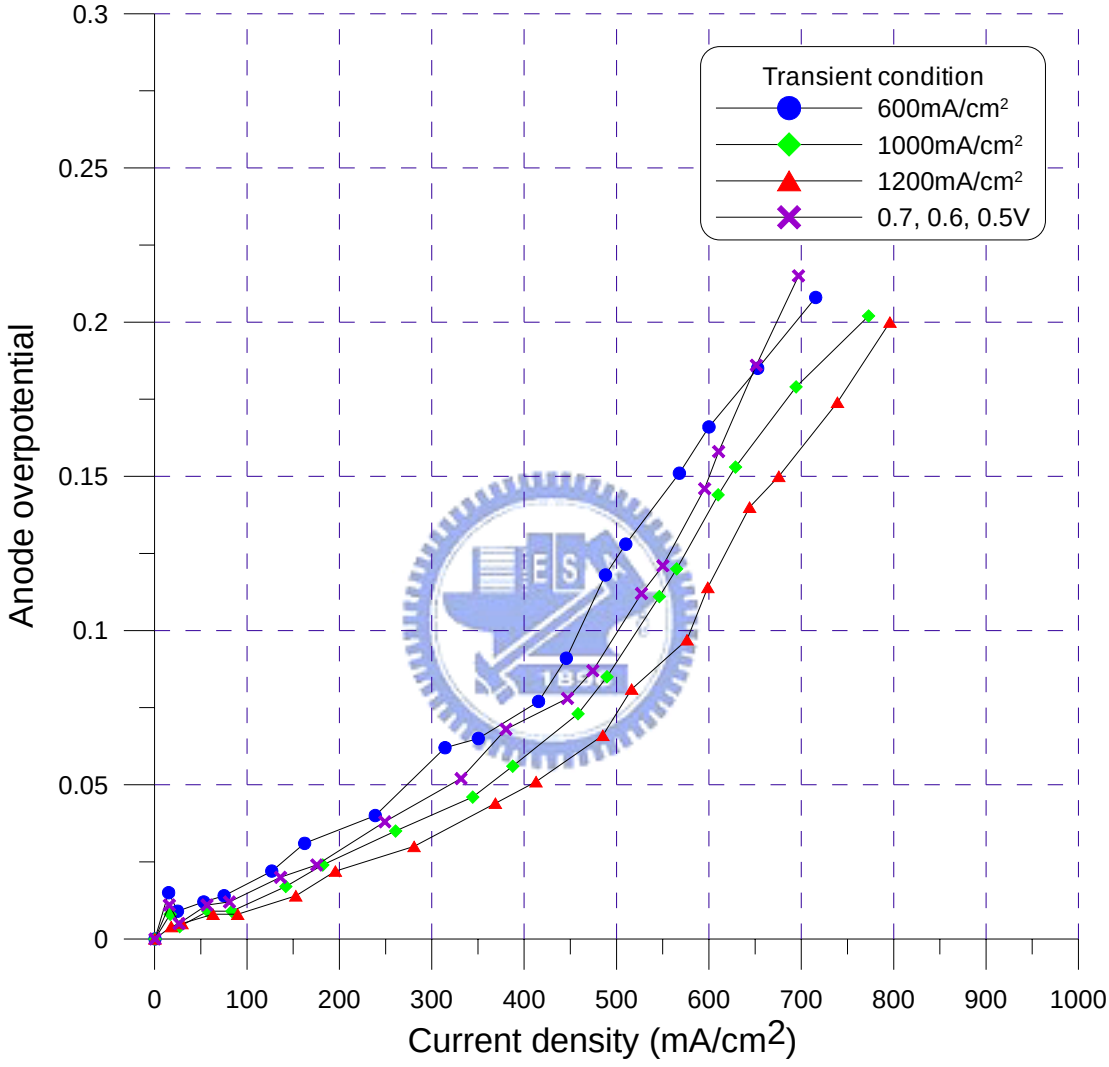

Fig. 4.5 Anode potential due to CO (52.7ppm) poisoning with different transient poisoning conditions (0.5, 0.6 and 0.7V), (600, 1000 and 1200 mA/cm^2)

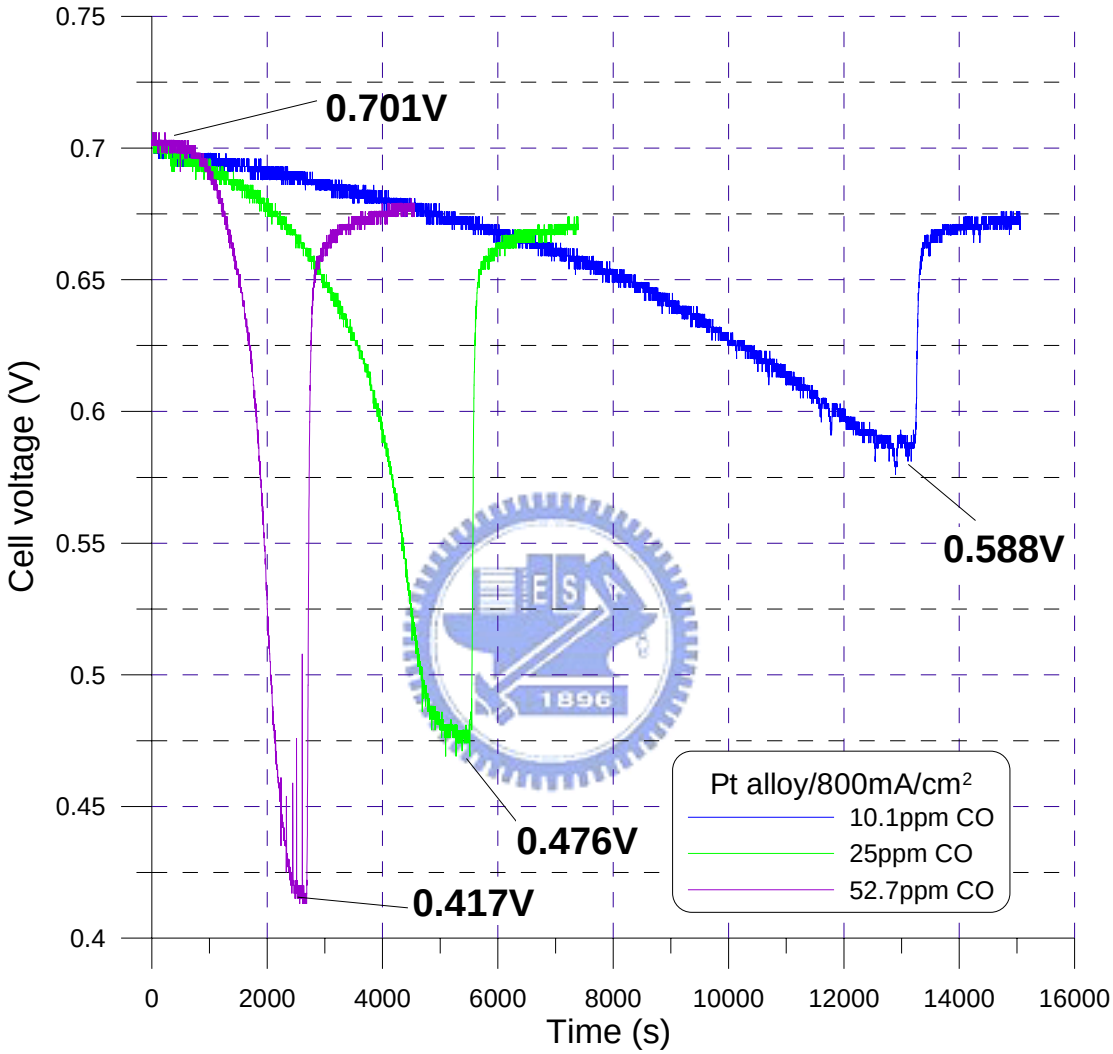

Fig. 4.6 Transients poisoning and recovery performances with different CO concentrations (10.1, 25 and 52.7ppm) at 800 mA/cm^2

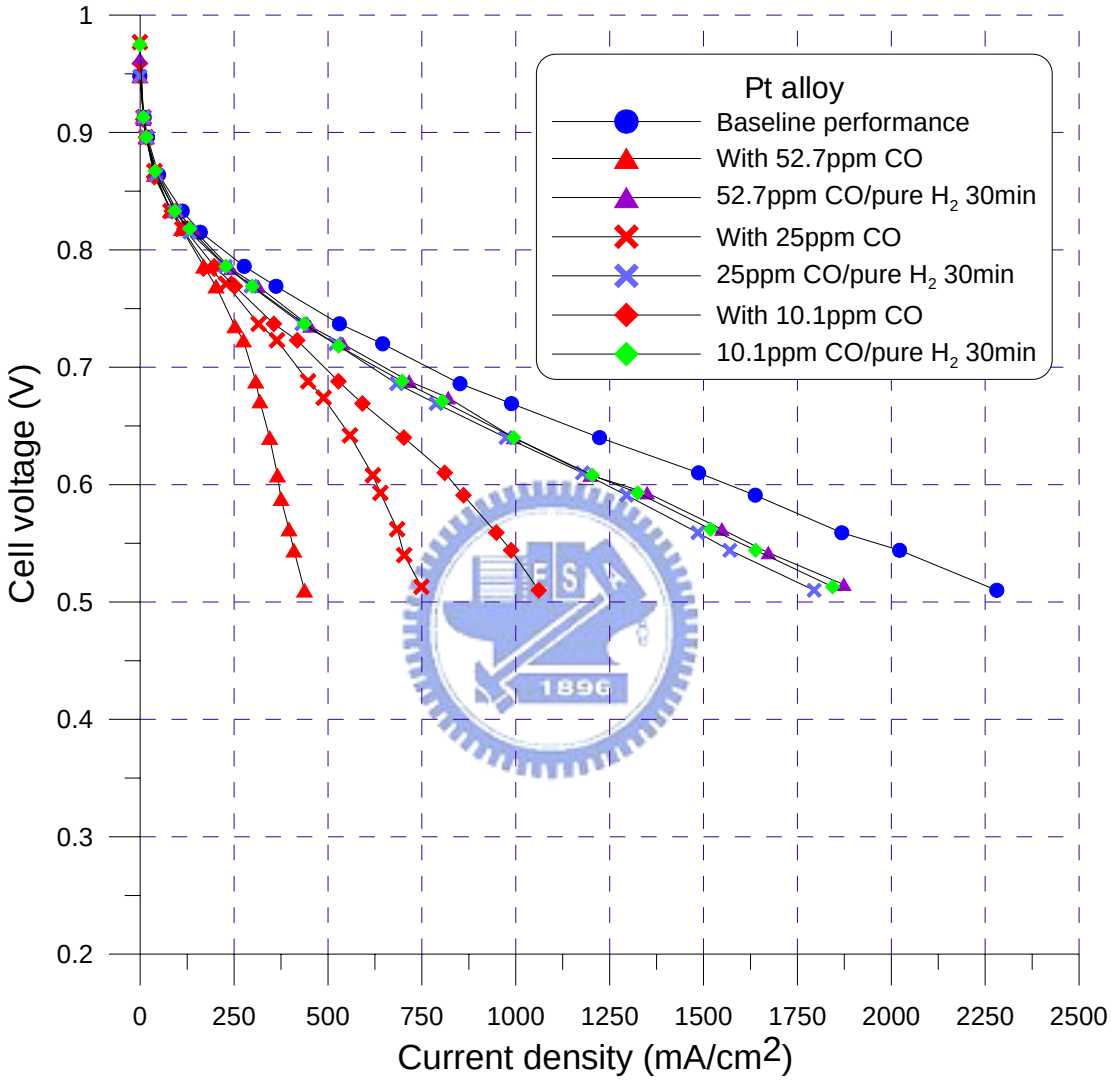

Fig. 4.7 The baseline polarization curve, the poisoned and recovered polarization curves with different CO concentrations (10.1, 25 and 52.7ppm)

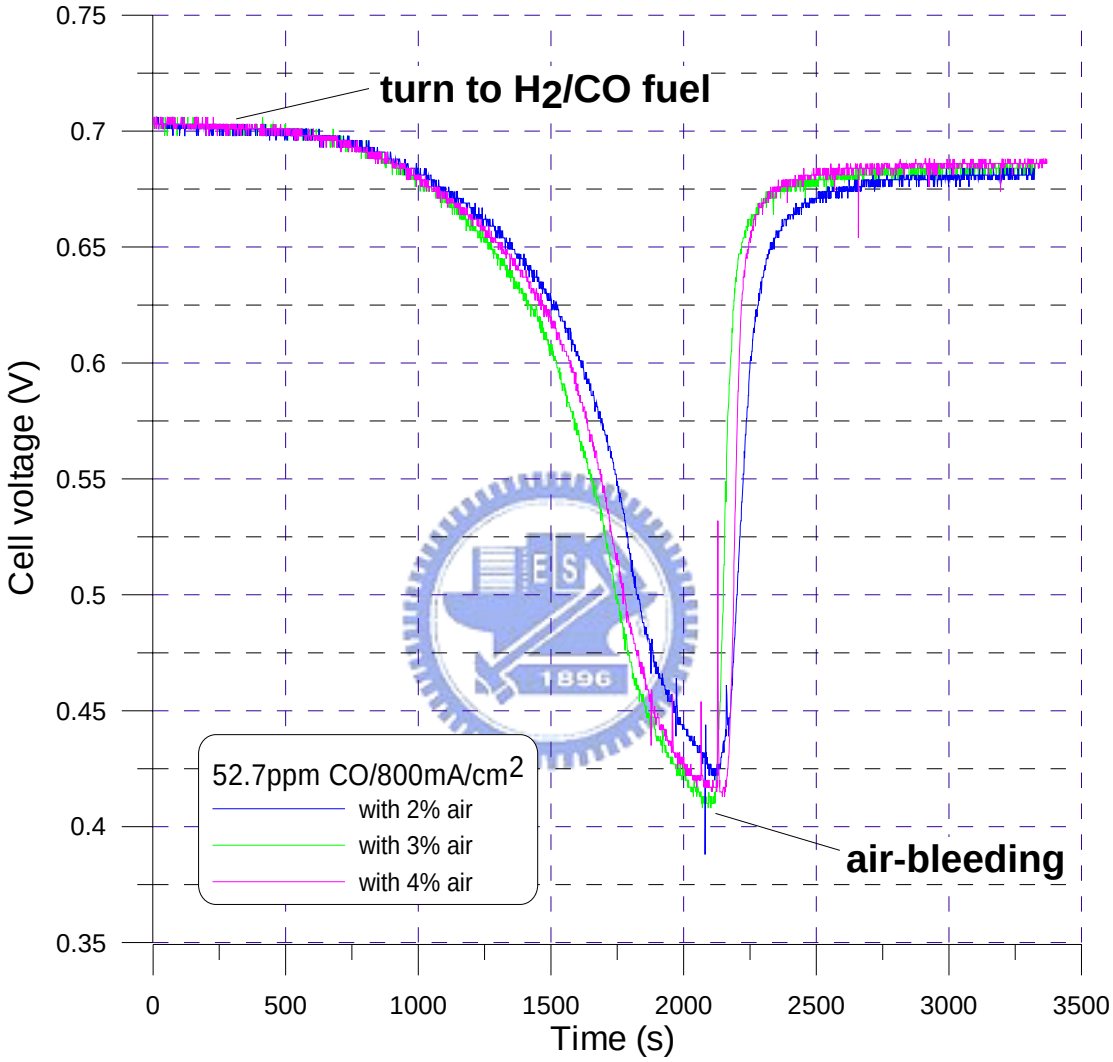

Fig. 4.8a Transient air-bleeding test with 52.7ppm CO at 800 mA/cm^2, the cell potentials recover to 0.681, 0.684 and 0.687V as the air-bleeding ratios are 2, 3 and 4%, respectively

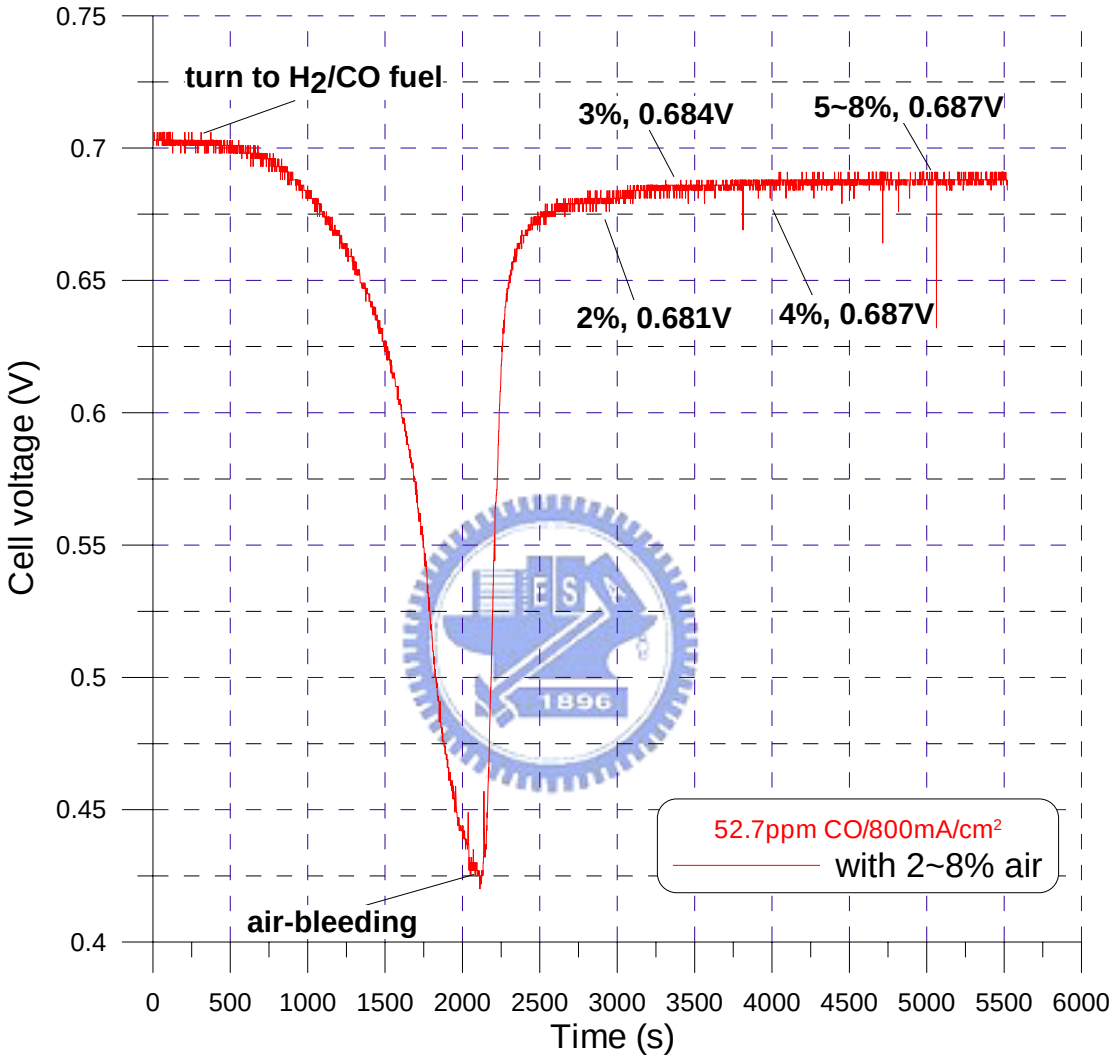

Fig. 4.8b Transient performance with continues changing air ratio and 52.7ppm CO

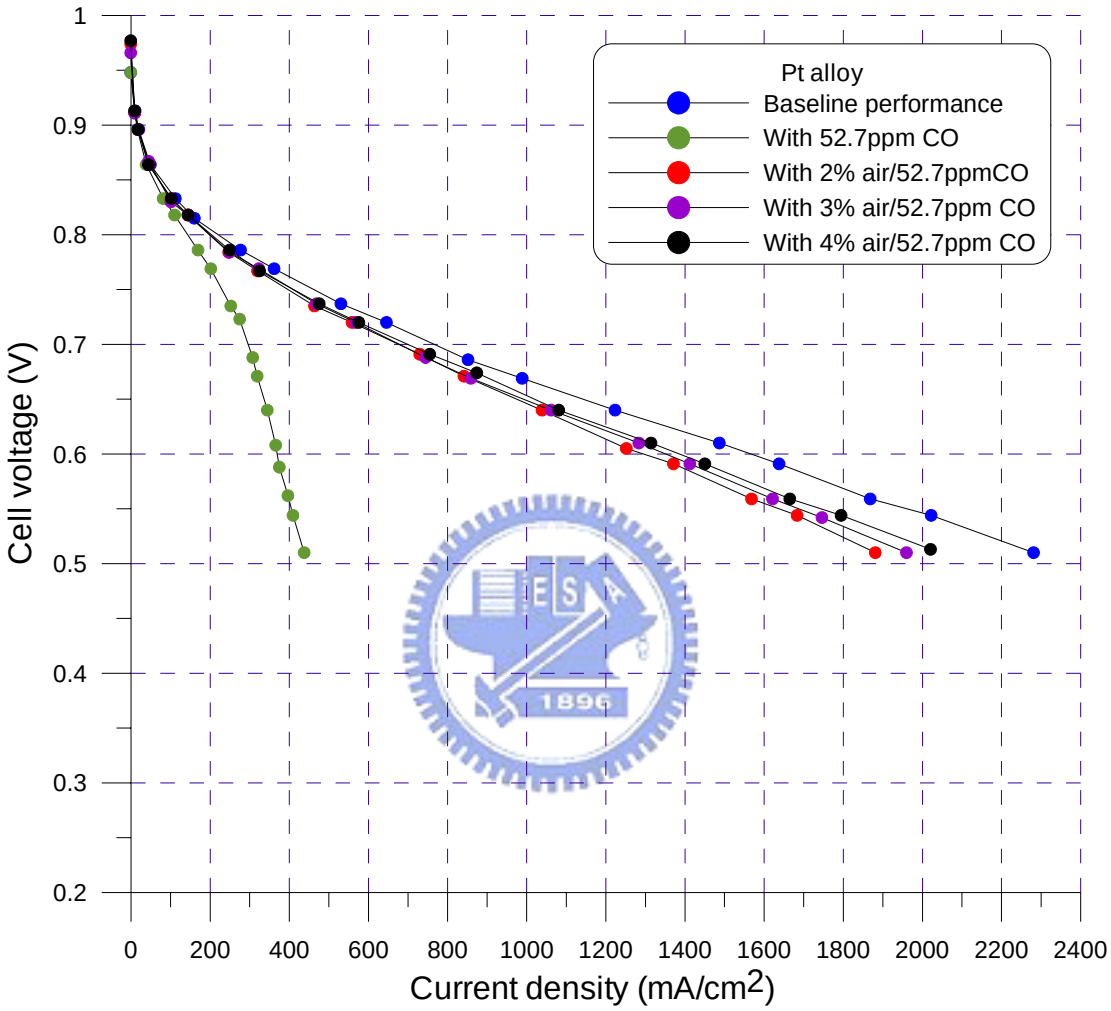

Fig. 4.9 The baseline polarization curve, the poisoned polarization curve and recovered polarization curves as a function of air-bleeding ratio

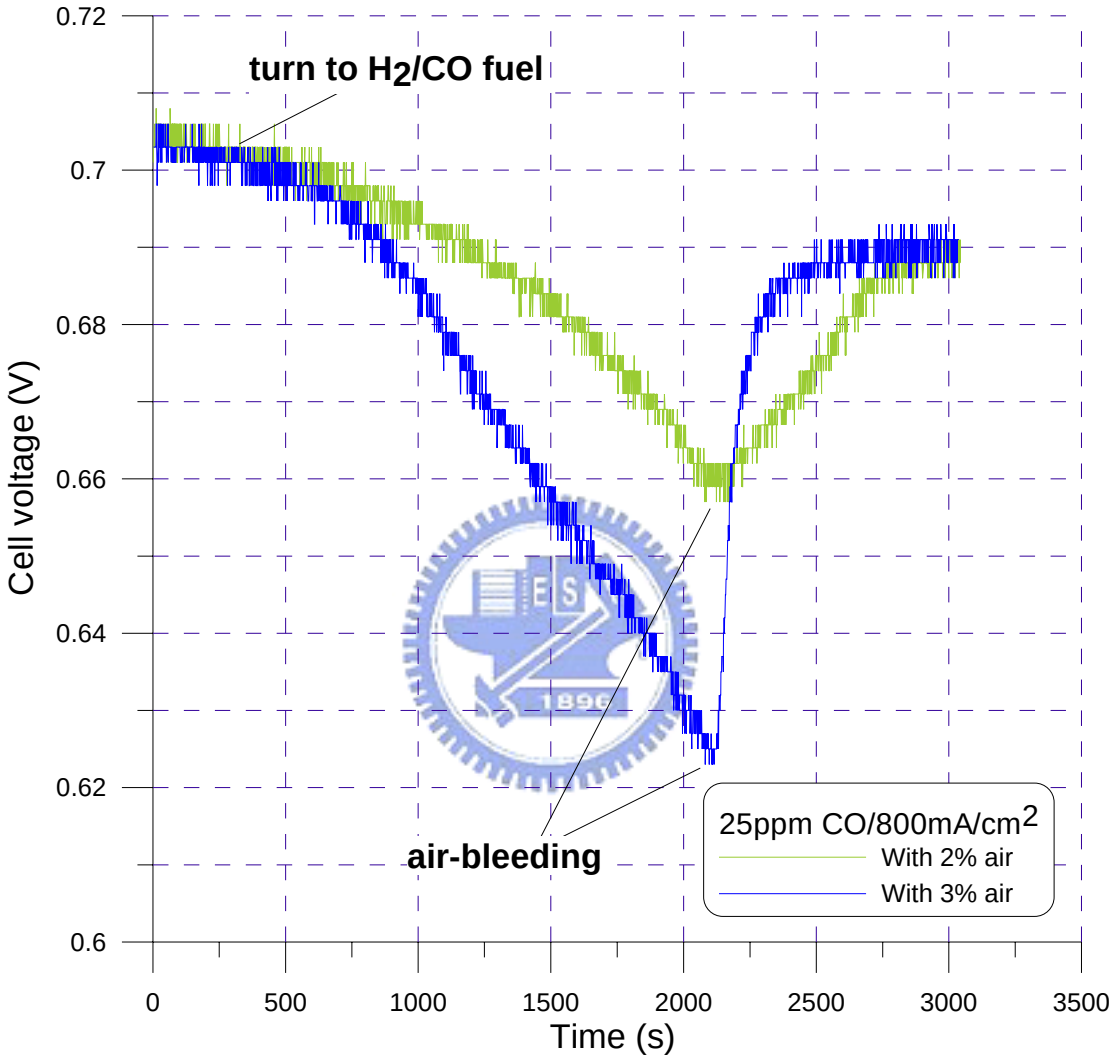

Fig. 4.10a Transient air-bleeding test with 25ppm CO at 800 mA/cm^2, the cell potentials recover to 0.688 and 0.691V as the air-bleeding ratios are 2 and 3%, respectively

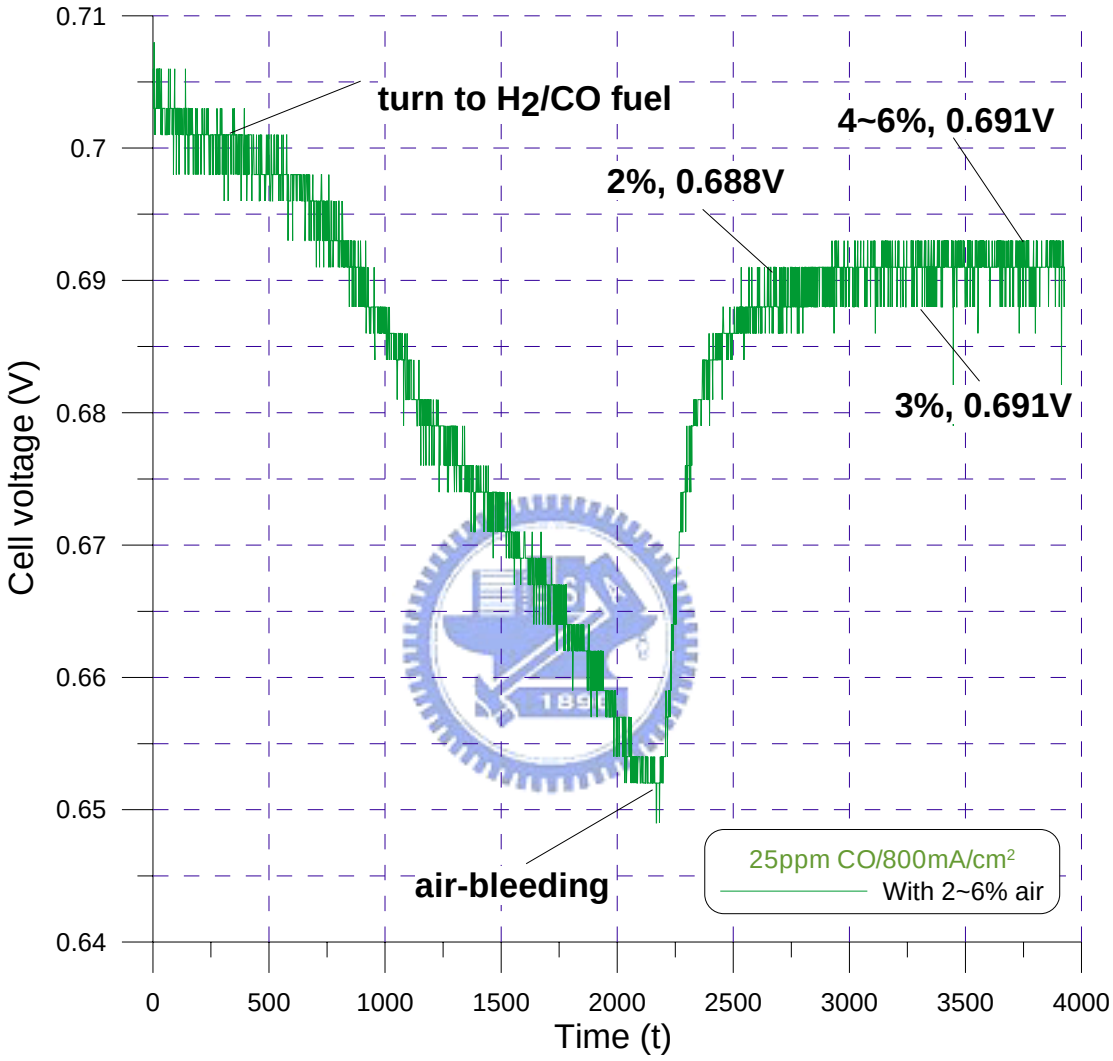

Fig. 4.10b Transient performance with continues changing air ratio and 25ppm CO

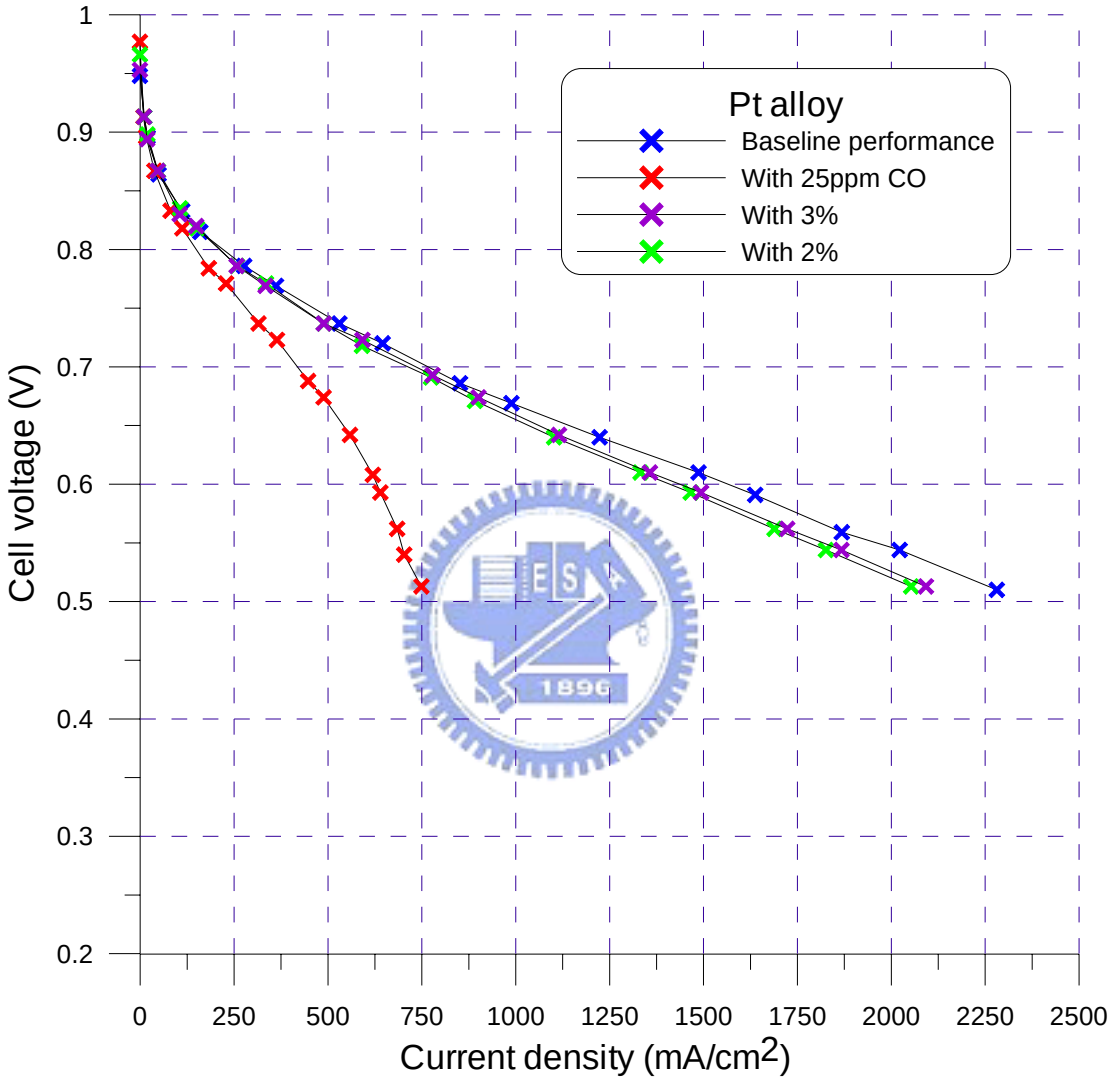

Fig. 4.11 The baseline polarization curve, the poisoned polarization curve and recovered polarization curves as a function of air-bleeding ratio

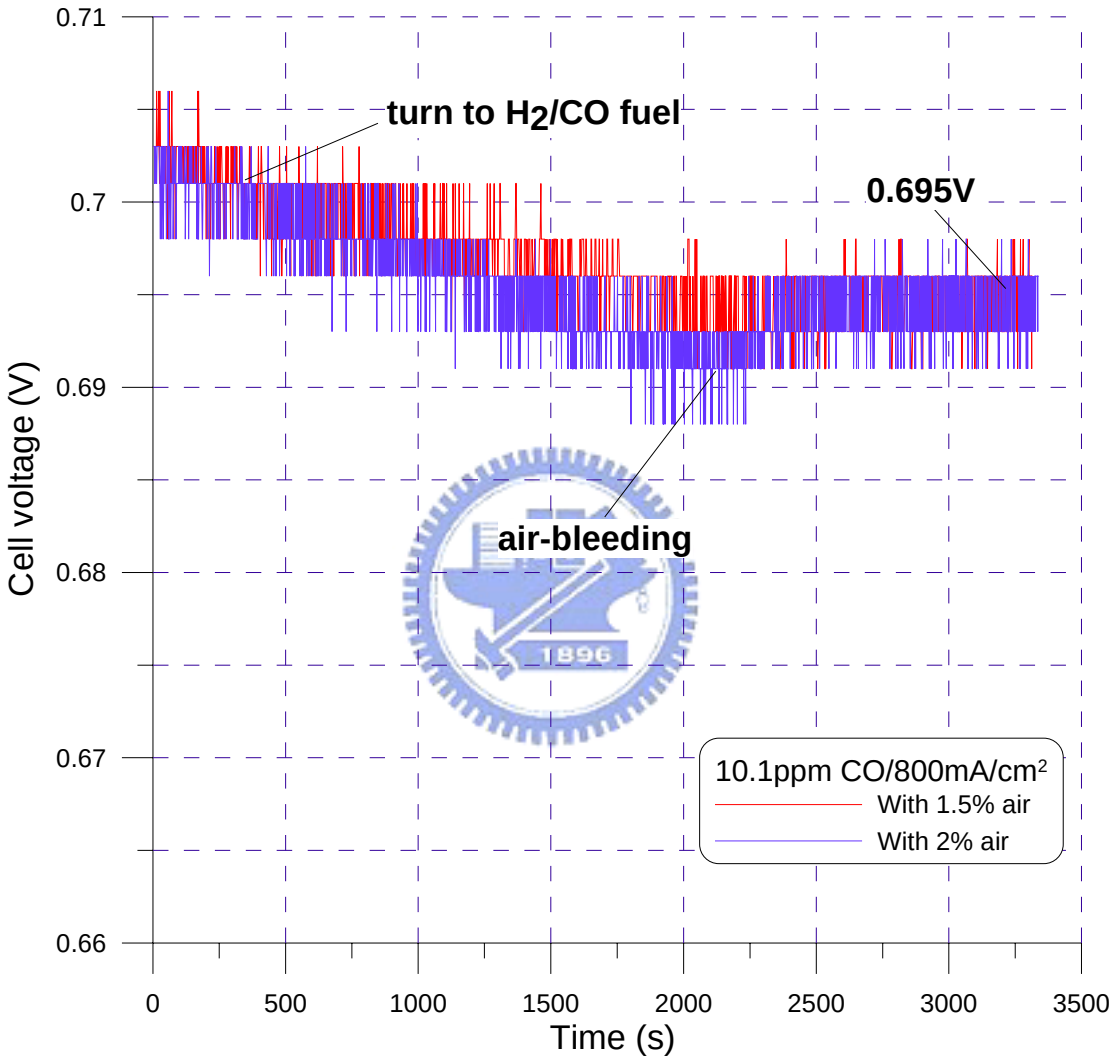

Fig. 4.12a Transient air-bleeding test with 10.1ppm CO at 800 mA/cm^2, both 1.5 and 2% of air-bleeding ratios let cell potentials recover to 0.695V

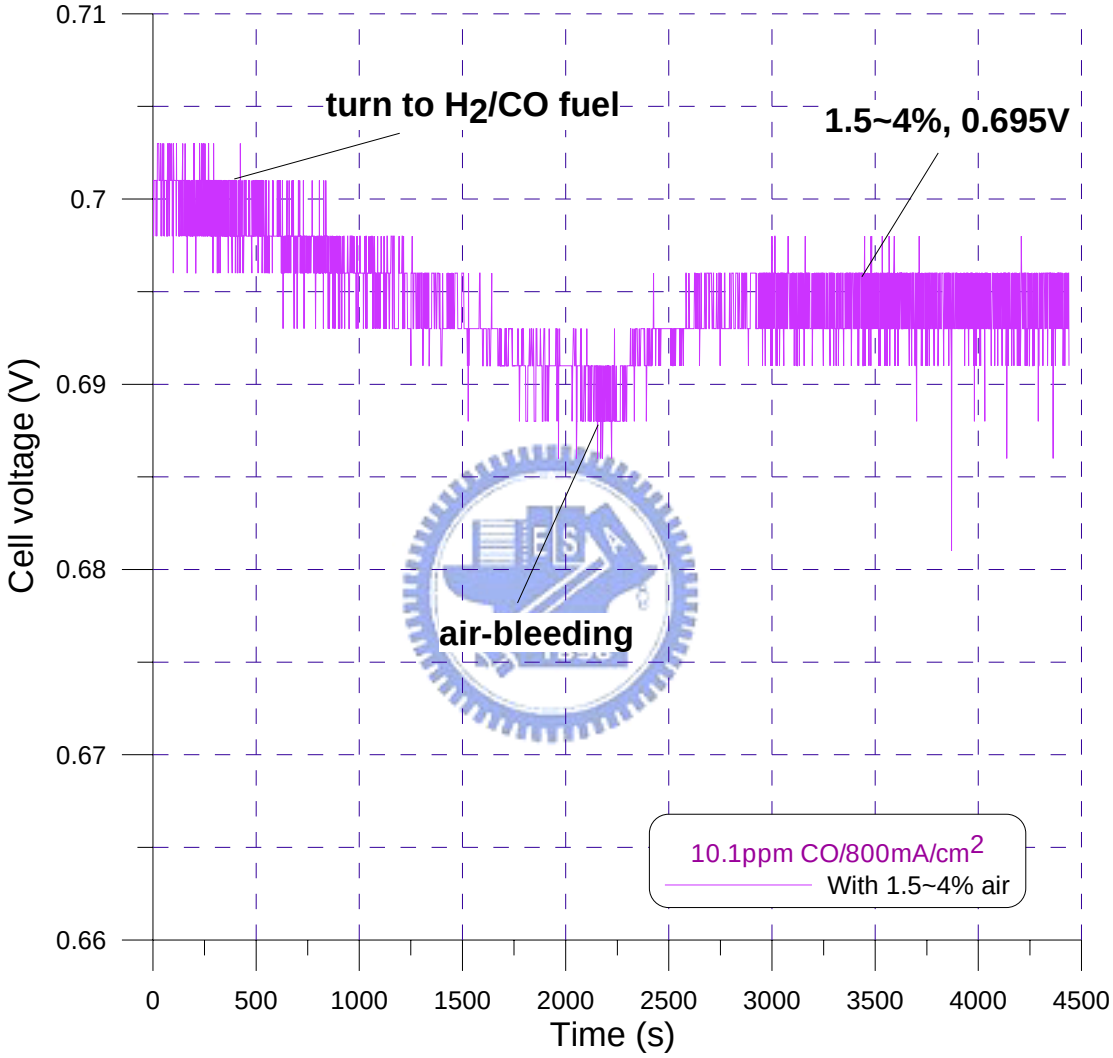

Fig. 4.12b Transient performance with continues changing air ratio and 10.1ppm CO

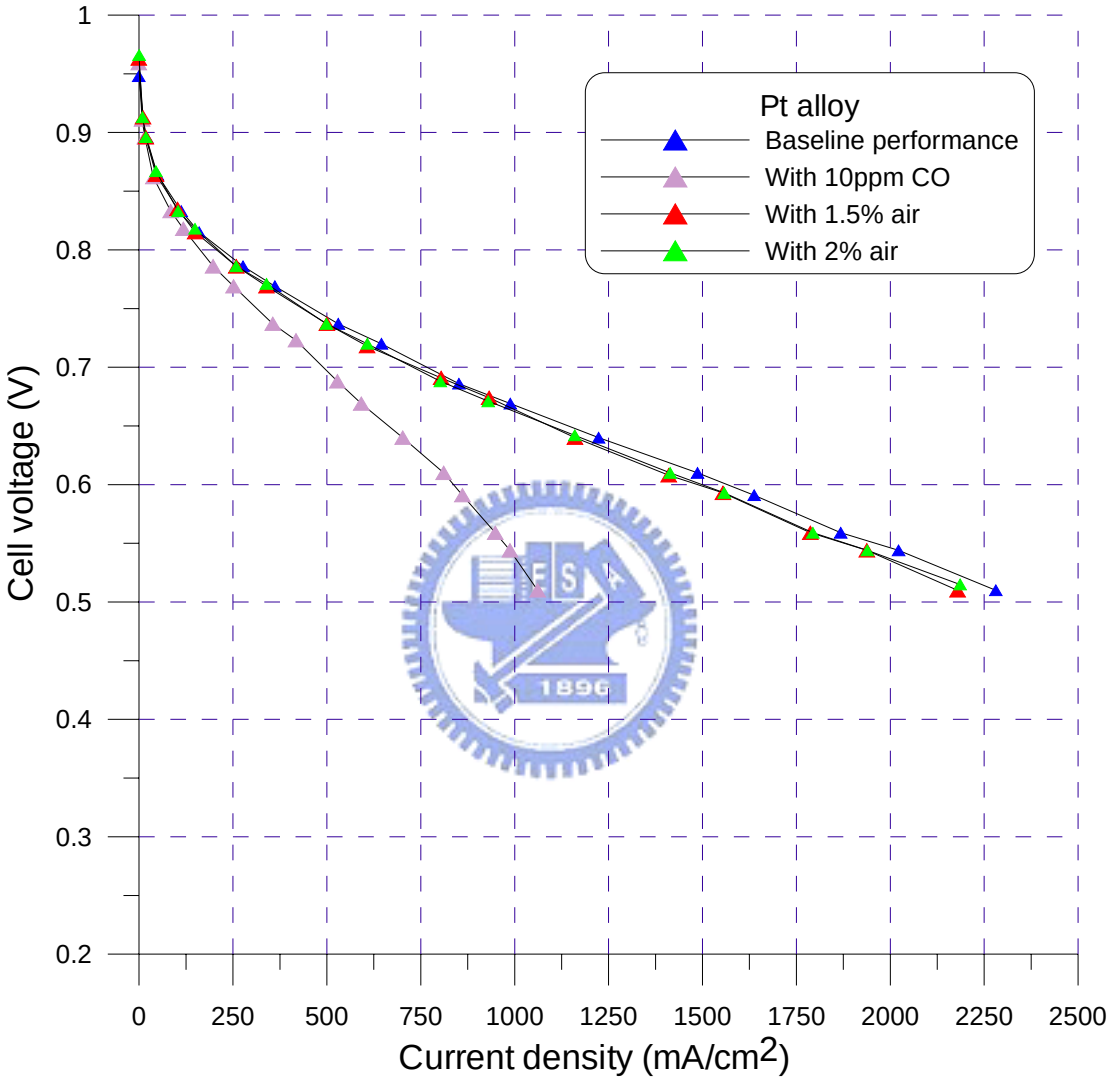

Fig. 4.13 The baseline polarization curve, the poisoned polarization curve and recovered polarization curves as a function of air-bleeding ratio

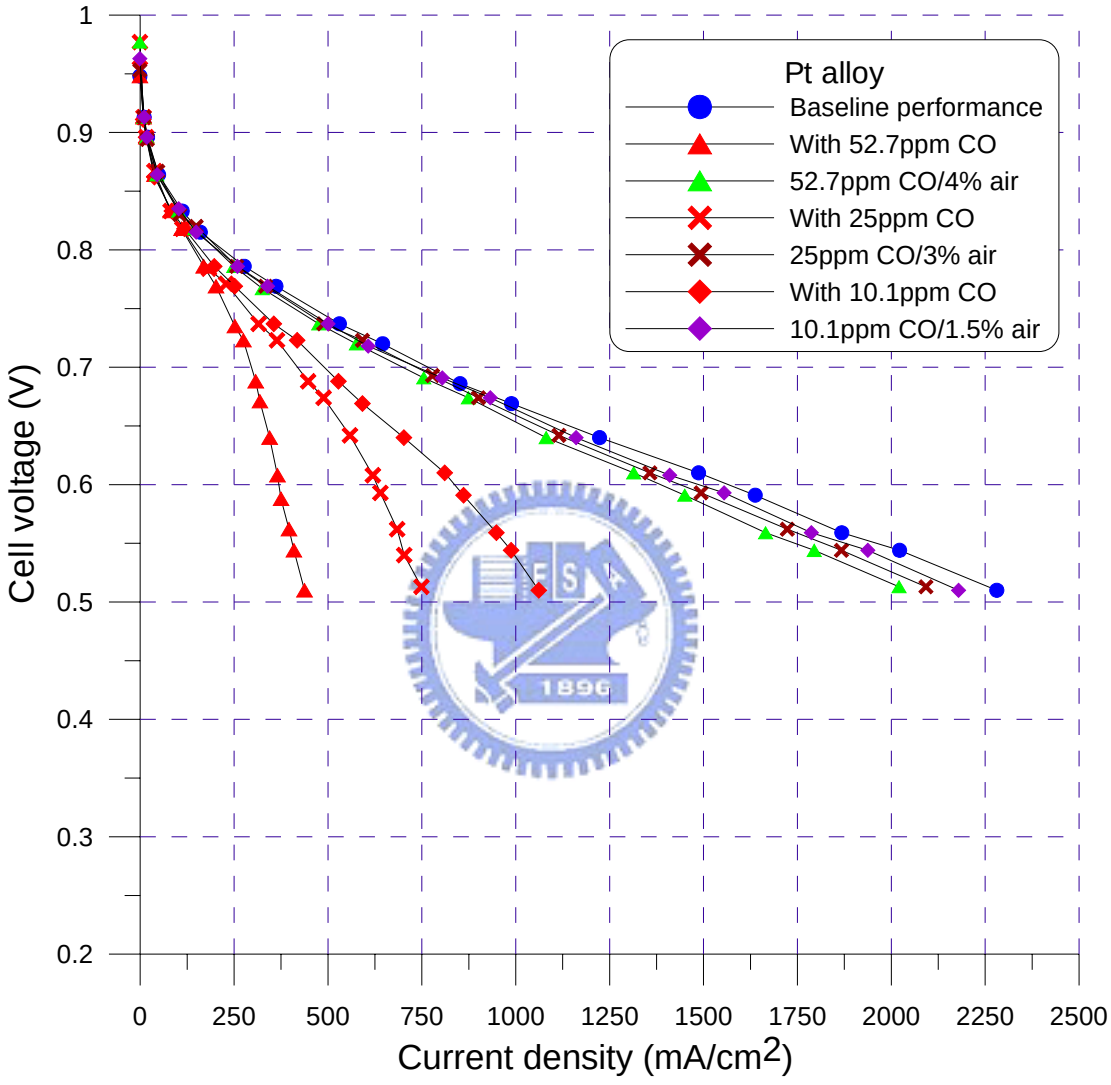

Fig. 4.14 Summarizes the recovered steady-state polarization curves by air-bleeding with different CO poisoning concentrations (52.7, 25 and 10.1ppm)

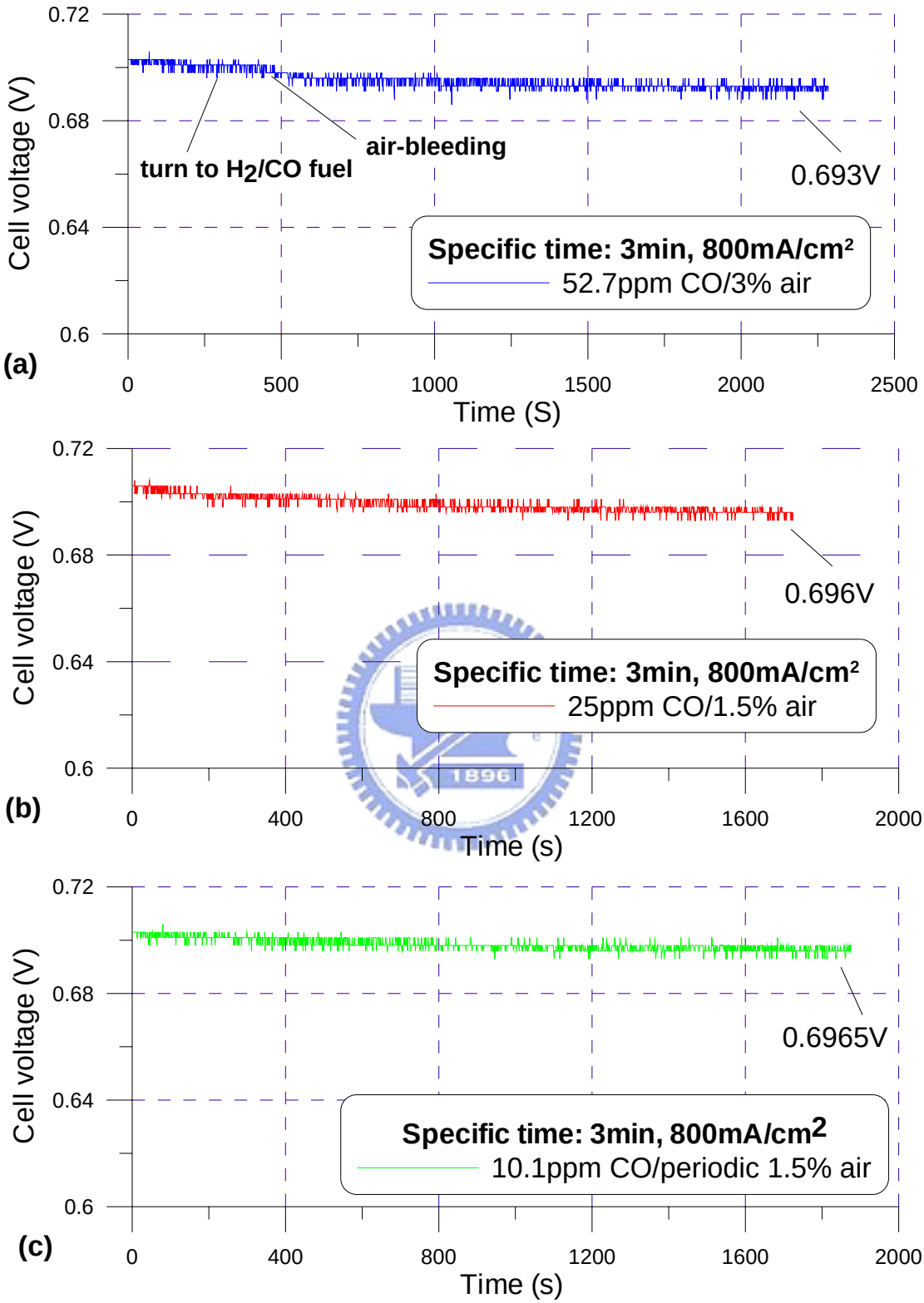

Fig. 4.15a, b and c Transient air-bleeding test with different CO poisoning concentrations (52.7, 25 and 10.1ppm), the timing of air-bleeding is 3min

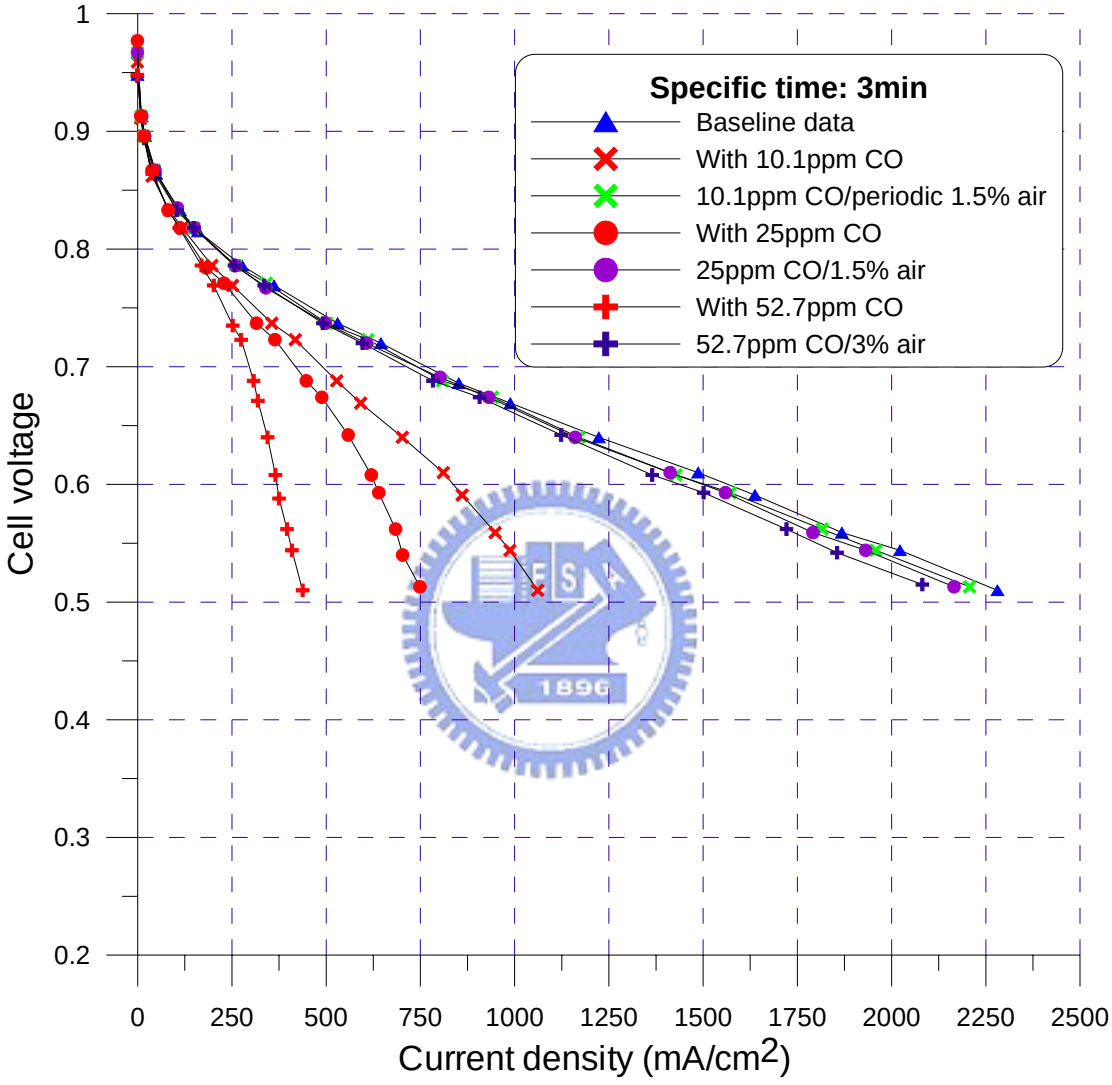

Fig. 4.16 Summarizes the recovered steady-state polarization curves by air-bleeding with different CO poisoning concentrations (52.7, 25 and 10.1ppm), the timing of air-bleeding is 3min in transients tests

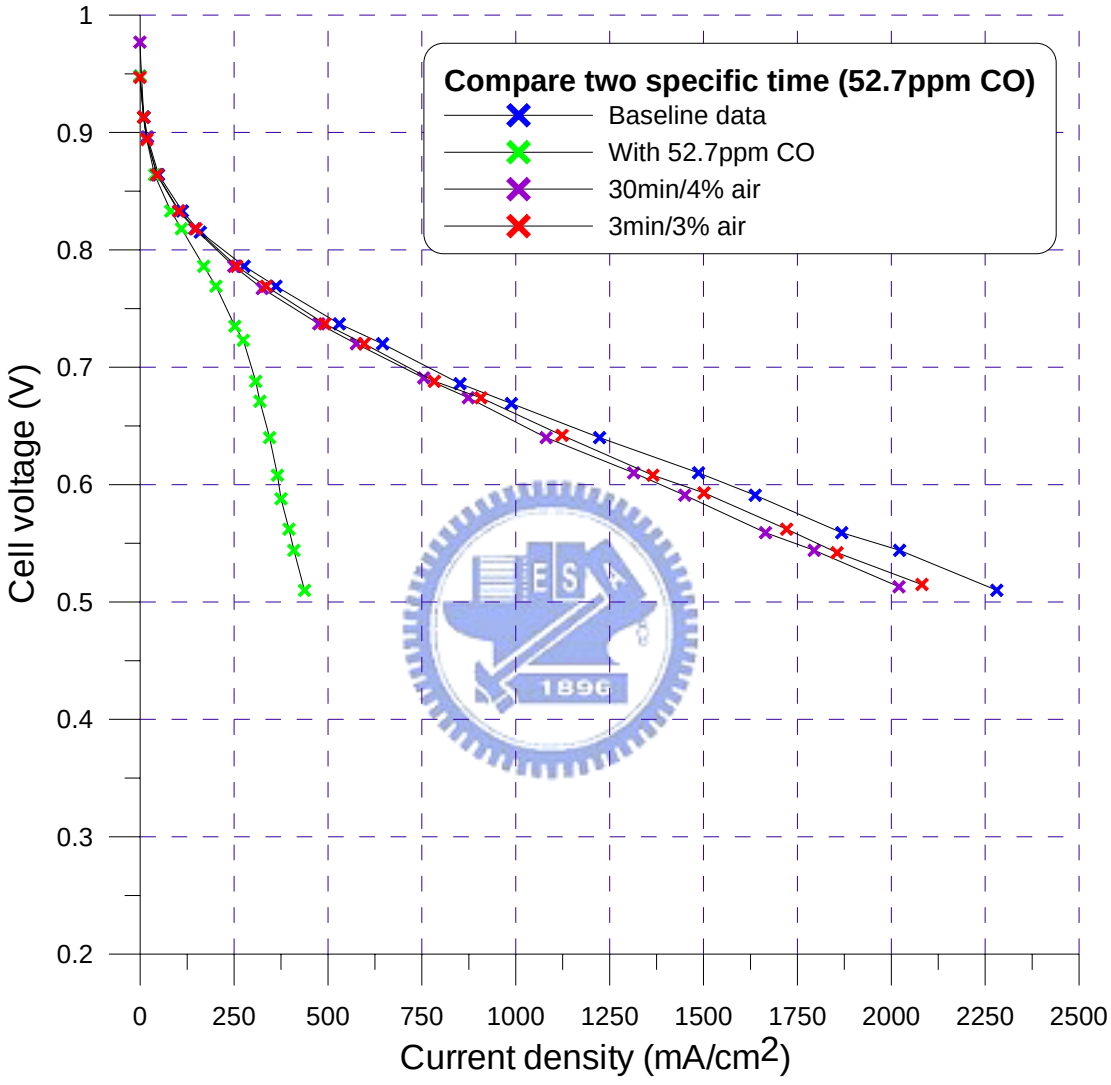

Fig. 4.17 The comparisons of recovered steady-state polarization curves with different air-bleeding timing (3 and 30min), with 52.7ppm CO

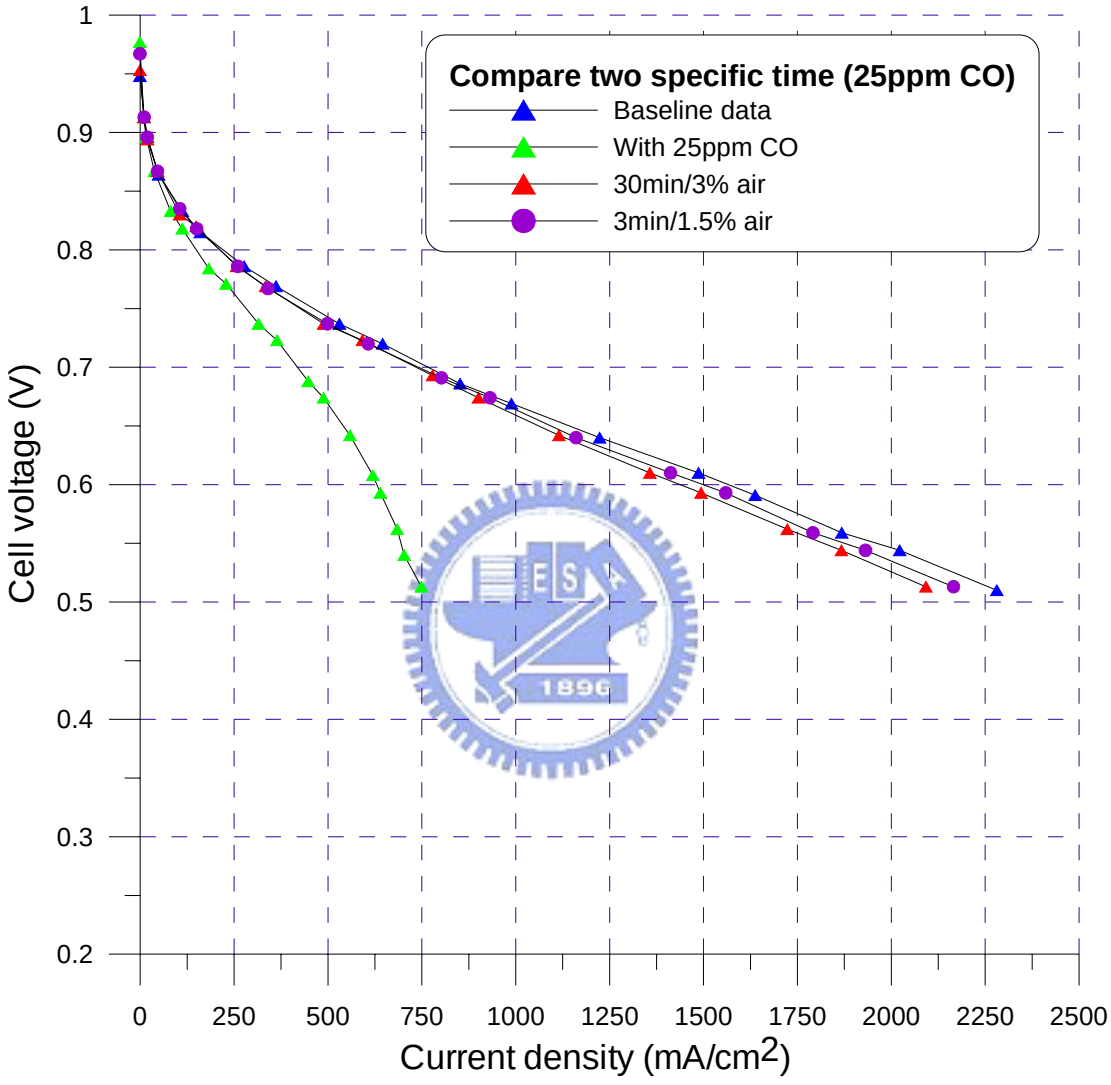

Fig. 4.18 The comparisons of recovered steady-state polarization curves with different air-bleeding timing (3 and 30min), with 25ppm CO

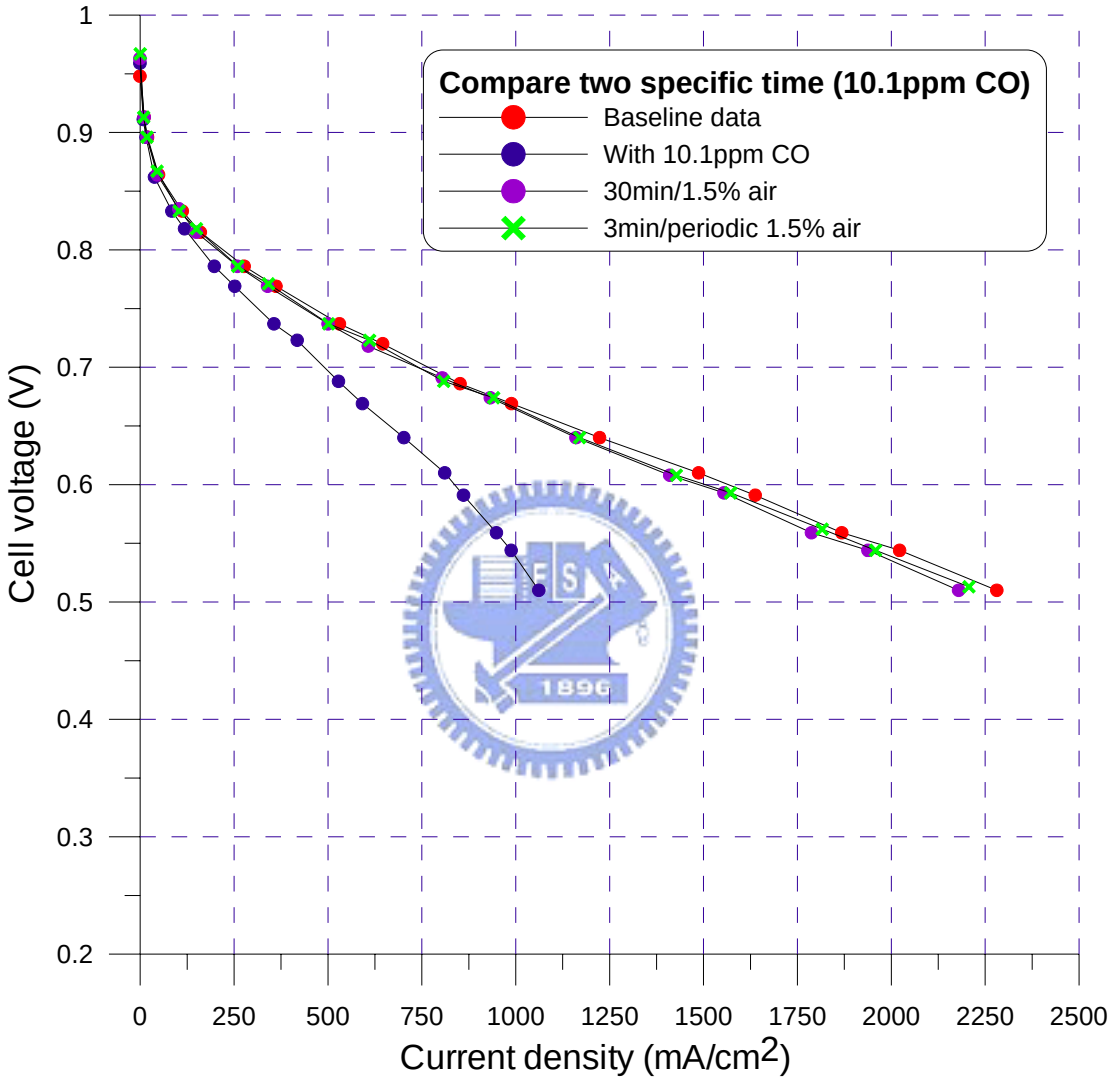

Fig. 4.19 The comparisons of recovered steady-state polarization curves with different air-bleeding timing (3 and 30min), with 10.1ppm CO

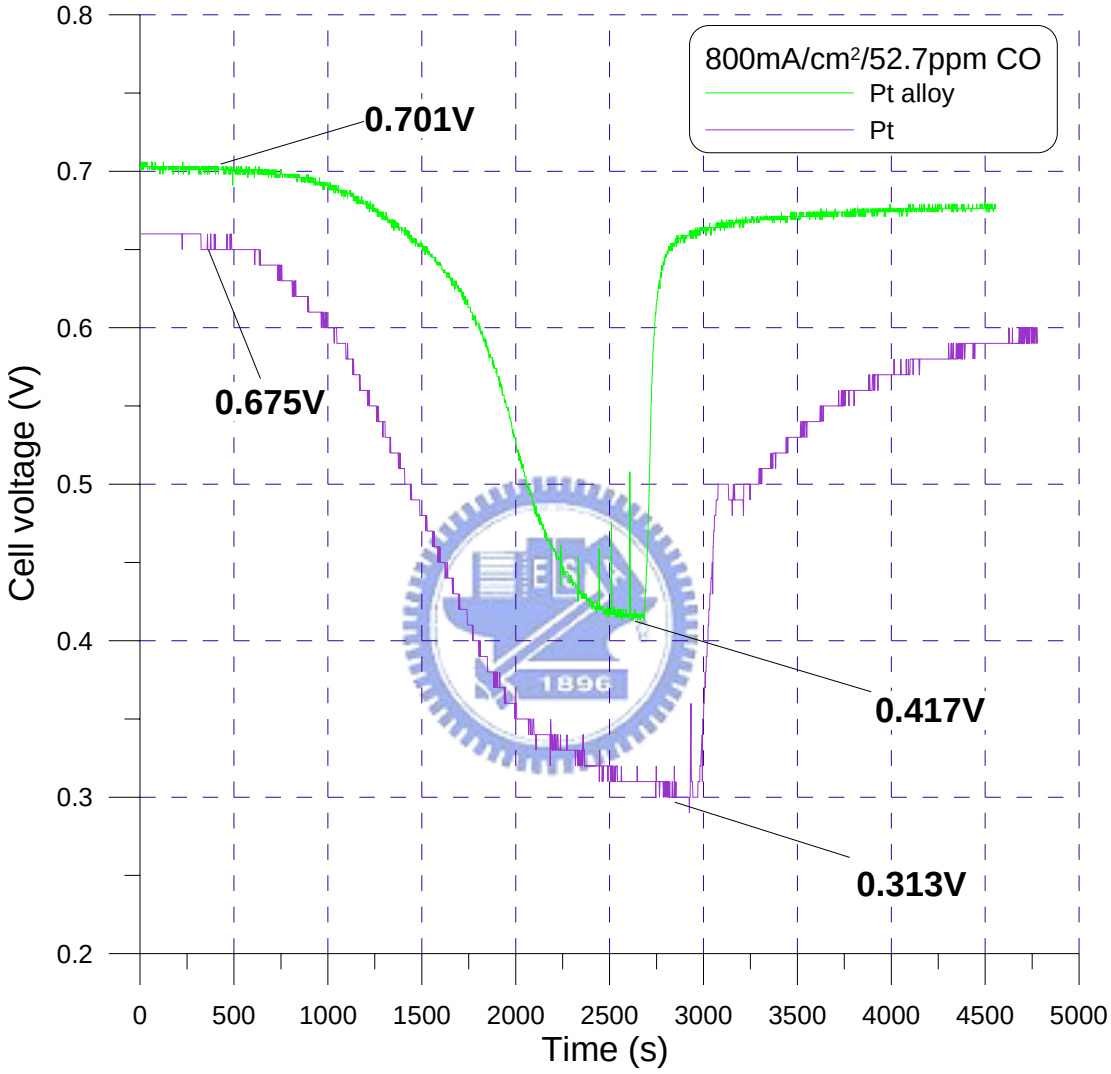

Fig. 4.20 Transients poisoning and recovery performances with different anode catalyst (Pt alloy and Pt), with 800 mA/cm^2 and 52.7ppm CO

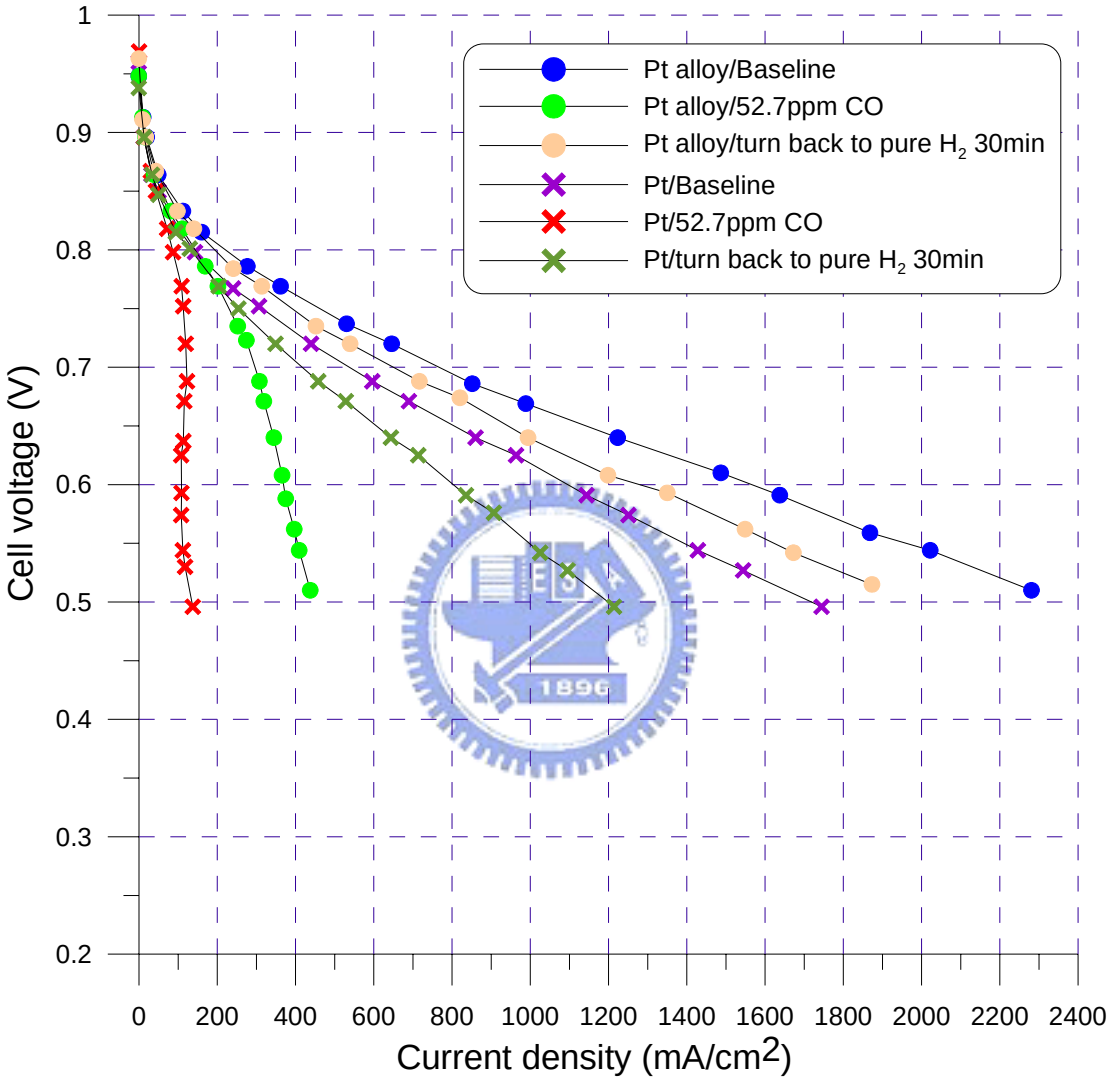

Fig. 4.21 The baseline polarization curve, the poisoned and recovered polarization curves with different anode catalyst (Pt alloy and Pt)

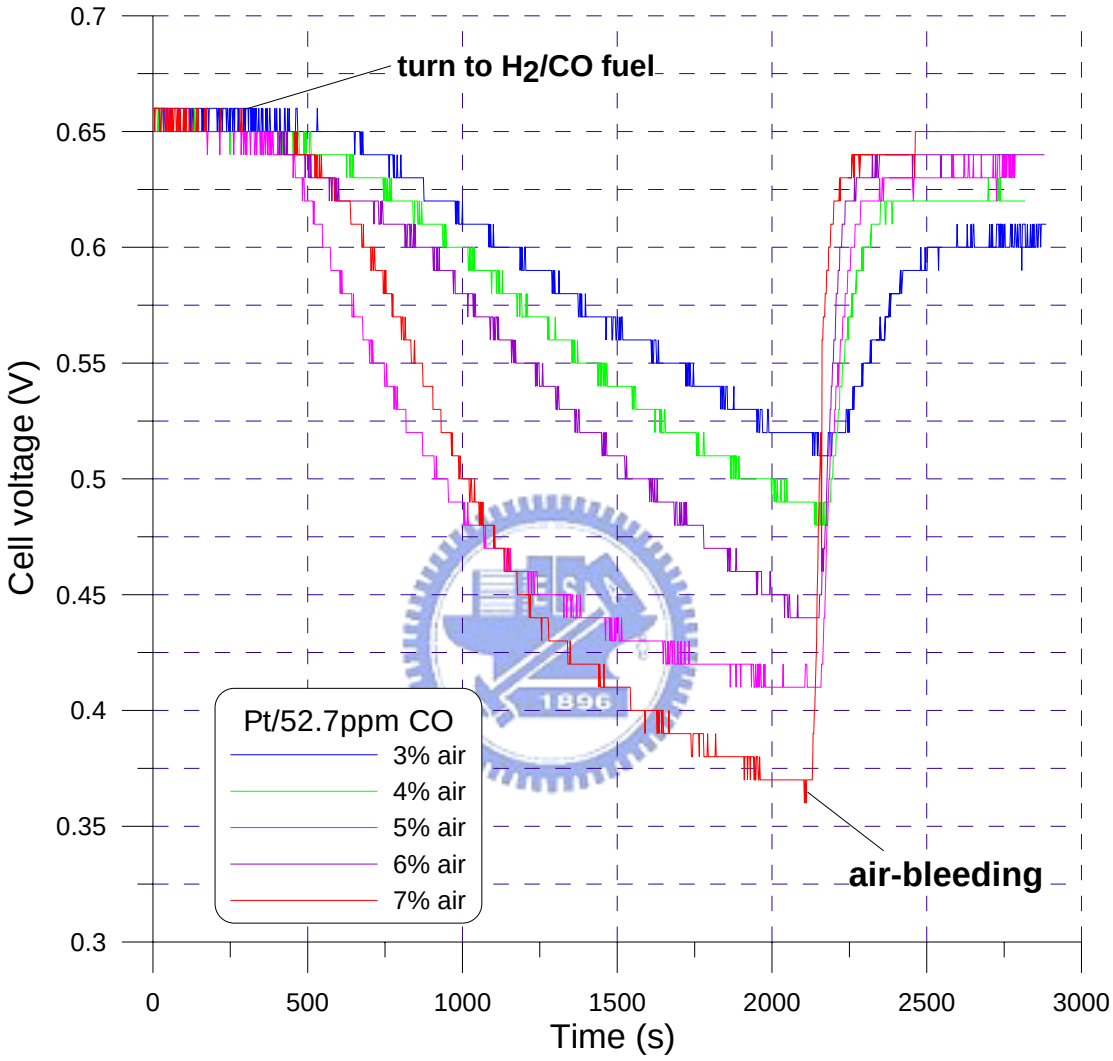

Fig. 4.22 Transient air-bleeding test with 52.7ppm CO at 800 mA/cm^2 and Pt anode catalyst, the cell potentials recover to 0.605, 0.620, 0.637, 0.642 and 0.649V as the air-bleeding ratios are 2, 3, 4, 5, 6 and 7%, respectively

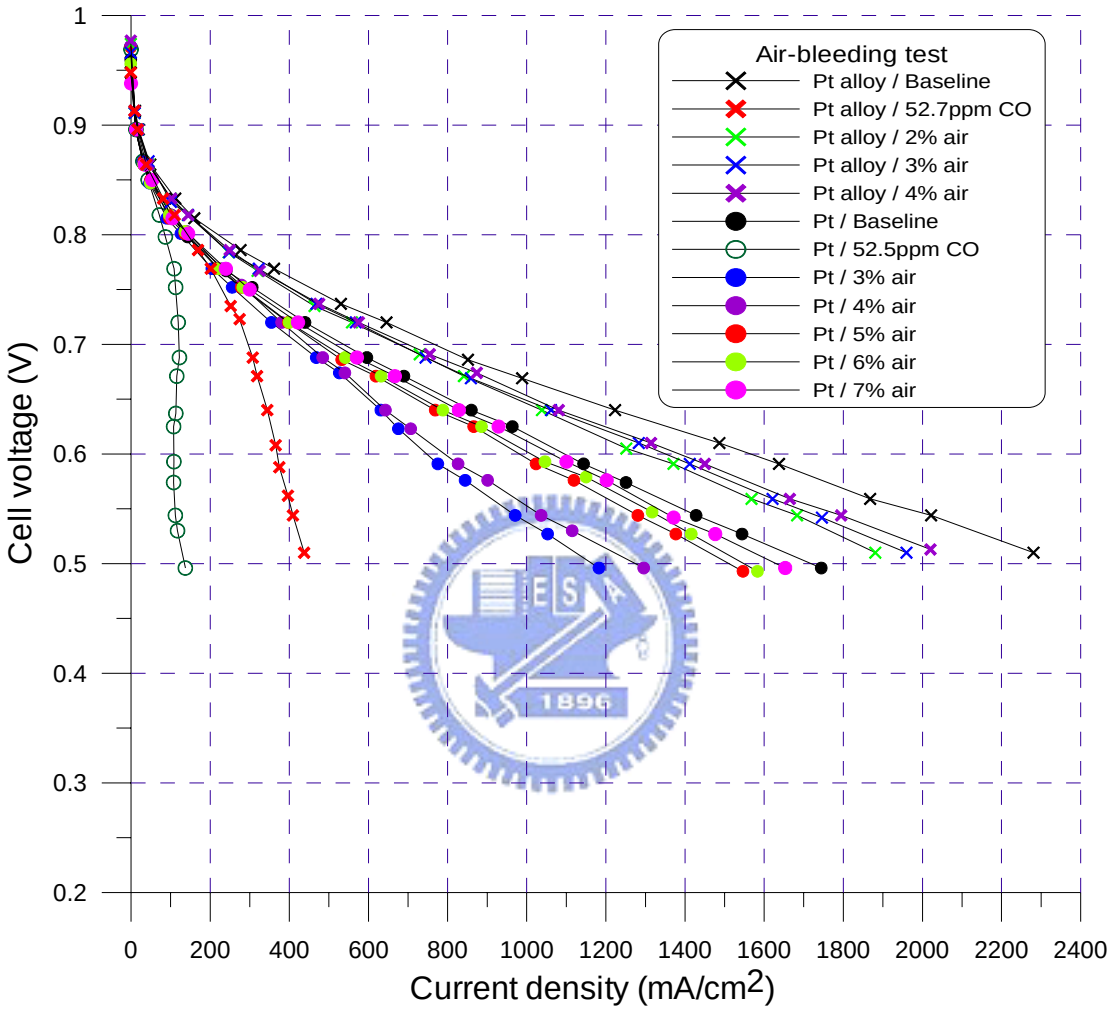

Fig. 4.23 Summarizes the recovered steady-state polarization curves as a function of air-bleeding ratio with different anode catalyst (Pt and Pt alloy), with 52.7ppm CO